On active layer processes and landforms in Western Dronning Maud Land, Antarctica

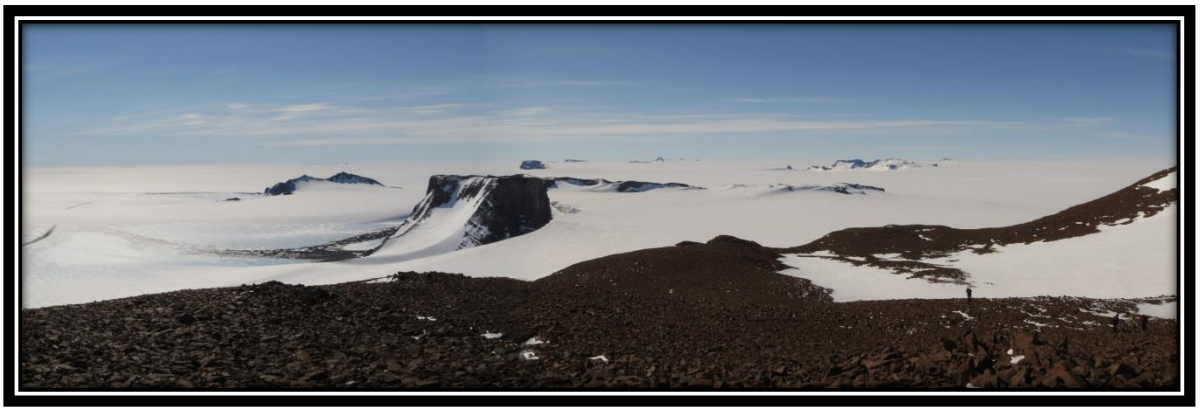

A thesis submitted in fulfilment of the requirements for the degree of

MASTER OF SCIENCE

of

Rhodes University

by

David Alan Scott

November 2014

Supervisor

Professor K.I. Meiklejohn (Department of Geography, Rhodes University)

Abstract

Permafrost is a variable in Antarctic terrestrial ecosystems, and the role it plays in the cryosphere is not well understood. There is much still to be learnt about the thermal state, physical properties, thickness and age of permafrost in Western Dronning Maud Land (WDML). Active layer dynamics and observed change over time have the potential to improve our knowledge of climate change. Understanding the effects of a warming climate on permafrost can also be of benefit to infrastructure, especially in areas with a large amount of frozen ground such as Scandinavia, Canada and Russia. Active layer and permafrost dynamics of WDML, Antarctica, are presented and discussed using data from six study sites, namely the Robertskollen, Vesleskarvet, Flarjuven, Grunehogna, Slettjfell nunataks and the Troll research station in the Jutulsessen area. Ground and ambient air temperature, as well as ground moisture data were collected for each site. An inventory of active layer and permafrost landforms was compiled, as were the frequency of cycles over the zero-degree isotherm, and the depth of the active layer. Furthermore, 3D models, geo-referenced maps and Digital Elevation Models were created of study areas with the use of an Unmanned Aerial Vehicle (UAV). Polygonal features are the most common landscape feature and are common to most of the study sites. Robertskollen has the deepest active layer at over 66cm and Slettfjell the shallowest at 9cm. A maximum recorded air temperature of 8.76°C (10/11/2014) occurred at Troll with the second highest maximum of 6.77°C (22/12/2010) recorded at Vesleskarvet. Robertskollen has the highest observable biological growth and a maximum recorded ground temperature of 22.84°C (10/01/2014). Troll and Valterkulten, registered the second and third highest ground temperatures respectively. The high ground Temperature observed for Robertskollen may be ascribed to it being the lowest altitude site. The highest number of cycles over the zero-degree isotherm was observed at Troll (11.01%), followed by Robertskollen (10.99%). For relatively warm areas, such as Robertskollen it is recommended that two metre borehole loggers are installed in order to capture a detailed understanding of the active layer. The UAV proved to be a beneficial tool for capturing aerial photographs for post fieldwork analysis and 3D modelling.

Keywords: Western Dronning Maud Land, Antarctica, permafrost, active layer dynamics, cryosphere, freeze/thaw, UAV, aerial photography, 3D modelling.

Acknowledgements

The author would firstly like to thank his parents who have given support and encouragement through his academic carrier. Gratitude is given to Professor Ian Meiklejohn of Rhodes University for his guidance and support throughout the two years of study undertaken to complete this dissertation. Rosie Dwight, Liezel Rudolph, Christel Dorothee Hansen, Gwyneth Dorothy, Dr Sebastiaan Swart, and Professor Ian Meiklejohn are thanked for their willingness to assist in the data collection and permission to use their photographs for display purposes. David Forsyth is thanked for his dedication to helping with the construction of the UAV for aerial photography. Rhodes University is thanked for their support throughout the M.Sc. studies. Funding by the NRF (National Research Foundation) is appreciated, without whose financial support the M.Sc. studies would not have been possible. DEA (Department of Environmental Affair) and SANAP (South African National Antarctic Programme) are thanked for providing logistical support during the fieldwork seasons conducted in the Antarctic. NGI (National Geo-Spatial Information) and GeoEye foundation (0.5m resolution satellite imagery) are thanked for the provision of data, as are those members of the 2012/13 and 2013/14 Austral summer relief voyage teams to SANAE IV that assisted during the fieldwork data collection process. Finally, thanks to all my friends at Rhodes University who have made my stay in Grahamstown a memory of a lifetime.

Table of Contents

Table of Figures

Table of Tables

Table of Equations

List of Abbreviations

3D – Three dimensional

Alt. - Altitude

C – Celsius

c – coefficient of variation

CF – Correction Factor

cm - Centimetre

CSDA- Confirmatory Spatial Data Analysis

DEA – Department of Environmental Affairs

DEM – Digital Elevation Model

DML – Dronning Maud Land

DSLR - Digital Single-lens reflex

ESRI – Environmental Systems Research Institute

GIS – Geographical Information Systems

GPS – Global Positioning System

DGPS – Differential Global Positioning System

GST – Ground near-Surface Temperature

m – Metres

Ma – Mega-annum (1 000 000 years)

MASL – Meters Above Sea Level

MAV – Manned Aerial Vehicle

mm - Millimetre

NGI – National Geo-Spatial Information

NRF – National Research Foundation

s – standard deviation

SANAE – South African Antarctic Expedition

SANAP – South African National Antarctic Programme

SCAR – Scientific Committee on Antarctic Research

TIN - Triangulated Irregular Network

UAV – Unmanned Aerial Vehicle

WDML – Western Dronning Maud Land

CHAPTER 1: Introduction

1.1. Background, Context and Motivation

Antarctica contains 90% of the World's ice and is the continent with the highest mean elevation at 3000m and the minimum mean annual air temperature at -40°C (Bockheim and Hall, 2002). A concentration of ice this large wields an influence on global atmospheric and cryospheric systems (Bockheim and Hall, 2002). Permanently frozen ground (permafrost) underlies 22 million km² which is approximately 17% of the global land area (Gruber, 2012). There is a need to develop our understanding of Antarctic permafrost (French and Guglielmin, 2000a; French and Guglielmin, 2000b; Bockheim and Hall, 2002; Vieira *et al*., 2010; Gruber, 2012; Bockheim *et al*., 2013). In recent decades, permafrost warming has been measured in boreholes in the Northern Hemisphere (North America, Russia, and Northern Europe) but very little is known about trends in Antarctica (Bockheim *et al*., 2013). There is little information on the permafrost component of the cryosphere regarding the thermal state, physical properties, thickness, age, and response to global change (Bockheim, 1995; Bockheim and Hall, 2002; Bockheim *et al*., 2008; Hallet *et al*., 2011; Guglielmin, 2012). No solid conclusions with regard to trends have been drawn up and there is the need for long term monitoring programmes.

Permafrost is one of the controlling and driving factors for Antarctic terrestrial ecosystems and it is, therefore, important for us to grasp a full understanding of its elements (Vieira *et al*., 2010; Guglielmin, 2012; Bockheim *et al*., 2013). Both cryospheric and life sciences are dependent on an in-depth understanding of permafrost properties and whereabouts. Permafrost can be found beneath almost all ice-free terrain except for certain areas of low elevation in the maritime Antarctic and on the sub-Antarctic islands (Vieira *et al*., 2010). Guglielmin (2012) and Bockheim *et al*. (2013) suggest that permafrost properties and active layer (seasonally freezing soil) dynamics are two fundamental indicators for assessing climate change in the northern polar regions. However, once again these authors stress that in Antarctica very little is known about these properties. Due to the importance of the permafrost and active layer properties, the scientific community fully supported the creation of a Scientific Committee on Antarctic Research (SCAR) and Geosciences Standing Scientific Group (GSSG) on Antarctic permafrost and periglacial environments (Guglielmin, 2006). A research project called Antarctic and Sub-Antarctic Permafrost, Periglacial and Soil Environments (ANTPAS) was created as a result of these groups. ANTPAS was coordinated by the International Permafrost Association's working group on Antarctic Permafrost and Periglacial Environments, and the Scientific Committee on Antarctic Research Expert Group on Permafrost and Periglacial Environments (Vieira *et al*., 2010). It addresses key issues in cryospheric science and was designed to

fill the gap, improving the monitoring protocols and quantity of monitoring sites around Antarctica and to promote the creation of an Antarctic network (Guglielmin, 2006; Vieira *et al*., 2010). All research will be added to the frozen ground data centre (Brown *et al*., 2003). ANTPAS aims at addressing key issues of Antarctic permafrost science with two main objectives (Vieira *et al*., 2010:183):

- "Integrating existing datasets on permafrost, ground ice, active layer dynamics and soils; and
- Implementing borehole, active layer, periglacial process and soils monitoring networks as the Antarctic component of the 'IPA-IPY Permafrost Observatory Project' (TSP) and of the Circumpolar Active Layer Monitoring programme (CALM)".

Understanding Antarctic life and how it evolves is one of the six research priorities recently identified (Kennicutt II and Chown, 2014). Furthermore, two of the key fields for future studies raised by leading Antarctic scientists directly relate to this research project (Kennicutt II *et al*., 2014):

- Question 39: What are and have been the rates of geomorphic change in different Antarctic regions, and what are the ages of preserved landscapes?
- Question 42: How will permafrost, the active layer and water availability in Antarctic soils and marine sediments change in a warming climate, and what are the effects on ecosystems and biogeochemical cycles?

Since the 1960's ground temperatures have been measured and monitored for a variety of reasons but unfortunately there was no form of standardised protocols (Bockheim, 1995; Turner *et al*., 2009). In 1999 a network of boreholes was implemented to monitor permafrost conditions over long term durations.

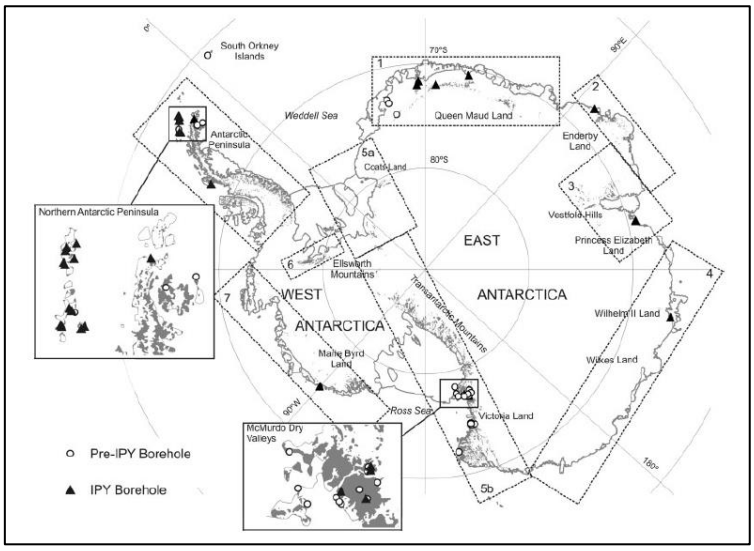

Figure 1: Antarctic permafrost monitoring boreholes areas (Vieira *et al*., 2010:184).

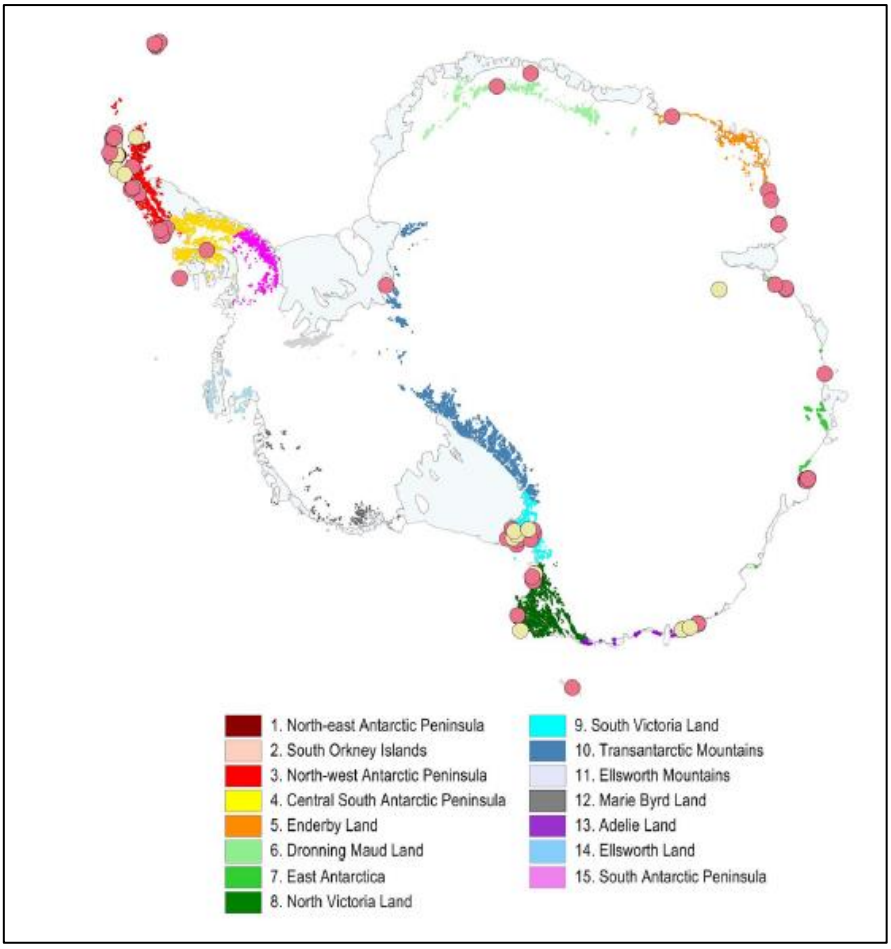

Figure 2: Location of Antarctic Specially Protected Areas (ASPAs) and Antarctic Conservation Biogeographic Regions (ACBRs) (Shaw *et al*., 2014:2).

1.2. Landscape features – Patterned ground formation

The repeated annual, seasonal, diurnal, and/or permafrost derived from freezing and thawing of the active layer in permafrost soils can produce interesting features, termed patterned ground (Kerfoot, 1972; French, 2006; Marchant and Head, 2007; Hallet *et al*., 2011). The features of interest for this research are; polygons, terraces, steps, stripes, and sorted and non-sorted stones and sediments (self-organisation) (Kessler and Werner, 2003; Haugland, 2004). The sorting of the ground via freeze/thaw cycles is due to interplays between two feedback mechanisms: 1) the formation of ice lenses and 2) the transportation of stones along the axis of elongation (Kerfoot, 1972; Kessler and Werner, 2003; Marchant and Head, 2007). When water freezes it expands and the repeated freezing and thawing of groundwater forces larger stones towards the surface as smaller soils flow and settle underneath these larger uplifted stones (Kessler and Werner, 2003; French, 2006). The water saturated areas of finer sediments have a much greater ability to expand and contract as freezing and thawing occur, leading to lateral forces which ultimately pile larger stones into clusters and stripes (Kessler and Werner, 2003; French, 2006). According to Andre (2003), the formation of patterned ground is associated with diurnal, seasonal and/or permafrost derived from freeze/thaw cycles. Many scientists have conducted

field and laboratory studies in order to better understand the exact mechanism involved in these formations, however, they are still not entirely understood (Lundqvist *et al*., 1995; Harris and Davies, 2000; Hall and André, 2001; Hall, 2002; Boelhouwers *et al*., 2003; Guglielmin *et al*., 2003; Kessler and Werner, 2003; Matsuoka *et al*., 2003; French, 2006).

Kessler and Werner (2003) suggest that formation of patterned ground could take a century in Polar latitudes; however, Ballantyne and Matthews (1982) believe that stabilization of sorted circles occurs within 50 years of ground exposure and Matthews *et al*. (1998) recognise it to be a 60-year time frame. A study in southern Norway on the small features (<1 m), suggest that the relatively small time period (60-years) for stabilization to occur is linked to paraglacial processes (Matthews *et al*., 1998). Shortly after deglaciation; the ground temperatures increase, sediments become consolidated and drained, slope angles decline, and then vegetation establishment occurs (Matthews *et al*., 1998; Haugland, 2004). Ballantyne and Matthews (1982) conclude that the formation of patterned ground is influenced more by the immediate local environment of the glacial margin rather than the expected regional or local climatic conditions. The processes responsible for the reworking of glacigenic material in deglaciated terrain are termed paraglacial (Haugland, 2004). The idea behind this term (paraglacial) refers to the instability in a system soon after deglaciation and most of the previous research done refers to slope adjustments; however, the concept may also be concerned with patterned ground formation after deglaciation (Haugland, 2004). Patterned ground formation can be associated with marginal environments, cool glacier winds and saturated conditions (Haugland, 2004). The surface temperature of a glacier will not increase beyond melting point as warm air which has been heated by nearby bare soil and rocks will be advected over the melting ice by winds and therefore the air near to the surface will be cooled once again and will flow down the glacial slope due to the negative buoyancy of cold air (Obleitner, 1994 and Van Den Broeke, 1997). Ballantyne and Matthews (1982) discovered that there was a difference of 11°C between 5cm deep boreholes at the ice margin and at a distance of 100m from the ice margin, and concluded that areas near to the ice margin are more likely to be associated with patterned ground formation. Haugland (2004) noted that what this then implies is that periglacial processes exist within a small geographical zone (the periglacial zone). As the ice margin retreats; frost activity decreases and allows for the onset of vegetation which then stimulates the genesis of soils (Hall and Walton, 1992; Haugland, 2004).

Patterned ground diversity is due to a variety of mechanism; particle sorting, freezing and thawing, deformation of frozen soil, soil creep, and contraction cracks (Levy *et al*., 2008a and Goodfellow *et al*., 2009). According to Kessler and Werner (2003:380) the ground sorting process is as follows (Fig. 3):

A. “Frost heave expands soil perpendicular to the freezing front (cross section). Horizontal lines indicate zone of lateral frost heave near the stone-soil interface; vertical lines indicate zones of vertical frost heave near the ground surface.
B. Surface stones creep toward stone domains, subsurface soil is driven toward the interior of the soil domain, and stones are pushed toward stone domains by frost heave near the stone-soil interface (cross section).
C. Stones avalanche away from regions where stone domains are thicker, which experience greater uplift by lateral squeezing (vertical section along the stone domain axis).
D. Regions where stone domains are wider experience greater uplift owing to lateral squeezing (plan view); stone motion (open arrows) is away from wider areas and parallel to the stone domain axis”.

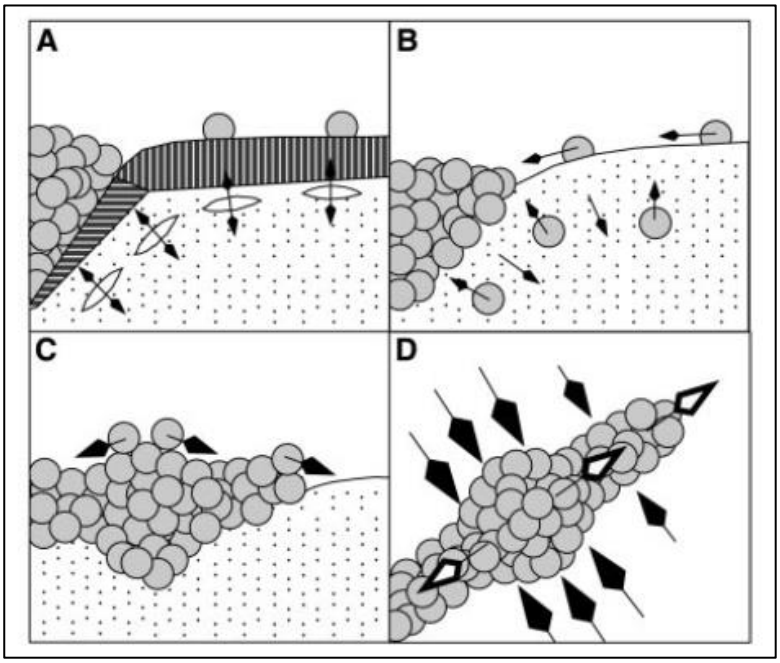

Figure 3: The feedback mechanisms for sorted ground (Kessler and Werner, 2003:380).

Typical formations developed from the freeze/thaw cycles show; sorted and non-sorted ground, patterned ground, stripes and contraction cracks found in different areas around the Arctic (Fig. 4). Polygon crack patterns occur in permafrost when a rapid temperature drop causes a contraction of the permafrost material and if water is present in the cracks it will freeze during the colder periods and produce an ice vein (Black, 1976; van Gasselt *et al*., 2005). The ice vein will then cause a mechanically weak zone in the permafrost and will be reopened in future cycles, however, if conditions are not favourable to moisture then sand will fill the empty space and cause sand wedges (Pewe, 1959).

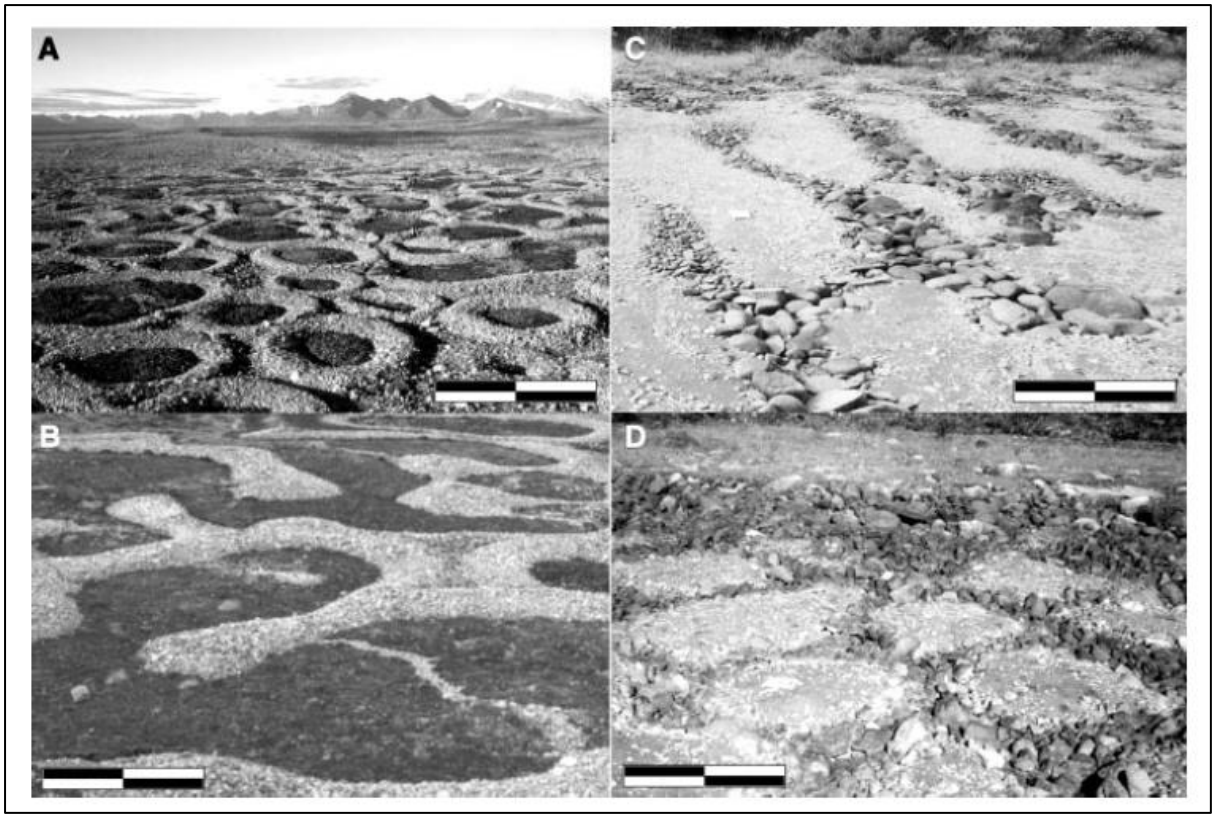

Figure 4: Sorted and patterned ground found in the Arctic, similar to that of Antarctic patterned ground (Kessler and Werner, 2003:380).

Examples of polygon features found at some of the study areas in WDML, were identified as part of the current study (Fig. 5 and 6). A variety of studies, both theoretical and quantitative, have attempted to explain patterned ground formation e.g. Ray and Krantz, 1983; Hallet *et al.,* 1990; Krantz, 1990; Boelhouwers *et al*., 2003; Kessler and Werner, 2003; Matsuoka *et al.,* 2003; Marchant and Head, 2007; and Minsley *et al*., 2012. However, patterned ground formation is a complex process and a universal explanation is still absent. Patterned ground can be found in a wide range of environments so therefore similar-looking features in different environments do not necessarily share a common genesis (Washburn, 1980). Most studies have focused on areas where processes may have been active for a very long time; however, Haugland (2006) argues that recently deglaciated areas must not be neglected as the local factors may prove to be equally relevant. Studies done on recently deglaciated Jotunheimen Norway; on microtopography, drainage, exposure of substrate and distance from the ice margin can also explain patterned ground formation (Ballantyne and Matthews, 1982, 1983; Harris and Matthews, 1984; Hall and Walton, 1992; Ballantyne and Benn, 1994; Matthews *et al*., 1998; French and Guglielmin, 1999). The formation of patterned ground and stabilisation in recently deglaciated areas can occur within a few decades (Haugland, 2006). Observations have been made in the Jutenheimen region where patterned ground is most active on glacial deposits (textured ground) which are bordering ice margins as these areas are where temperatures and soil moisture appear to be

favourable towards the rapid reworking processes (Ballantyne and Matthews, 1982, 1983; and Matthews *et al*., 1998). Furthermore, these ideal conditions decline with withdrawal of the ice margin.

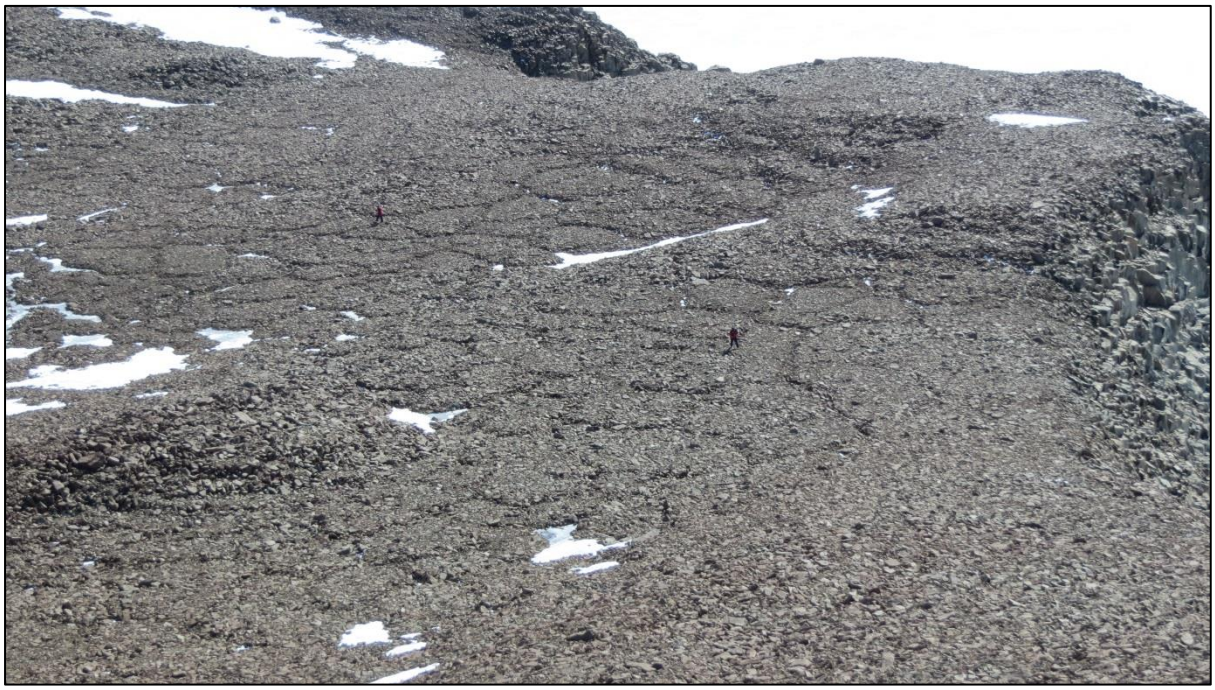

Figure 5: Polygon formations due to contraction cracks from the current study's Flårjuven study site. Note the people for scale (Photo: Scott, D.A).

Figure 6: Polygon formations due to contraction cracks from the current study's Troll study site (Photo: Scott, D.A).

Ballantyne and Matthews (1982), Obleitner (1994) and Van Den Broeke (1997) suggest that the microclimates around the ice margins have cooler temperatures than the surrounding glacial deposits due to katabatic winds which flow directly onto the ground along the margin which in turn increases the occurrence of freeze/thaw cycles and hence the beginning of patterned ground formation. Haugland's (2006) research found with increasing distance from the ice margin, vegetation colonization occurs, as soils thicken with age. A theoretical model (Fig. 7) from Haugland (2006) displays his research findings on the development of patterned ground features. The model is based on post-deglaciated development of relatively small patterned ground forms. The model suggests the abiotic factors that drive the initial processes associated with patterned ground formation. The time scale for this model is measured in decades and the working of the ground is directly linked to increased soil moisture and freeze/thaw activity (Ballantyne and Matthews, 1982, 1983; Matthews *et al*., 1998). Ice margins retreat from the local area of study after time and there is a reduction in frost activity, soil moisture, and substrates drain and consolidate (Matthews *et al*., 1998). Thickness of the arrows indicates relative importance of that stage. Stage D is where vegetation cover begins to form, ultimately stabilizing the land, impacting the amount of frost activity (Haugland, 2006). Model stages show the two-way relation between vegetation colonization and soil development within these patterned ground features and rely heavily on the subsidence of frost activity (Haugland, 2006). Bockheim *et al*. (2013) suggest that the depth of the permafrost (or the active layer depth), can be vaguely predicted in Antarctica based on the latitude due to climatic differences. Permafrost is likely to become continuous at 69°S to 74°S, with the change from maritime to a continental climate (Bockheim *et al*., 2013). There are at least five major groups of periglacial features that are indicative of permafrost systems: 1) cryoplanation terraces, 2) ice-cored moraines, 3) ice-wedge and sand-wedge polygons, 4) rock glaciers and protalus lobes, and 5) open-system pingos (Harris, 1982; Bockheim, 1995; Serrano *et al*., 2008).

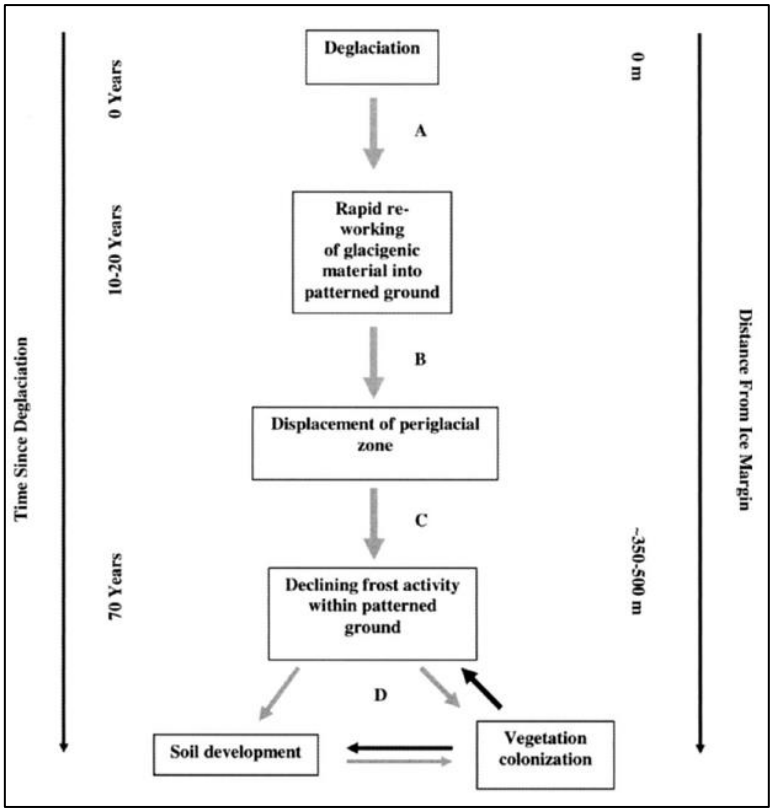

Figure 7: A theoretical model of microsite landform development across recently deglaciated terrain (Haugland, 2006:87).

1.3. Permafrost and active layer thermal regime

The International Polar Year (IPY) project ANTPAS has provided for a snapshot of the thermal regimes in permafrost and active layer, however, there is the need for continued research in order to monitor change (Vieira *et al*., 2010). Vieira *et al*. (2010) and Guglielmin (2012) among other authors have provided and been adding to the active layer sites inventory for many years. Boreholes have varied in depth according to their geographical location and are classified as follows; deep (>125m), intermediate (25m to 125m), shallow (10m to 25m), surface (2m to 10m) and boreholes under 2m of depth are distributed mainly in two areas: Maritime Antarctica and in Victoria Land, Antarctica (Hauck, 2007; Vieira *et al*., 2010; Guglielmin, 2012). It is important to note that the active layer is highly variable at a local scale and directly influenced by surface cover and micro-morphological features (Cannone *et al*., 2006; Guglielmin, 2006; Guglielmin *et al*., 2008; Guglielmin, 2012; Guglielmin *et al*., 2014). Furthermore, water content in the active layer is poorly understood even though various authors have done long term monitoring but it has been determined that local climatic/microclimatic conditions and topography strongly influence the water content (Seybold *et al*., 2010; Guglielmin, 2012). The effects of a changing climate are noticeable and have become a focus of many scientists (Cannone *et al*., 2006; Guglielmin, 2006; Guglielmin *et al*., 2008; Guglielmin, 2012; Guglielmin *et al*., 2014).

1.4. Permafrost in a climate change environment

Antarctica is one of the areas of the world least disturbed by anthropogenic impacts and it is therefore a key area for global climate change studies. Permafrost is present beneath most of the ice-free terrain in Antarctica, with the exception of the low elevations of the sub-Antarctic islands (Guglielmin, 2012). As mentioned earlier, permafrost occupies only 0.36% (49,800 km²) of the Antarctic region and has been identified by the World Climate Research Programme as a key element of the Earth System for the focus of future research (Intergovernmental Panel on Climate Change, 2001). There have been numerous studies done in the Arctic and mountainous areas around the world which define the characteristics of permafrost and its response to climate change, however, studies of the same intensity have not been done in the Antarctic (Goryachkin *et al*., 1999; Hall, 2002). According to Hauck *et al.* (2007), the reason for this lack of knowledge is due to very scarce network of permafrost monitoring boreholes and active layer monitoring sites. Without these networks climate models cannot be applied and an understanding of the Antarctic permafrost dynamics cannot be established (Hauck *et al.*, 2007 and Guglielmin, 2012). Hauck *et al.* (2007) stresses that the current permafrost distribution should be determined to establish a baseline which could then be used for measuring the impact of climate change on permafrost in Antarctica in the future.

Geophysical techniques can be used to improve knowledge of ground ice distribution in Antarctica and have a low impact which is especially useful in sensitive and protected areas (Hauck *et al.*, 2007). According to the IPCC (Intergovernmental Panel on Climatic Change) assessment there are large feedbacks between climate and its impacts on the landscape, on the geomorphic processes and on the ecosystems in which permafrost degradation and active layer thickening occur (Hauck *et al.*, 2007; Guglielmin, 2012). Although these impacts are related more to Arctic conditions, some aspects still apply; hydrological changes at the surface, slope instability, release of methane, changes in vegetation, increases in dissolved materials in rivers and oceans (Lewkowicz and Harris, 2005; Cannone and Guglielmin 2010; Guglielmin, 2012). Changing wind regimes are a resultant of climate change in cold areas and can impact more complex processes like the freeze/thaw cycles and the related landforms (Guglielmin, 2012). Patterned ground activity can be reduced in mild areas (maritime Antarctica) by depletion of freeze/thaw cycles through the increase of air and surface temperatures, however, these cycles may increase in colder areas due to warming (Guglielmin, 2012). Furthermore, soil formation and all the related processes (i.e. sorting and cryoturbation) can be affected through active layer thickening (Guglielmin, 2012).

In contrast to the Arctic, the physical properties of Antarctic permafrost is less well known, especially with regards to the thermal regime, the active layer thickness and the presence of ground ice (Vieira *et al*., 2010). Maritime Antarctica is one of the areas of the world greatly affected by the by warming air temperatures and it therefore provides a unique opportunity for scientific research into the

understanding of the impacts of climate change on permafrost and its related ecosystems (Guglielmin, 2012 and Bockheim *et al.*, 2013). Research in the Arctic has given an insight into many aspects of effects.

1.5. Permafrost, the carbon cycle and Northern Hemisphere developemnt

Thawing permafrost and microbial decomposition is one of the most significant potential feedbacks from terrestrial ecosystems to the atmosphere in a changing climate (Schuur *et al*., 2008; Turner *et al*., 2009). The global biogeochemical cycle of carbon is a major concern for modern science. Unlike the Arctic, the permafrost in Antarctica is low in carbon and therefore its role in contributing to greenhouse gasses is minimal (Turner *et al.*, 2009). However, areas where the active layer is thickening could act as carbon sinks in the long term through the colonisation of new microbial communities and plant species and hence an increase in biomass (Anderson *et al*., 1998; Brinkmann *et al*., 2007; Vieira *et al*., 2010). Understanding the potential environments where such a prediction may occur is important for a long term all round understanding of these conditions. The warming of the Earth's climate is a huge concern and a common topic among scientists nowadays (e.g. Blunier and Brook, 2001; Lavelle, 2012; Skuce, 2012). In the Arctic there has been a large amount of research done on the effect of a warming climate on permafrost. The process of methane release into the atmosphere through thawing permafrost and the harmful release of CO_2 and methane into the atmosphere is illustrated in Figure 8. It is common knowledge that methane bubbles to the surface of lakes and accumulates under the ice (Fig. 9); however, more recent research in Alaska has shown that seeps are also fed by thermal compression of organic matter in deeper older sediments (Skuce, 2012). Scientists are beginning to discover how detrimental the effects of a warming climate have been and will become if the climate continues to change.

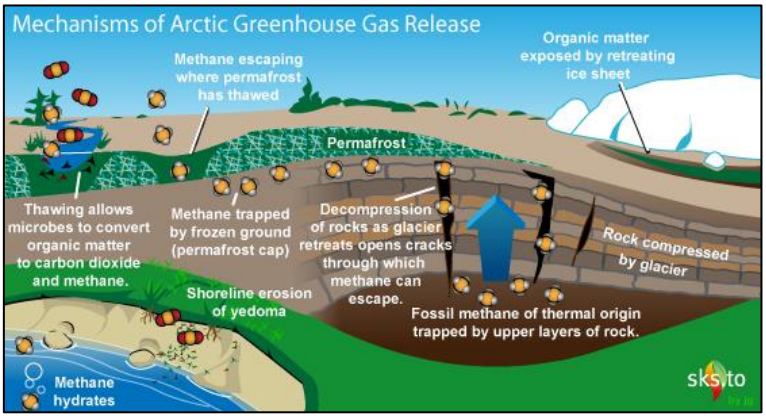

Figure 8: The process of methane release into the atmosphere through thawing permafrost is illustrated in this image. 1) Organic matter is exposed by retreating ice margins. 2) Thawing allows microbes to convert organic matter into carbon dioxide and methane. 3) Thawing of permafrost, shoreline erosion and decompression of rock cracks allows for methane to escape into the atmosphere (Lavelle, 2012).

Figure 9: The images show trapped methane bubbles in Arctic lakes (left) and the explosive flammability release of this methane gas (right) (Lavelle, 2012).

1.6. Consequences of thawing permafrost on the Antarctic Peninsula, infrastructure and Extra-terrestrial applications of permafrost research

Permafrost distribution is poorly known for Antarctica and there is a scarcity of active layer and permafrost monitoring sites (Bockheim, 1995; Guglielmin, 2006). The Antarctic Peninsula is a good study area for permafrost adaptations to temperature fluctuations due to its latitude. The ground surface temperature (GST) is a delicate indicator of the local climate as it integrates many climatic elements above the ground surface, such as; air temperature, wind factor, and seasonal snow cover and includes their interactions with the ground surface characteristics like vegetation cover and surface micro-relief (Guglielmin, 2006). On the other hand, deeper indicators of climate change include the active layer and permafrost levels. In order to create future climatic models there needs to be a long record of ground thermal temperatures and active layer development (Guglielmin, 2006). International programmes such as the Circumpolar Active Layer Monitoring (CALM) and Permafrost and Climate in Europe (PACE) are focussed on continuous monitoring of these indicators in the Arctic and Europe respectively (Brown *et al*., 2000; Harris *et al*., 2001; Guglielmin, 2006).

Permafrost has been degraded in the South Shetland Islands by climate warming and this is visible through thermokarst features, debris flows and active layer detachment slides (Vieira *et al*., 2008). This general thawing can lead to mass movements, especially on hill slopes and moraines, which can be noticed on Elephant, Livingston, and King George Islands (Bockheim *et al*., 2013). Furthermore, Bockheim *et al*. (2013) also notes that there are hydrological implications to the thawing of permafrost which can lead to very rapid changes in lacustrine areas. Permafrost degradation in coastal areas such as the South Shetland Islands of Antarctica infers sediment transportation from the slopes

to the seacoast (Bockheim *et al*., 2013). Permafrost is a delicate indicator of climate change where a noticeable increase of 2.4°C to 3.4°C has occurred along the western Antarctic Peninsula over the past 50 years according to Bockheim *et al.* (2013). The general degradation in permafrost has had major impacts with regards to change in soil depths (Bockheim *et al.*, 2013). According to reports prior to 1980, permafrost was at a depth of around 0.30m in organic soils near Palmer Station, however, recent results show levels reaching 14m in depth (Bockheim *et al*., 2013).

Understanding the effects of a warming climate on permafrost can also be of benefit to infrastructure, especially in areas with a large amount of frozen ground such as the coastal zones of Antarctica (Vieira *et al*., 2010). Infrastructure may not cover much of the continent but the financial investment is substantially large for these areas (Vieira *et al*., 2010). Only the McMurdo Dry Valleys (MDV) area and some areas in the locality of several research stations around Antarctica have been studied intensively for permafrost activity (Bockheim *et al*., 2007).

In addition to Earth's terrestrial features, there has been interest in the features found on Mars for many decades. Similar features have been studied in cold weather environments on Earth. The progression of technology has made it possible to understand the similarity between Earth and Mars features, and since, increasing interest and new motive for better understanding Antarctic geomorphological activity (Belcher *et al*., 1971; Lucchitta, 1981; Rossbacher and Judson, 1981; van Gasselt *et al*., 2005; Levy *et al*., 2008b; Levy *et al*., 2009a; Levy *et al*., 2009b; Mellon *et al*., 2009; Levy *et al*., 2010). Guglielmin (2012) says that thermal contraction polygons of Phoenix lander on Mars are very similar to those of the Antarctica Dry Valleys which suggests the working of sublimation with the absence of moisture and processes driven by ground ice. In addition to this, ice-blisters and wind action have been studied in Northern Victoria Land, Antarctica, to better understand related processes on Mars (Guglielmin, 2009; Guglielmin 2012). According to Guglielmin (2012) permafrost areas of Antarctica can be directly compared to extra-terrestrial landscapes like those found on Mars due to its extreme dry and cold conditions and can be considered a leap towards future studies. The polygonal features captured on Mars and their similarities to those found in the Arctic and Antarctic are strikingly similar (Fig. 4, 5, 6 and 10). It is important for scientific research to continue into all the mentioned fields and new technique and strategies should be used whenever appropriate.

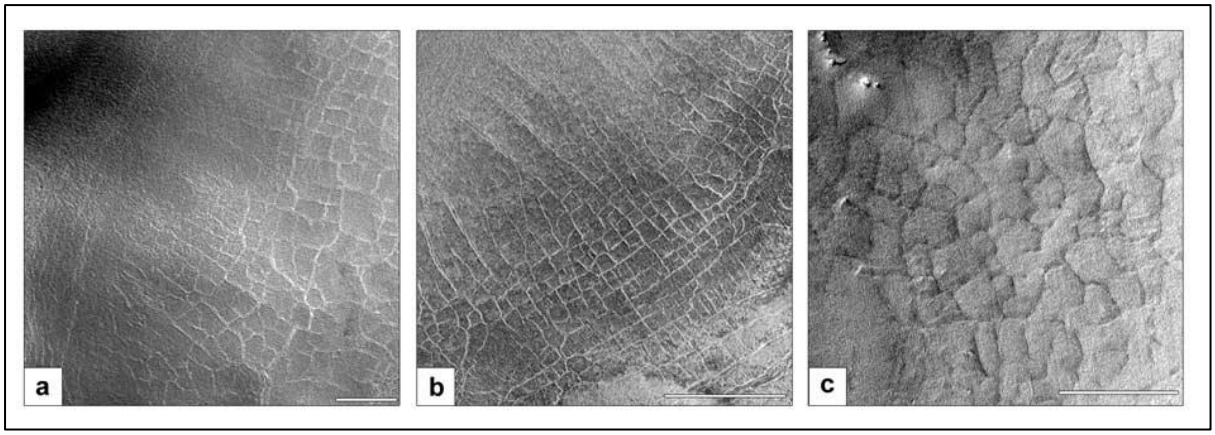

Figure 10: Examples of characteristic polygonal terrain located in the Martian mid-latitudes, images were taken by the MOC-NA instrument during its primary mapping phase. The polygon formations appear on crater slopes and show striking similarities to terrestrial polygons found in Antarctica caused by thermal contraction cracking (van Gasselt *et al*., 2005).

1.7. 3D modelling of Antarctic landscapes and features

One of the ways of assessing landscape features was by the use of Unmanned Aerial Vehicles (UAVs). UAVs have been used widely across the world and are becoming popular in many academic and research fields (e.g. Eisenbeiss, 2004; Bendea *et al*., 2007; Zongjian, 2008; Lucieer *et al*., 2010; Remondino *et al*., 2011; Lucieer *et al*., 2012; Turner *et al*., 2012; Vieira, 2014). UAVs have provided an easy system for capturing aerial imagery. These radio controlled vehicles are often referred to as; drones, Remotely Piloted Vehicle (RPV), Remotely Operated Aircraft (ROA), and Unmanned Vehicle Systems (UVS), and with the correct components on board they can be programmed to fly certain GPS navigated routes (Remondino *et al*., 2011). UAVs were first developed for military and police force situations where the risk of sending a human piloted aircraft was undesirable or the situation for a manned aircraft was impractical (Dragonfly Innovations Inc., 2014). Aerial torpedoes were designed for World War One to be fully autonomous UAVs and relied on technology such as mechanical gyroscopes to maintain straight flight paths. Although these were primitive in comparison to the UAVs of today they were the catalyst to all modern UAV capabilities (Dragonfly Innovations Inc., 2014). As technology advanced, the use of radio transmission for UAV guidance was used to navigate the vehicle for a mission and return to base. Although this was a huge step in the UAV world it required constant control via a human pilot and therefore could not fly autonomously (Dragonfly Innovations Inc., 2014). The invention of integrated circuitry allowed engineers and designers to build sophisticated UAVs which had electronic autopilot capabilities (Chao *et al*., 2010). UAVs were then widely used in the military to fly themselves to a location and attack the target with on-board weapons or to simply survey the area with cameras and sensor equipment. The UAVs of today combine these technologies allowing for manual flight controls and fully autonomous flight which allows for highly complex mission capabilities (Remondino *et al*., 2011).

CHAPTER 2: Setting, Research Question and Objectives

2.1. Setting

The study areas for the project are located in Dronning Maud Land, Antarctica, and focus areas are based around the South African base (SANAE IV) and the Norwegian base (Troll). South Africa, Argentina, Australia, Belgium, Chile, the French Republic, Japan, New Zealand, Norway, Russia, the UK and the USA signed the Antarctic Treaty on the 1st December 1959 (ATS, 1959). South Africa furthermore committed to being a full member of SCAR (Scientific Committee on Antarctic Research) (SCAR, 2010; SANAP, 2012).

Western Dronning Maud Land geology is classified by the Ahlmannryggen-Borgmassivet and Kirwanveggen-Sverdrupfjella mountains with scattered rocky outcrops (nunataks) (SANAP, 1992). The Borgmassivet intrusive is the major range of WDML and these nunataks which are exposed at the surface form part of it (SANAP, 1992). These rocks are classified as Mesoproterozoic origin (SASCAR, 1984). According to Grosch *et al*. (2007) at 1107Ma the mafic Borgmassivet sill intruded into the Ritscherflya Supergroup and at 600Ma mafic sills intruded into the north-eastern and south-western part of the Maud belt. The WDML nunataks consist of doleritic and dioritic sills and minor dykes which are massive rocks and generally resistant to mechanical weathering (Briggs, 1977a, SASCAR, 1984). However, their large crystal sizes make them susceptible to both mechanical (thermal stress, granular disintegration, and freeze-thaw action) and chemical weathering (hydration and hydrolysis, solution weathering, salt weathering, and oxidation) (French, 1996).

The climate is that of a cold desert receiving very little precipitation (SANAP, 1992). WDML receives between 55-81mm precipitation in the form of snowfall annually (Reijmer and van den Broeke, 2001). The mean annual air temperature for the SANAE IV area -16.4°C, the monthly average lowest temperature is -24°C and the average highest temperature is -14°C (Hansen *et al*., 2013). The mean annual air temperature at the Troll site is -14.3°C (Lee *et al*., 2012).

The six study sites investigated in this study will form part of the Permafrost Monitoring Borehole Network (Fig. 11, Pg 19). The following are descriptions of the six study sites in order of landscape feature abundance for the SANAE IV area, followed by the Troll area (Alberts, 1995):

1) **Flårjuven** (Old - S72°01'26.4", W3°22'47.6", alt. 1278m), (New - S72°01'01.7", W3°23'49.1", alt. 1380m): A flat-topped mountain approximately 44km to the south west of the SANAE IV base (Vesleskarvet). It is ideal for conducting research into active layer dynamics. The 60cm

borehole logger data has been recorded from January 2008 to January 2014. Furthermore, an additional 60cm borehole and 20cm borehole data have been recorded from January 2013 to January 2014.

2) **Slettfjell** (S72°08'14.2", W3°17'02.8", alt. 1472):

Located 53km south of SANAE IV, Slettfjell is the second furthest site in this study. Being similar to Flårjuven it has clearly visible sorted and non-sorted patterned ground. 60cm borehole and 20cm borehole data have been recorded from January 2013 to January 2014.

3) **Valterkulten** (S71°53'50.0", W3°13'36.3", alt. 1021):

Valterkulten is a small buttress shaped nunatak 28km south west of SANAE IV. A brine lake can be found near the top which offers exceptional potential for investigating geochemistry and chemical weathering (Marshall *et al*., 1995). Thermal contraction cracks and terrace formations have also been identified on the nunatak. 60cm borehole and 20cm borehole data have been recorded from January 2013 to January 2014.

4) **Robertskollen** (S71° 29' 28.6", W3° 14' 03.72", alt. 468):

Robertskollen lies approximately 25km North East of SANAE IV and boasts the best geomorphological research potential with its sorted and unsorted patterned ground and high biotic life. Special caution was be taken at this site due to it having potential of being labelled as a protected area as it has considerably more biotic factors in the forms of lichen, tafoni, fungi, algae, and Antarctic Snow Petrel colonies. 60cm borehole and 20cm borehole data have been recorded from January 2013 to January 2014.

5) **Vesleskarvet** (S71°40'12.7", W3°50'32.5", alt. 848):

SANAE IV base is situated on the flat topped Vesleskarvet which can be divided into the northern and southern buttress. SANAE IV is located on the southern buttress with the study area based on the northern buttress which is particularly good boasting excellent examples of sorted patterned ground in slight depressions. 60cm borehole data has been recorded from February 2009 to January 2014. 20cm borehole data have been recorded from January 2013 to January 2014. Furthermore, high frequency 60cm borehole data were recorded for 15 days in January 2013 and high frequency 20cm borehole data were recorded over the duration of two weeks in December 2013 and January 2014.

6) **Troll** (Old - S72°00'40.6", E2°32'00.2", alt. 1283), (New - S72°00'39.66", E2°31'28.8", alt. 1290):

Troll is the furthest study site from the SANAE IV base which lies 190 km across the Jutelstraumen glacier to the east and consists of different geology. The Troll surroundings have the most pronounced and abundant patterned ground formation out of all of the study sites and it is therefore an excellent site for the analysis of active layer activities. 2m borehole logger data has been recorded from February 2007 to January 2014. An additional 2m borehole data have been recorded from January 2013 to January 2014. Furthermore, two 20cm boreholes (one in the centre of a polygon and one in the contraction crack) have been recorded from January 2013 to January 2014. Additionally high frequency 20cm borehole data was recorded over the duration of two weeks in January 2014.

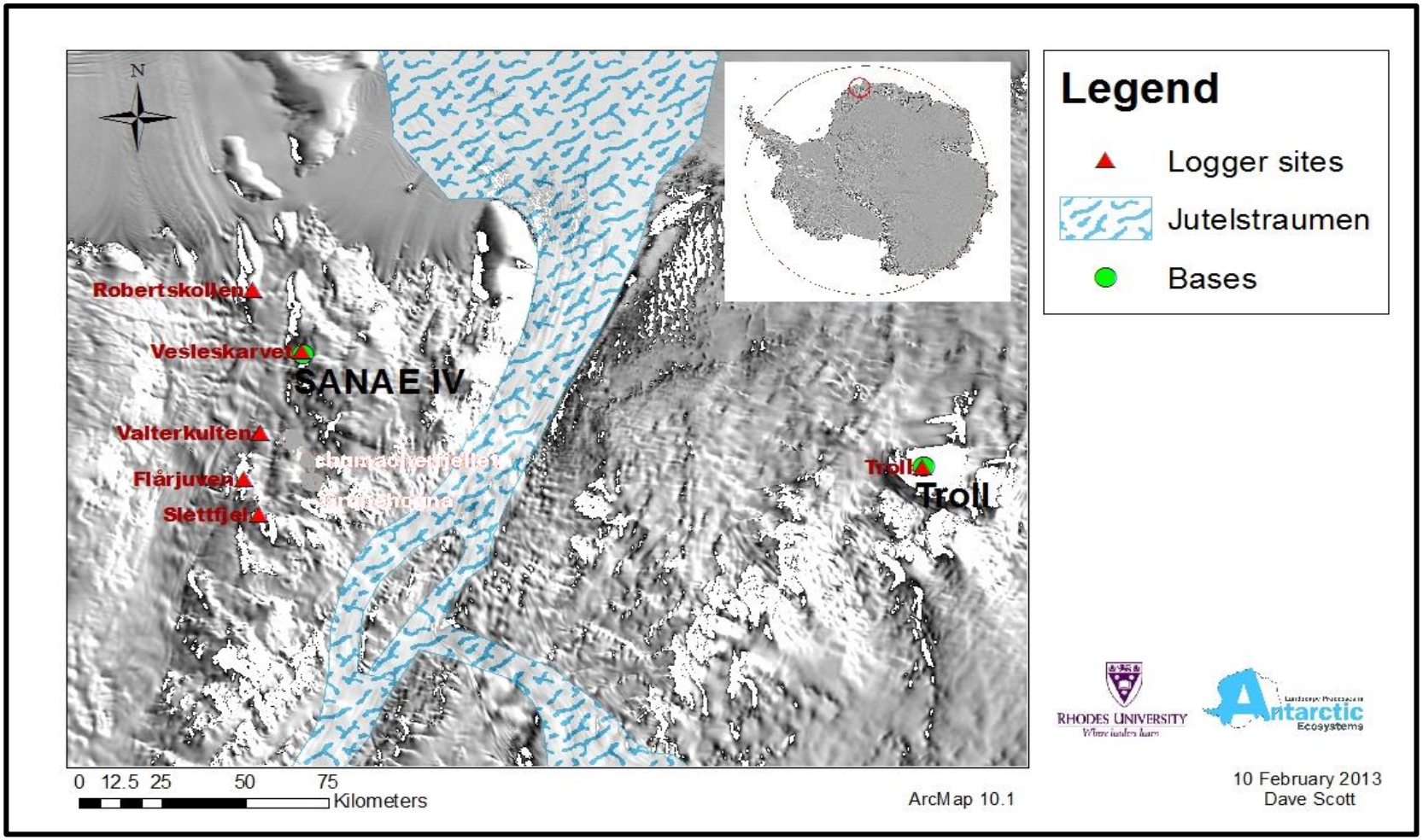

Figure 11: The six study sites in Western Dronning Maud Land, Antarctica. The South African base (SANAE IV) and the Norwegian base (Troll) are shown by the green dots. The areas around these two bases form two of the six study sites.

2.2. Research Question and Objectives

Bockheim (2002) strongly argues for the establishment of an observational network, as well as an interface, for monitoring sites in Antarctica, of the active layer. Along with the Circumpolar Active Layer Monitoring programme (CALM), Bockheim (2002) recommends certain protocol for measuring and describing the active layer. Landforms that result from processes within the active layer may contribute to our understanding of active layer/permafrost dynamics. Such processes provide insight into landform formation and development. Similarly, we may infer the presence of processes by investigating landforms that are known to develop within the active layer and permafrost from diurnal, seasonal, as well as annual variation. The current project aims to contribute towards these observational networks through establishing boreholes within Western Dronning Maud Land. An investigation into landforms that are resultant of active layer and permafrost dynamics will also be done. In order to achieve this, proxy data for these processes, in the form of ground thermal and moisture regimes, are used to identify processes. Furthermore, landforms are mapped using an UAV and these landforms are then linked to identify processes. Landforms that are investigated include thermal contraction crack polygons, terraces, steps, stripes, and sorted and non-sorted stones and sediments (self-organisation). The research question, aims and objectives are presented below.

2.2.1. Research Question

What are the environmental conditions, active layer processes and resultant landforms in Western Dronning Maud Land?

2.2.2. Objectives

To investigate and document environment conditions, processes and associated landforms on selected nunataks, the entire project was divided into six key objectives:

1. To determine air temperature, ground temperature and ground soil moisture variability and change at the six selected study sites;
2. To determine the depth of the active layer;
3. To develop an inventory of active layer and permafrost landforms;
4. To develop and utilise new technologies to document landforms;
5. To set up baseline data for future studies; and
6. To build Digital Elevation Models for the six different study sites.

CHAPTER 3: Data Requirements and Methods

This chapter details the methods employed and lists the instruments used in order to answer and address the objectives and overall aim of the project. The chapter is divided into the following sections:

1. Data requirements for the project (pg. 22).
2. Instruments used in the field are presented under Automatic Logging Stations (pg. 22).
3. Documenting and mapping landscape features on pg. 24 gives an overview of how landforms and features are mapped in the field.
4. Activities conducted and methods employed during fieldwork are detailed under Section 3.3 (pg. 24) through to Section 3.7 (pg. 34).
5. Laboratory methods used are presented under Sediment analysis (pg. 35).

3.1. Data Requirements

Geomorphology is in essence a holistic science and therefore it was important to follow all-inclusive processes (Sack and Orme, 2013). These include fieldwork, lab work, as well as analyses (statistical and imagery). Data in the form of images, temperature/moisture data, information on geology and lithology, climate data etc. was collected.

3.2. Automated Logging Stations

Between February 2007 and January 2014, a systematic investigation of permafrost landforms was initiated in Western Dronning Maud Land, study sites were identified in areas near the South African base, SANAE IV, and the Norwegian base, Troll. At each of these study sites a series of sensors were installed in order to measure the air temperature and ground temperature at a variety of depths. Pace XR5 logger/s and ACR logger/s in combination with Madgetech EC5 soil moisture sensors, were installed in order to achieve this. All loggers have been capturing data since their installation date, up to the latest collection in January 2014. Essentially there are two logger borehole types: deep boreholes to a depth of 60cm or 2m and shallow boreholes which measure the ground temperature to a depth of 20cm.

The loggers record the air and ground temperature, as well as ground moisture at hourly intervals. At the selected sites a borehole was dug and a rod with the attached sensors was let down into the hole. The terrain was then restored to its approximate initial state. Logging only commenced two weeks

after installation to allow for adjustment and settlement of the ground. Observations of ground temperatures were made at specific intervals to a depth of 20cm (1cm, 2.5cm, 5cm, 10cm, 15cm, and 20cm), 60cm (1cm, 15cm, 30cm, 45cm, and 60cm), 2m (1cm, 0.5m, 1m, 1.5m, and 2m), air temperature was logged at a height of 1.5m above the ground surface and soil moisture at 1cm below the ground surface (Fig. 12 and 13).

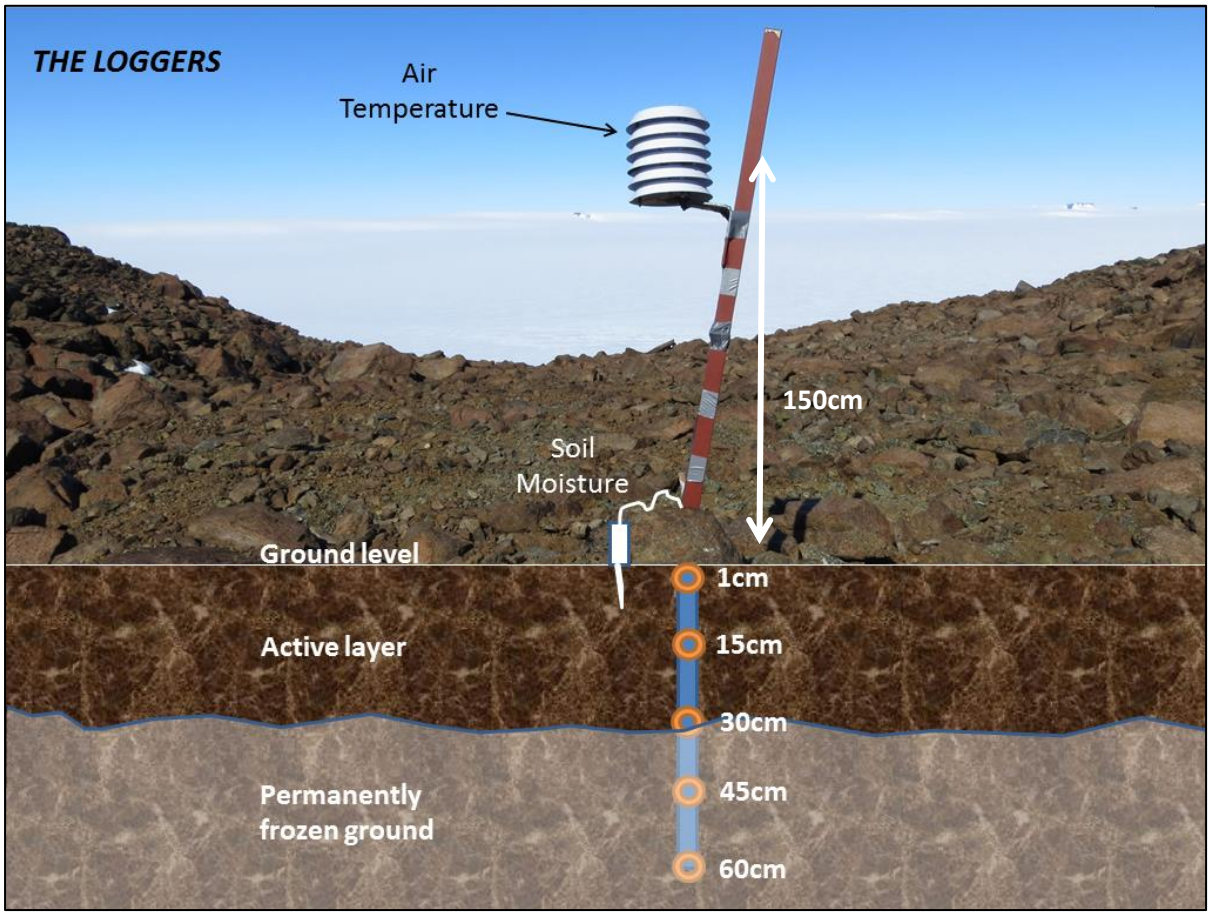

Figure 12: Diagram showing a deep logging station (XR5) with the thermal sensors indicated, their depths and positions in relation to their support.

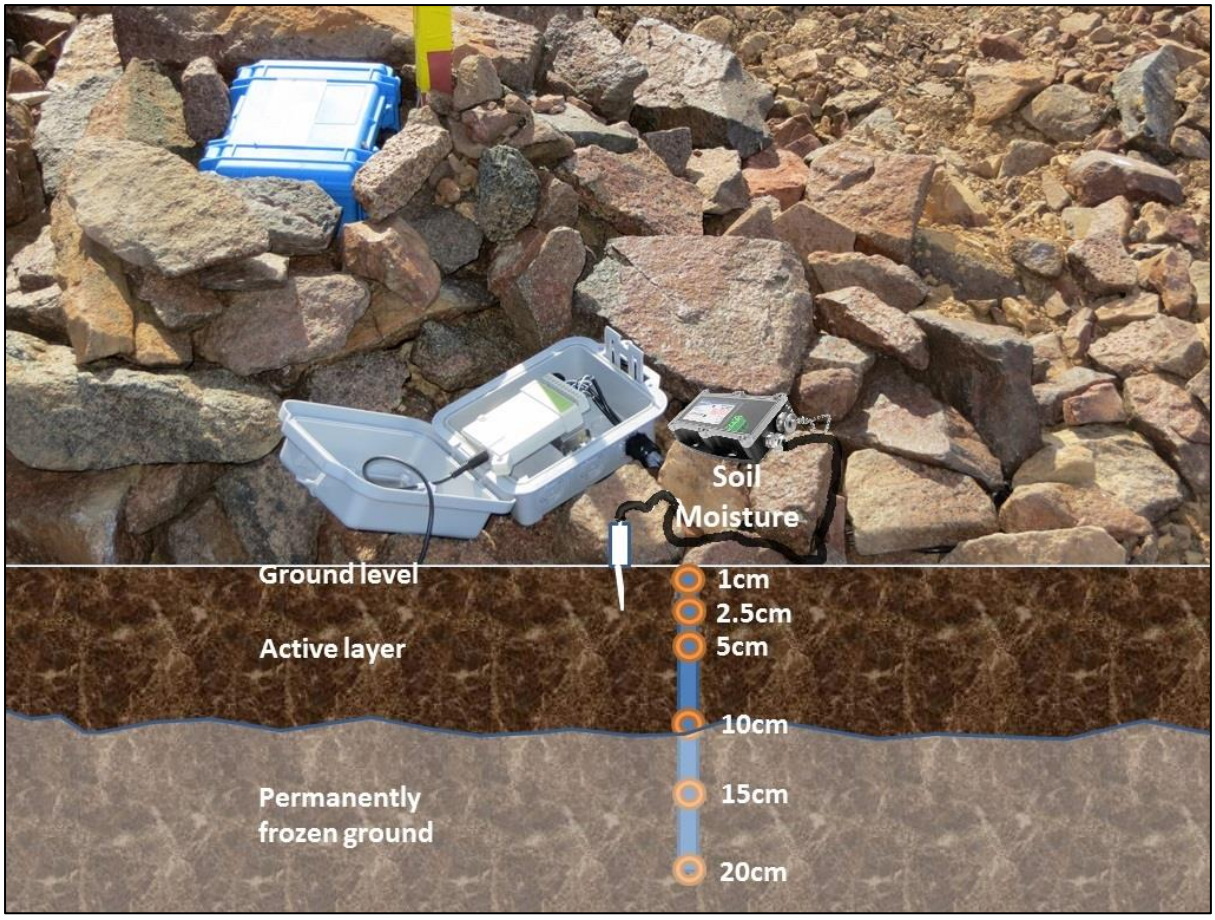

Figure 13: Diagram of a shallow logging station (ACR) with thermal sensors, their depths and the Madgetech EC5 soil moisture logger indicated.

3.3. Documenting and mapping landscape features

An inventory of periglacial landforms commenced in 2006 and was added to annually until January 2012 (Bockheim, 2005, Goodfellow *et al*., 2009, Guglielmin *et al*., 2005, Hall and André, 2006, Vieira et al., 2008, Vieira et al., 2010). All landforms and features identified during the duration of this study were added to this inventory. In addition, the mapping of polygons was undertaken using aerial photographs from an Unmanned Aerial Vehicle (UAV), a Garmin GPSmap 60CSx, a differential GPS, Google Earth Imagery, GeoEye imagery and GIS software. The use of a Spectra Precision® EPOCH® 35 differential GPS allows for precision accuracy and provides for the ability to return to a site and record change over time in centimetre accuracy. Handheld GPS's allow for the quick and easy navigation to landforms in the field and provide a general outline of investigated features. Aerial photographs and GeoEye imagery allows for the digital identification of landforms of interest using GIS. Aerial photographs were obtained from an UAV that was flown over the study sites during the 2013/14 Austral Summer. The GIS used the following datum and projection; WGS84 and Transverse Mercator-3 (TM-3) for SANAE IV study area and WGS84 and TM3 for the Troll study area.

3.4. Three-dimensional mapping of sites by structure from motion photography

UAVs, although having their birthplace in the military field are nowadays used for many non-lethal applications such as: real estate photography, mining, environmental management, farming and game management, whale watching, pest control, TV and filming industry, tracking wildlife etc. UAV photogrammetry opens various new opportunities for low-cost alternatives in comparison to the classical manned aerial photogrammetry (Remondino et al., 2011). However, they do come with certain limitations: reduced pay-load limits quality and quantity of on-board equipment, more images are needed for high quality results, limited flying time, and limited to low wind conditions (Remondino et al., 2011). Although these limitations could be an issue for some projects, the conventional UAV mounted with a simple point and shoot camera has an unarguable cost benefit result. Drones come in many shapes and sizes, however, for use in the Antarctic landscape it was decided that a hover drone would be best due to the rocky, variable gradient and size of landing sites. A hexacopter (six propeller copter) was built for this exact purpose which was able to be manipulated depending on the severity of the cold temperatures. Having an UAV which could hover made it possible to land in areas as small as 1m² which was often a necessity when having to land on steep rocky slopes in order to change battery packs. Landsat imagery is of a very low quality for the remote areas of Antarctica and therefore new high quality images were necessary and this is where the UAV fits in.

Agisoft PhotoScan®, modelling software, is used to convert the aerial photographs into 3D models. Agisoft PhotoScan® software is an advanced image-based 3D modelling software aimed at creating professional quality 3D content from still images (Agisoft PhotoScan® User Manual: Professional Edition, Version 1.0.0., 2013). Generally the final goal of photograph processing with PhotoScan® is to build a textured 3D model. Structure from Motion (SfM) is an advanced system through which topography/objects can be mapped and modelled in three-dimension (3D) and space. For the purpose of this project the multi-rotor UAV was used to take multiple images of the study site as it flew over with a 60% and 80% overlap on adjacent photographs. These images were used in Agisoft PhotoScan® software in order create 3D models, mosaicked images, and georeferenced outputs. Digital Elevation Models (DEMs) were created from the aerial images in order to gain a more in-depth understanding of the landscape and features.

Prior to flying of the sites four flags were positioned on the ground as far from one another as possible and accurate GPS coordinates taken for each of their positions. This allows for georeferencing images in the software at a later stage (Fig. 14). The flag positions were used in the software to illustrate four points which are common among multiple photographs and can be used to give those points x, y, and

z coordinates. Georeferencing brings the entire mosaicked 3D layer into real space with accurate elevation parameters.

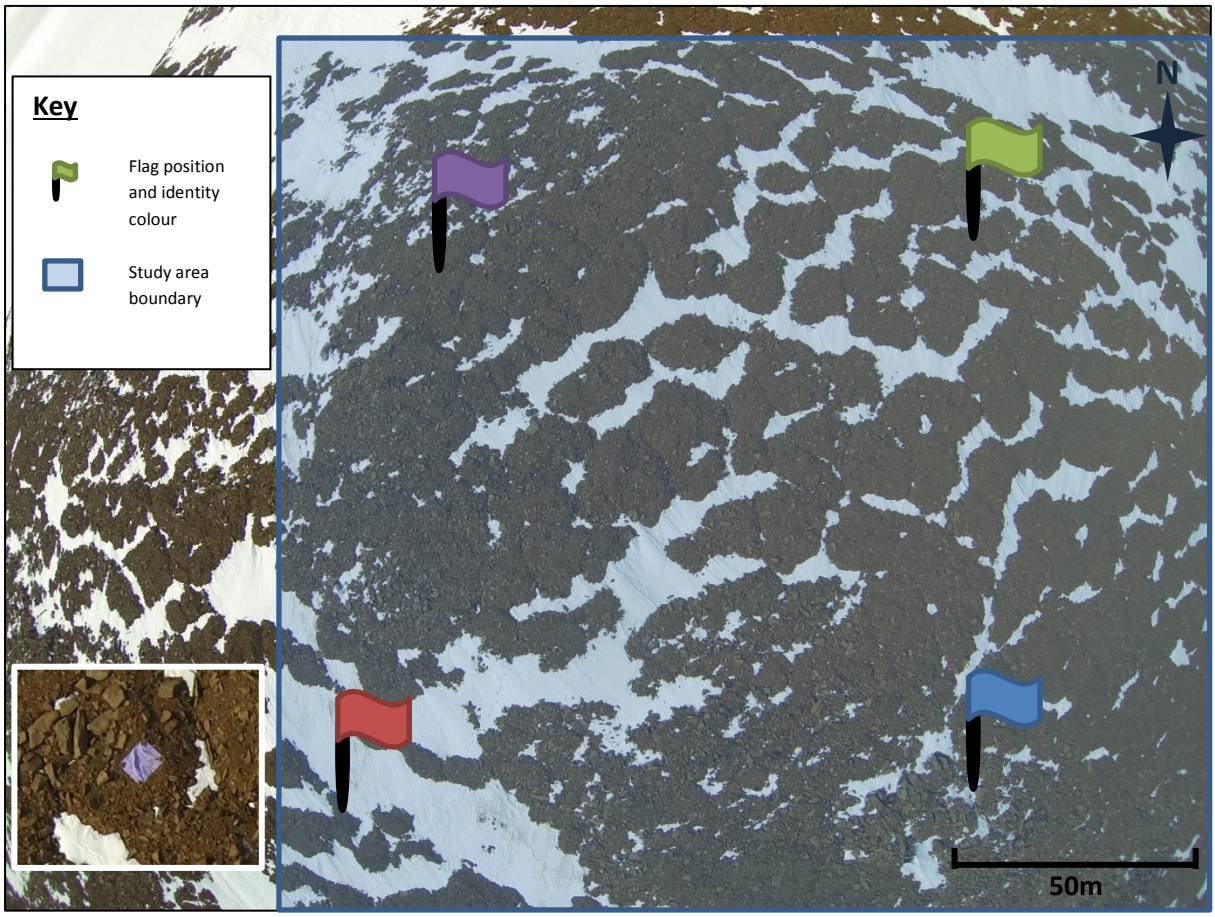

Figure 14: An example of flag positioning and marking techniques used for georeferencing images taken per study site.

A GoPro Hero 3 Black Edition camera was mounted to the UAV facing directly downward and set to a one-second time lapse interval (Fig. 15). The UAV was flown in a grid pattern and at reasonably low speeds in order to get at least 60-80% overlaps in every adjacent photo (Fig. 16, 17, 18, and 19). The altitude of flights was kept as constant as possible but varied according to site topography, size of study area, and quality of images required. Agisoft PhotoScan® software is an advanced image-based 3D modelling software aimed at creating professional quality 3D content from still images (Agisoft PhotoScan® User Manual: Professional Edition, Version 1.0.0., 2013). Generally the final goal of photograph processing with PhotoScan® is to build a textured 3D model. A comparison of the images from a GoPro Hero 3 camera to a DSLR camera will be done.

The procedure of photograph processing and 3D model construction comprises four main stages (Remondino *et al*., 2011):

1. Stage one is the camera alignment stage which entails searching for common points/features on the photographs and then matching them as well as determining the camera positions. This process is called automatic aerial triangulation (AAT) (Fig. 16).
2. Stage two is where the dense point cloud is made which is based on the estimated camera positions and pictures themselves.
3. PhotoScan® then builds a 3D polygonal mesh (Triangulated irregular network (TIN) model) from the point cloud which represents the object surface (Fig. 20).
4. The final stage is to add texture or generate an orthophoto.

Once the model is complete it is possible to export the data as an image (TIFF, JPEG, PNG), Google KMZ, or DEM file which can then be used in other software such as ArcMap for further analysis. For the purpose of this project the exported image was georeferenced in ArcMap in order to create polygons around the perimeter of the objects of interest (polygons, terraces, stripes, melt water). Graphs and statistics of the areas of the shapefiles were then created.

Figure 15: The UAV in action at the Troll study area, Antarctica. The UAV was flown at a maximum height of 50m above the ground level for this area (photos by Dwight, R).

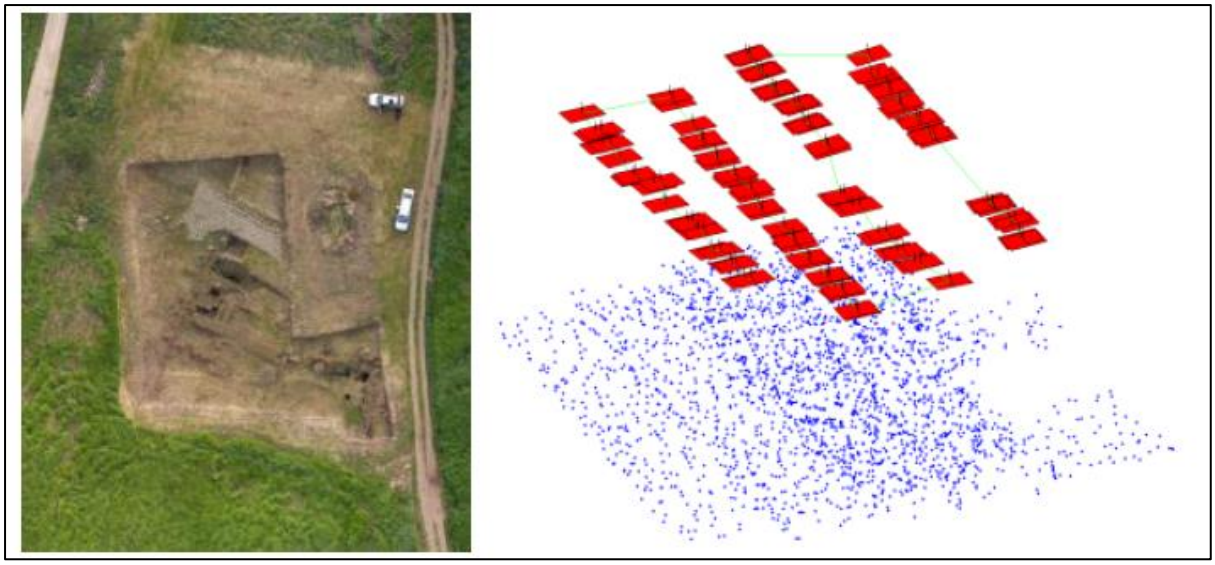

Figure 16: AAT results from a study done by Remondino *et al*. (2011) on an area of Veio, Italy (35m by 20m).

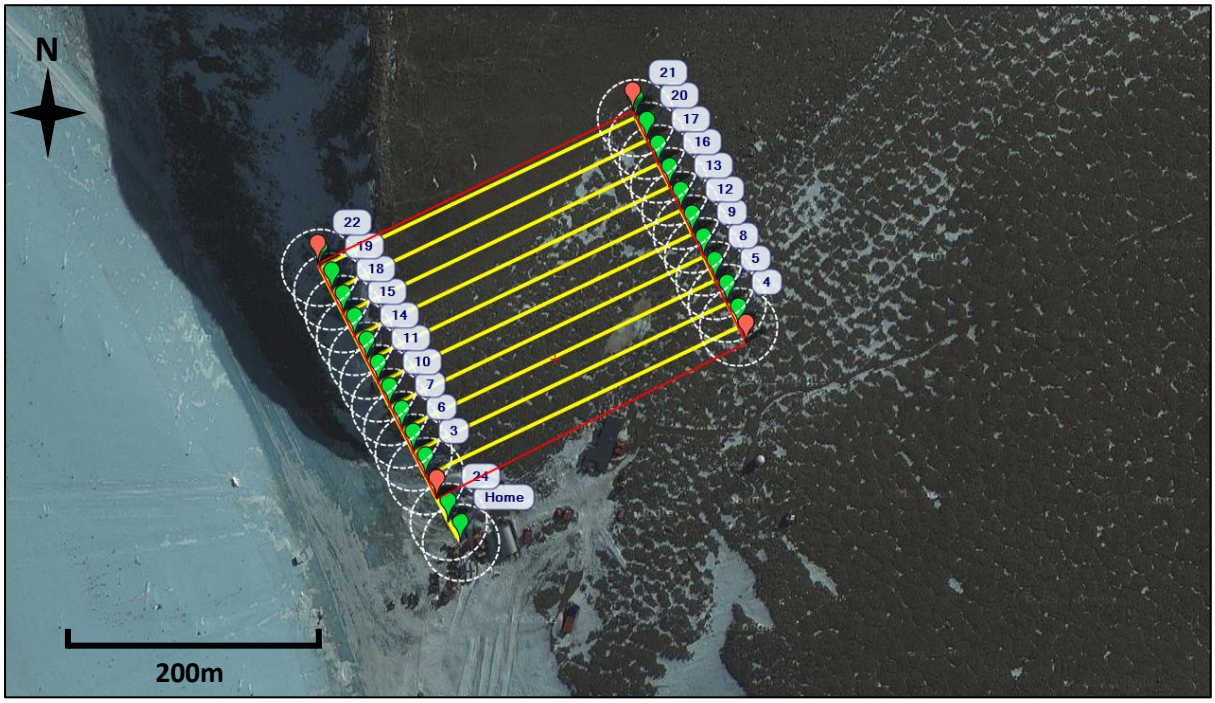

Figure 17: A computer generated grid pattern created to demonstrate the flight pattern of a UAV over one of the Troll study sites. Flight paths constitute a 60% overlap of images.

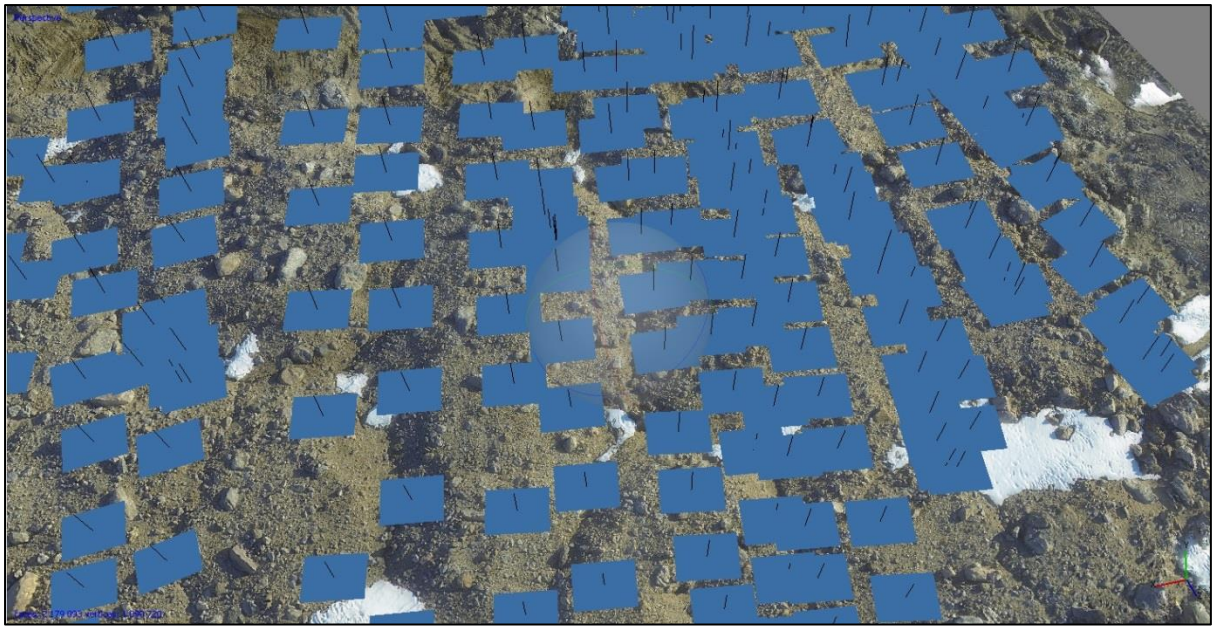

Figure 18: An example of a flight path grid pattern flown by the UAV over a polygon field at the Troll study site. Each blue rectangle presents the position and height at which a photograph was taken.

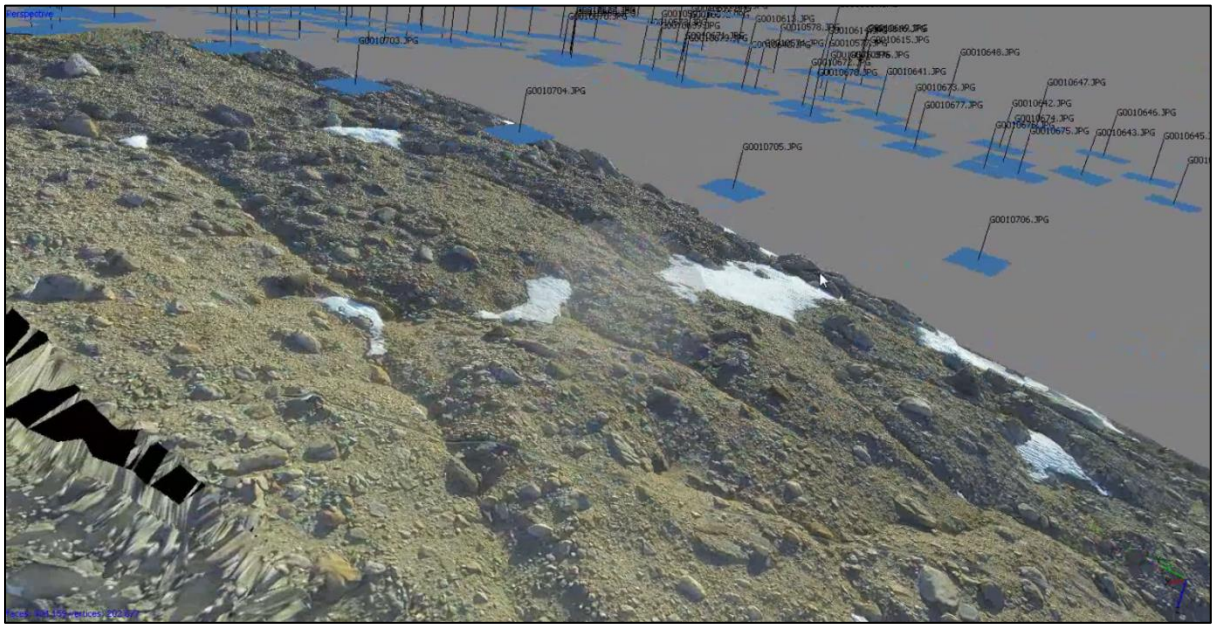

Figure 19: A 3D model example of the Troll study site created in Agisoft. Each photograph's position is illustrated by a blue rectangle and the photo identity labelled. Blue rectangles represent the position and height at which each photograph was taken. The black area shows the triangulated areas, which are missing aerial data.

The exported image was georeferenced in ArcMap in order to create polygons around the perimeter of the objects of interest (polygons, terraces, stripes, melt water *etc.*).

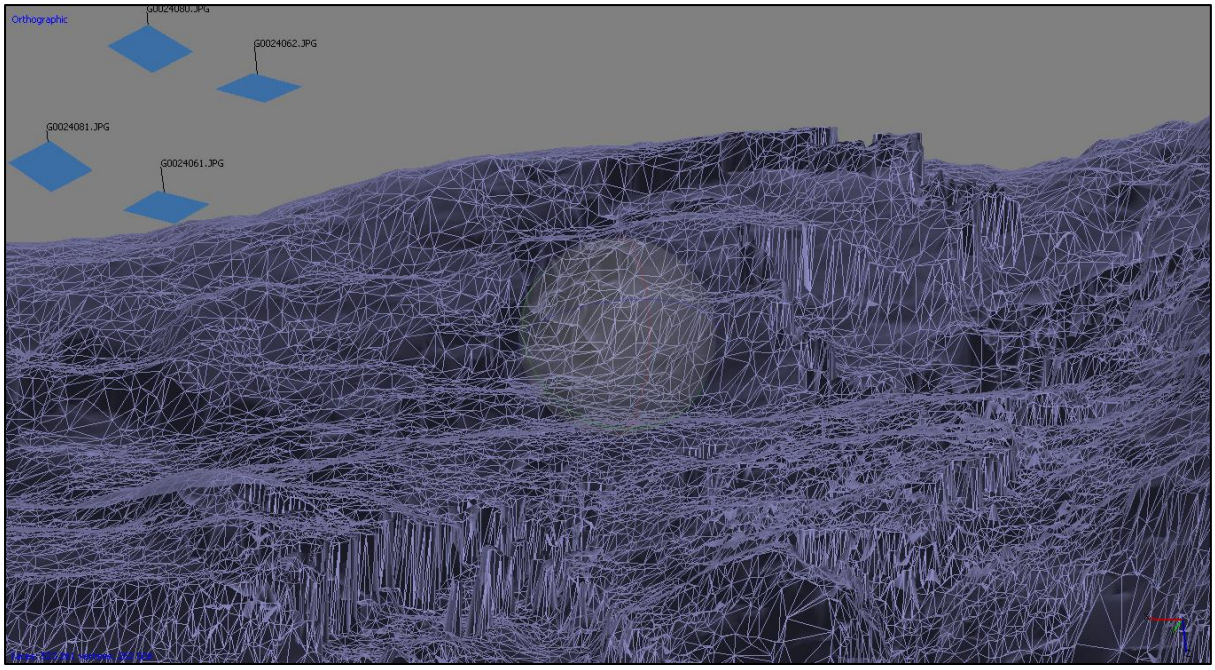

Figure 20: PhotoScan® builds a 3D polygonal mesh from the point cloud which represents the object surface.

3.5. Polygon sampling

The process of polygon sampling involved taking a variety of measurements, readings and samples from the randomly selected polygon positions within a polygon field, which were navigated to by a handheld GPS. A number of polygon morphological characteristics were taken in order to gain insight into polygonal movement across a slope, their size, and development. Instruments used in the field include a Garmin GPSmap 60CSx, 5m and 50m measuring tapes, a magnetic compass, and a clinometer. Moisture content is determined comparing the dry weight of soil samples to their field weight. The following data was collected, from each polygon (Fig. 21):

- The perimeter was measured using a measuring tape and recorded in meters (m);
- The longest axis was measured (a-axis; m);
- The second longest axis perpendicular to the longest axis was measured (b-axis; m);
- The gradient of the slope (degrees) was recorded with a Silva clino master clinometer;
- The orientation of the slope (magnetic, degrees) was recorded with a Brunton Transit compass;
- The orientation of the longest axis was measured (magnetic, degrees) if it varied to the slope orientation;
- Soil moisture readings at the centre and crack of polygon were taken with a Fieldscout TDR300 soil moisture reader. The crack reading was taken at the furthest downslope extent of the crack;

- Soil samples were taken with a customised container for the centre and crack of polygon (where possible). The crack sample was taken at the furthest downslope extent of the crack;
- Snow cover in centre/crack was noted; and
- Notes were taken on any other additional information.

The collected data were then used to find similarities and strengthen the DEM models of the polygon formations. They were studied in order to look for commonalities in longest axes, orientations, diameter, size and any other features.

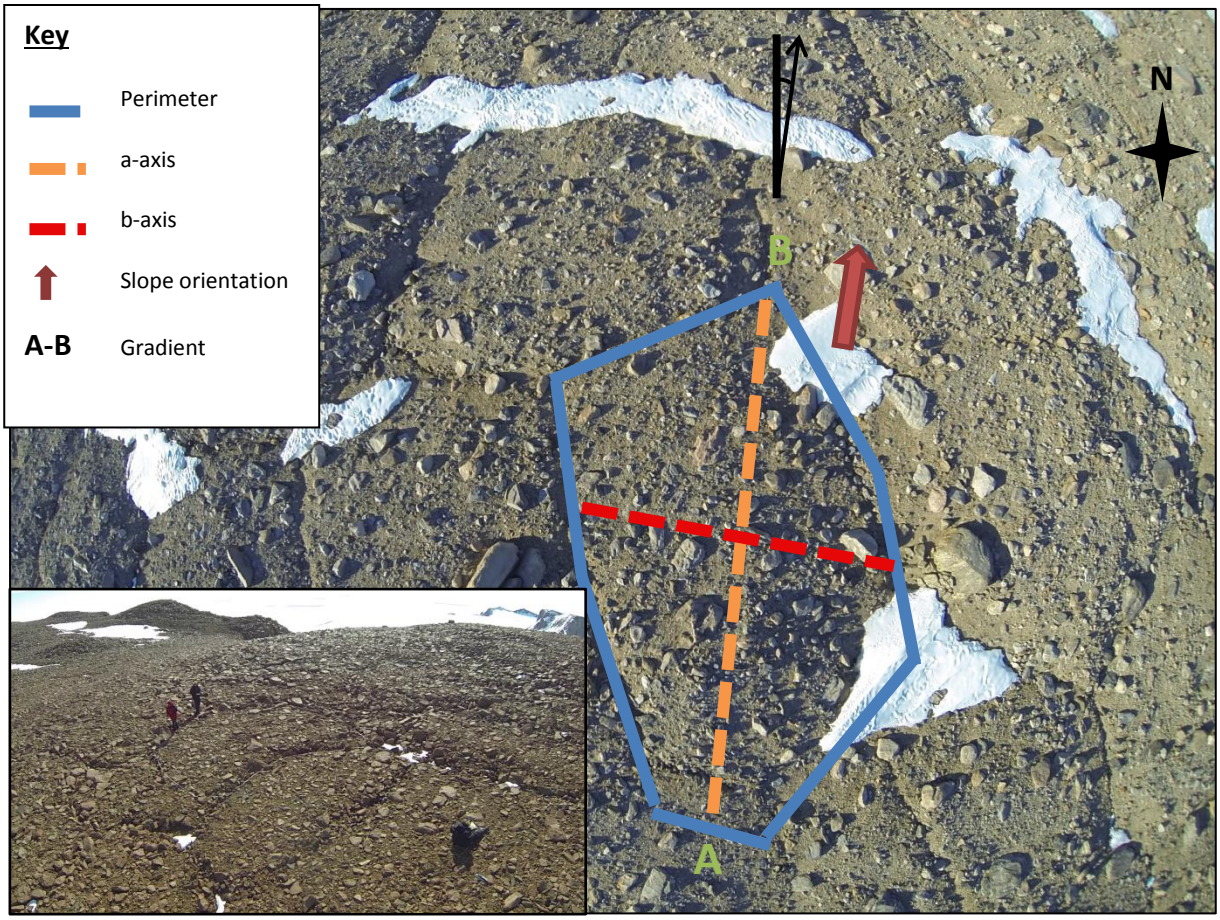

Figure 21: A diagram detailing sampling methods for polygons in the field. Note the people for scale in the inset.

3.6. Terrace transects sampling

The process of terrace sampling involved taking soil samples and GPS coordinates at the bottom and middle of every terrace feature on a transect line directly up the slope of a hill (Fig. 22). Instruments used included a Garmin GPSmap 60CSx, a customised soil container was used to determine bulk density, and a Spectra Precision® EPOCH® 35 differential GPS. The DGPS was used to take approximately 100 random points on the slope in order to build a DEM of the study site and get a precise understanding of the gradient and topography of the study site. Statistics on average area, slope, and long axis were calculated.

Figure 22: A typical terrace transect at the Valterkulten study site. The blue dots illustrate the sample points at the bottom of the terraces and the red dots illustrate the sample points at the top centre of the terraces. It must be noted that terraces are difficult to sample in this area due to their irregularity. As such, 3D modelling is used to strengthen the positional accuracy and topographical data collected for this study site.

3.7. Slope movement

Site experiments were set up at Grunehogna, Schumacherfjellet, and Valterkulten to investigate the movement of rock down slopes. In order to achieve this, transects were created: Five ten meter long transects (each containing 20 rocks in varying sizes) (Fig. 23) were measured out at a distance of 10 meters apart up the slopes (Fig. 24). The rocks were marked and a differential GPS was used to log the coordinates of each rock. Further points (50-100) were recorded around the site in order to get an accurate idea of the gradient and topography. The precise positions will be recorded each Austral Summer and movement, if any, will be mapped. This provides insight into the movement of clasts downslope. It is recommended that coloured metal plates with a point indentation are glued to the rock surfaces in order to make this a long term experiment.

Figure 23: A transect line containing 20 clearly marked rocks. This transect is located at the Grunehogna study site.

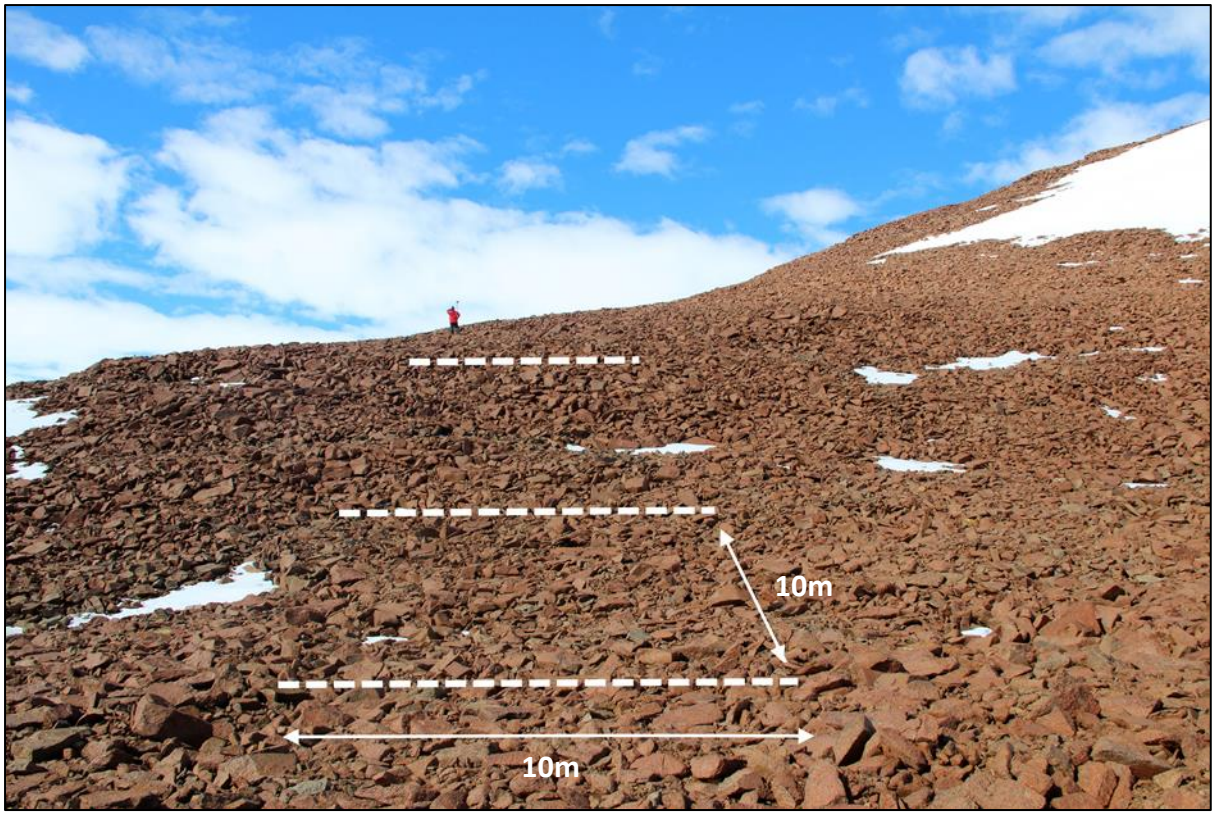

Figure 24: Three transects located parallel upslope at Flårjuven. Each transect is 10m across and located 10m from the next parallel transect.

3.8. Sediment analyses

Sediments were analysed to determine the level of weathering processes active within a specific region, as sediment is a product of weathering (Briggs, 1977a). Weathering is the physical and chemical alteration of rock at the Earth's surface and this occurs in Antarctica only once deglaciation has exposed the rock to the elements of nature (Birkeland, 1984; Gislason *et al*., 2009). Climate is considered as one of the most important factors influencing weathering processes, and moisture and temperature are the controlling factors of soil properties (Birkeland, 1984; Gislason *et al*., 2009). Mechanical weathering is the process related to stresses and fracturing of the rock, whereas chemical weathering occurs due to the non-equilibrium state of near-surface waters, temperatures and pressures (Gislason *et al*., 2009). The process of weathering and, depending on what stage of weathering the material is at, causes the production of clay and silts. Therefore the longer the site has been exposed to weathering processes, the greater this clay proportion is expected to be (Gislason *et al*., 2009). Furthermore, the slope orientation and topography can result in micro-climatic conditions for weathering processes (Gislason *et al*., 2009). Sediment and textural analyses can, therefore, provide insight into the weathering processes a surface has undergone. The greater the proportion of clay in the fine earth fraction, the greater the expected force and duration of certain weathering processes may be.

Sediment particles are conventionally graded into categories and arranged in an ordinal scale. The categories are in increasing order of size and shown in Table 1 below. There is no international agreement on these sizes. However, the Soil Survey of England and Wales will be used for this project.

Table 1: Table depicting particle sizes and classification according to Briggs (1977b).

Category	Size (mm)
Clay	<0.002
Silt	0.002-0.06
Sand	0.06-0.6
Gravel	2-60
Cobble	>60

A sieve analysis (gradation test) is a procedure used to assess the particle size distribution (gradation) of a granular material (Briggs, 1977a). A sieve analysis can be performed on any type of non-organic or organic granular materials including sands, crushed rock, clays, granite, feldspars, coal and soil. Its ease of use and simplicity make this the most common method for determining textural analyses. For each of the samples: the weight before, dry weight, bowl weight and net weight were recorded and then total water loss was calculated. A Labcon forced-circulation oven was used to dry the samples for 24 hours at 60ºC (Fig. 25) (Briggs, 1977b). Once dried the samples were then disaggregated with a mortar and pestle and sieved in a sieve stack (Fig. 26) for ten minutes (Briggs, 1977b). The sediment in each sieve was weighed to determine the dry mass proportion of sediment within each size class. The bottom dish tray contained the fine earth fraction. This fraction, containing clay particles, underwent proportional analyses in a Malvern Mastersizer 3000. The Mastersizer is based on Stokes' Law presented in Equation 1. Stokes' Law states that the velocity of a particle falling under its own weight in a viscous medium (such as water) is directly proportional to the diameter of the particle: the heavier the particle, the faster it falls (Briggs, 1977a; 1977b).

Equation 1: Stokes' Law. D = size of the particle; ν = terminal velocity of the particle; η = viscosity of the liquid; ρ = density of the particle material; ρ0 = density of the liquid; g = gravity (Briggs, 1977a).

$$D^2 = \frac{18\nu\eta}{(\rho-\rho 0)\, g}$$

Figure 25: The Labcon forced air circulation oven. Samples are dried at 60^{o}C for 24 hours.

Figure 26: The Endecott test sieve shaker. Each sample is sieved for 10 minutes. Sieve mesh sizes include <63µm, 63µm, 125µm, 250µm, 500µm, 1000µm, 2000µm, 4000µm, 8000µm.

CHAPTER 4: Results

In this section the results for each of the sites are presented. The topographical analysis is presented and landscape features are displayed and all posible models are presented. The temperature, moisture and zero-degree isotherm depth graphs are then presented and briefly discussed. The results will be compared and interpretted further in the next chapter.

Topographical Analysis

An Unmanned Aerial Vehicle (UAV) was used to fly over the areas of interest in order to obtain aerial images for the study sites for use in Structure from Motion. Structure from Motion (SfM) is an advanced system through which topography/objects can be mapped and modelled in three-dimensional (3D) space and therefore visually representing morphological features of interest in the landscape. The UAV was flown over the study sites in order to take 200 to 800 aerial photographs per site (size dependant). Agisoft PhotoScan® software was used to georeference, overlay and mosaic the images together in order to create 3D models of the study areas. Furthermore, Digital Elevation Models (DEMs) were created to gain an understanding of the topography of the landscape and features. The mosaicked images were imported into ArcMap and ArcScene for further analysis which allowed for delineating the landscape features. Taking measurements in the field in such extreme environments can be challenging and field work can be limited by weather conditions and time. Post fieldwork desktop analysis has proven to be an exceptional advancement in this study.

Thermal Environments - Depth, temperature and moisture graphs

In order to identify the trends in the maximum, minimum and zero-degree isotherm (freeze/thaw) depth of the logger sites, a depth graph is used. Permafrost is defined as ground which has been below 0°C for two or more years (van Everdingen, 2005). Therefore, the zero-degree isotherm will be used as the artificial observation point in this study. Pressure and chemical concentrations affect the freezing point of water from 0°C to below -2.5°C (van Everdingen, 2005). As previously mentioned there are different borehole depths, therefore several depth profile graphs will be presented. In each of the graphs the minimum and maximums for each depth per year of available data is presented by a single line and the zero-degree isotherm depth is shown by a short horizontal solid red line. Incomplete data sets were excluded from the graphs. A comparison of zero-degree isotherm depth for a year can be directly abstracted from a single graph; however, comparisons across sites must be done via several graphs. Finally, in order to compare the difference in sites, the summer data from 16 December 2013 to 25 January 2014 was used for all the sites in order to get an effective comparison. The 20cm borehole loggers were installed in 2013 and therefore for all the sites we have data for the

top 20cm of the ground (1cm, 2.5cm, 5cm, 10cm, 15cm, and 20cm). Air temperature data from the 60cm borehole logger was used for air temperature and the data from the Madgetech EC5 sensors was used for soil moisture as the ACR loggers do not have these sensors.

4.1. Flårjuven

Flårjuven contains two areas of interest for this study. Site 1 has a borehole dating back to 2008 but this area is small and isolated, and therefore cannot represent the entire nunatak. The second borehole site was setup in a more represented area for the site. Furthermore, the second borehole data is more representable of the landscape feature environments.

4.1.1. Topographical Analysis

Three perspectives are presented of the Flårjuven study area taken after the 3D model was created from the aerial images (Fig. 27). The modelling software allows for a complete 3D viewer interface similar to that of Google Earth. It was possible to identify many features in the 3D view which could not be obtained from the 2D mosaicked image alone or even from fieldwork data.

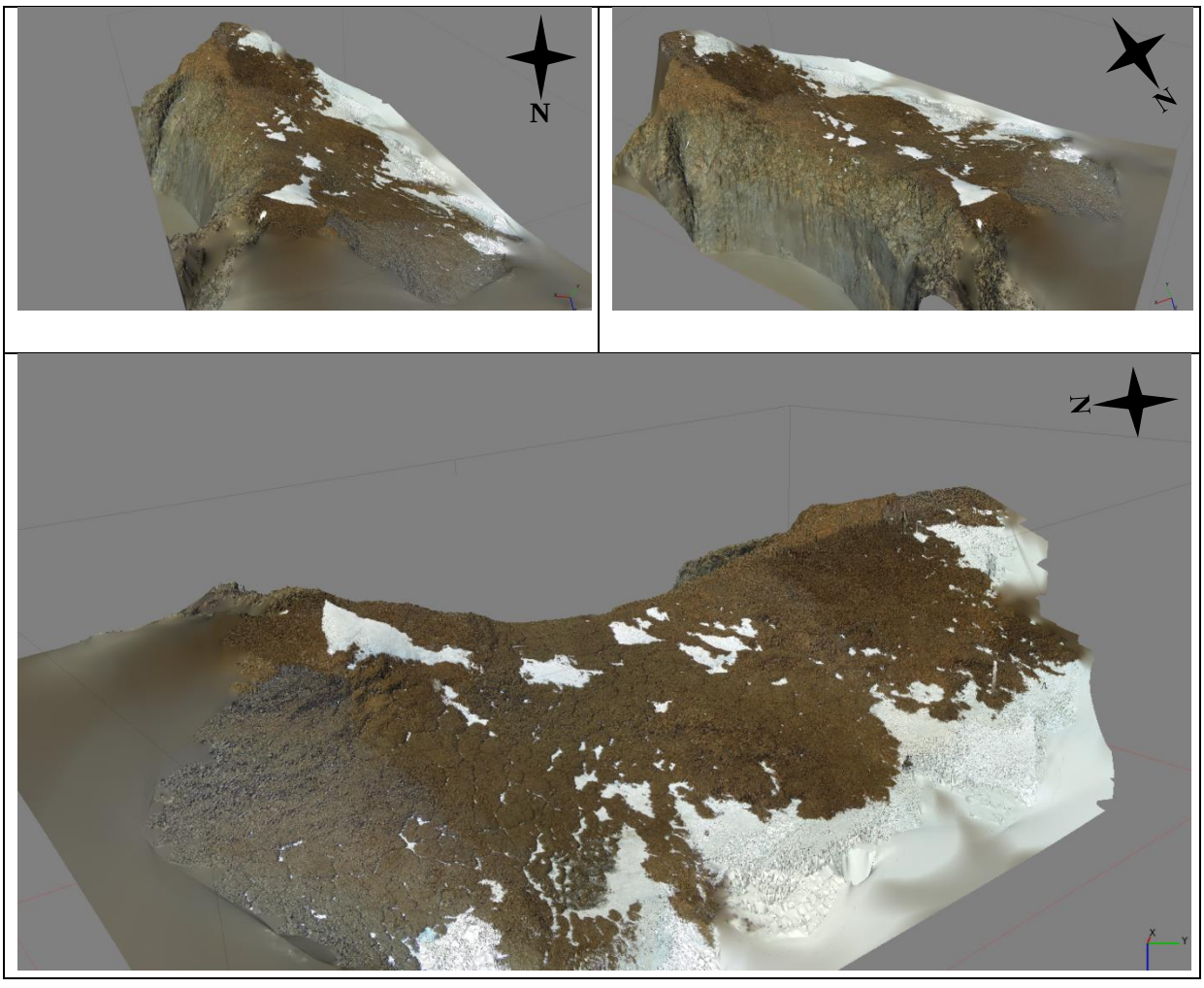

Figure 27: Model representation of the Flårjuven study site showing the topographic area of interest from three perspectives.

The terraces were the most difficult landform to differentiate as their borders are not well defined and therefore it must be noted that the delineated areas are not exact. The polygon formations are easy to delineate as there is direct shading noticeable where the larger rocks form which defines the perimeter. A visual for the area of Flårjuven can be seen in Figure 28 which contains polygon features. A total of 31 polygons were digitised, five of which were sampled in the field (green dots). Measurements of only the clearest polygons and terraces were taken for comparison across sites. The graduated colours represent the area of the polygons (m²) with yellow representing a small area and red representing large polygons. Statistics were calculated for these polygon areas (Fig. 30). The Flårjuven terrace features are displayed in Figure 29 and give a visual for the area. A total of 7 terraces were digitised, all of which were sampled in the field. Statistics were calculated for these terrace areas (Fig. 31).

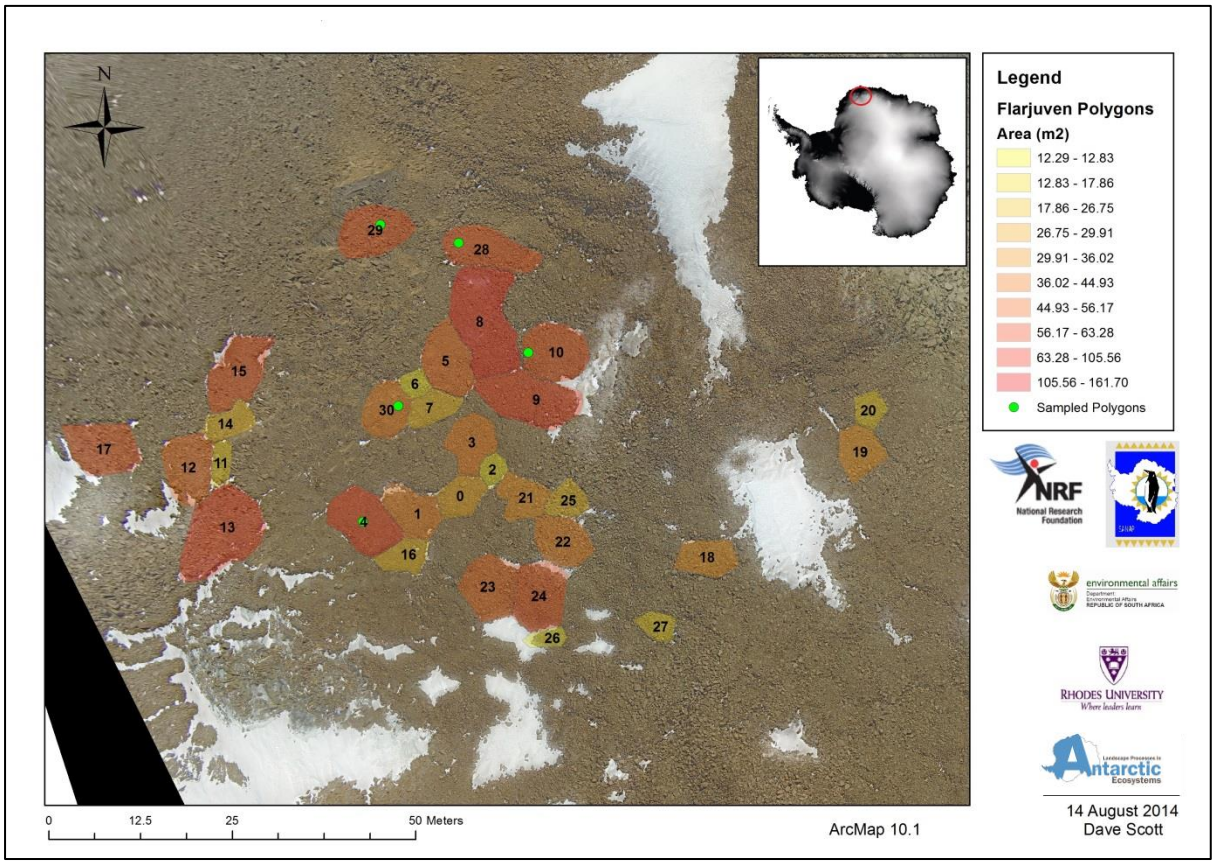

Figure 28: Map showing delineated polygons done in post fieldwork desktop analysis. Green dots show the five polygons which were measured on site. The graduated colours represent area of polygons (m²) with yellow showing small area and red representing large polygons.

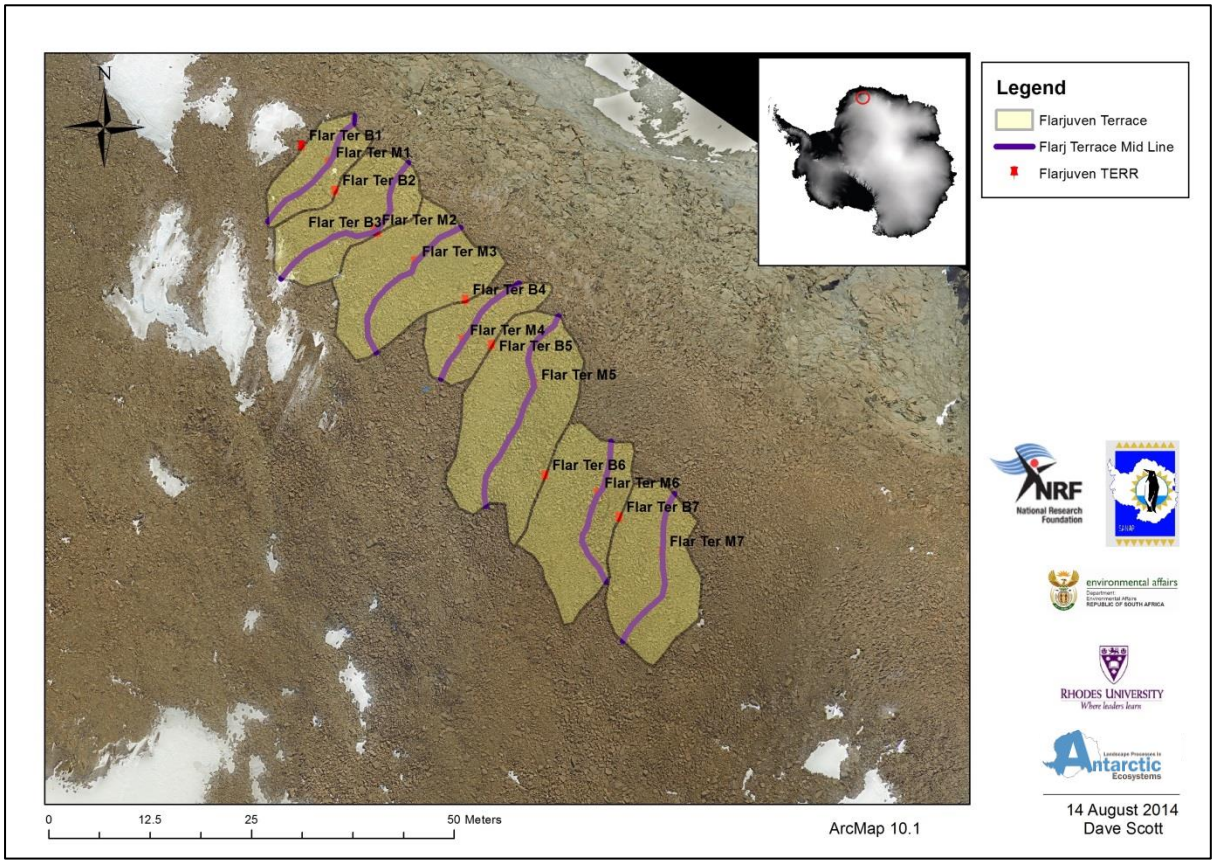

Figure 29: Map showing delineated terrace formations done in post fieldwork desktop analysis. The purple line represents the estimated centre line (flat section).

The polygon sample size was 31 with a minimum area of 12.9m², a maximum of 109.26m² and a mean area of 44.68m² (Fig. 30). The terrace sample size was seven with a minimum area of 90.92m², a maximum of 293.18m² and a mean area of 183.28m² (Fig. 31). The statistics show that there is much variation in the size of the landscape features found on the Flårjuven study site and become the baseline for change over time.

Field analysis and samples were taken on five randomly chosen polygons which were also delineated in post fieldwork analysis shown by the green dots in Figure 28. In order to check to accuracy of the Structure from Motion photography a direct comparison of the perimeter is presented in Table 2 which shows results with deviation of 0.45m² up to 3.6m². The deviation can be accounted to software modelling issues and/or user delineation error. The statistical relevance has shown that these methods can be used in future studies. The results of the other sites will be compared further in this section.

Flårjuven Polygon Area (m²) Statistics

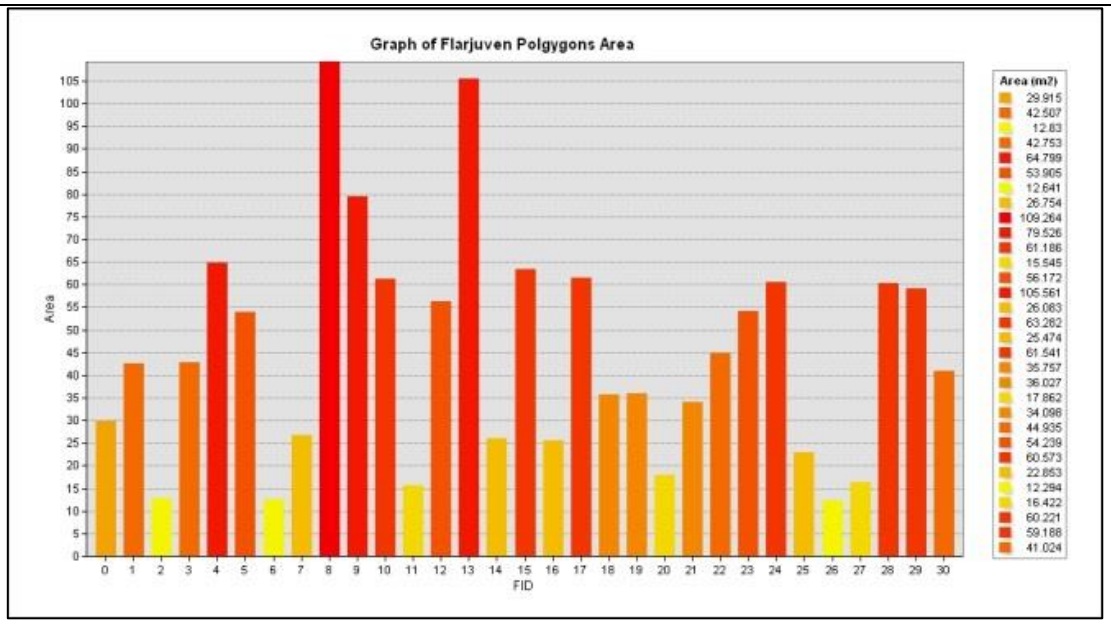

Count:	**31**
Minimum:	12.29
Maximum:	109.26
Sum:	1385.23
Mean:	44.68
Standard Deviation:	24.68

Figure 30: Graph and statistics of the Flårjuven polygon areas determined on ArcMap from aerial photographs.

Flårjuven Terrace Area (m²) Statistics

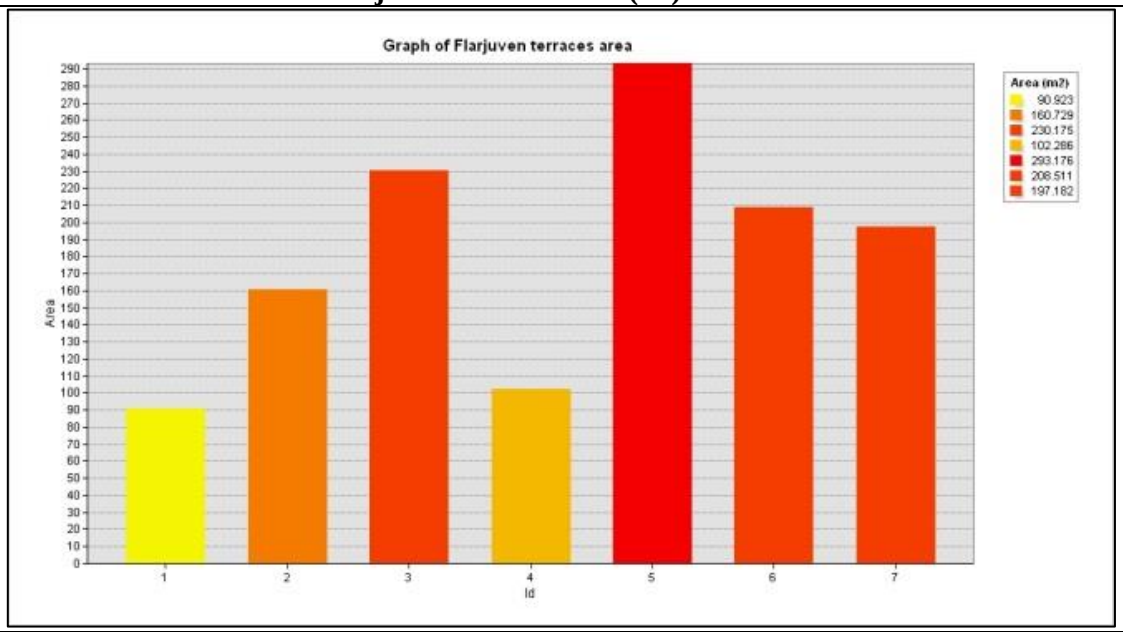

Count:	**7**
Minimum:	90.92
Maximum:	293.18
Sum:	1282.98
Mean:	183.28
Standard Deviation:	66.23

Figure 31: Graph and statistics of the Flårjuven terrace areas determined on ArcMap from aerial photographs.

Table 2: Comparative perimeter results of model data to field data.

	MODEL DATA	FIELD DATA
ID	Perimeter (m^2)	Perimeter (m^2)
1	31.3	32.55
2	23.8	20.2
3	28.5	25.4
4	33.3	34.4
5	29.2	29.65

Agisoft PhotoScan® allows for the output of DEMs which can be imported into GIS software for further interpretation. The DEM and contour map for the Flårjuven study site with the polygons and terraces displayed in graduated colours based on size is shown in Figure 32 and 33. On the eastern side of the site there is a cliff line with an altitude change of around 100m. Moving from South to North the gradient flattens out towards the middle of the site and then slowly increases once again towards the North. The polygon formations are found on the flattened area of land whereas the terrace formations can be seen on the southern 27^0 gradient.

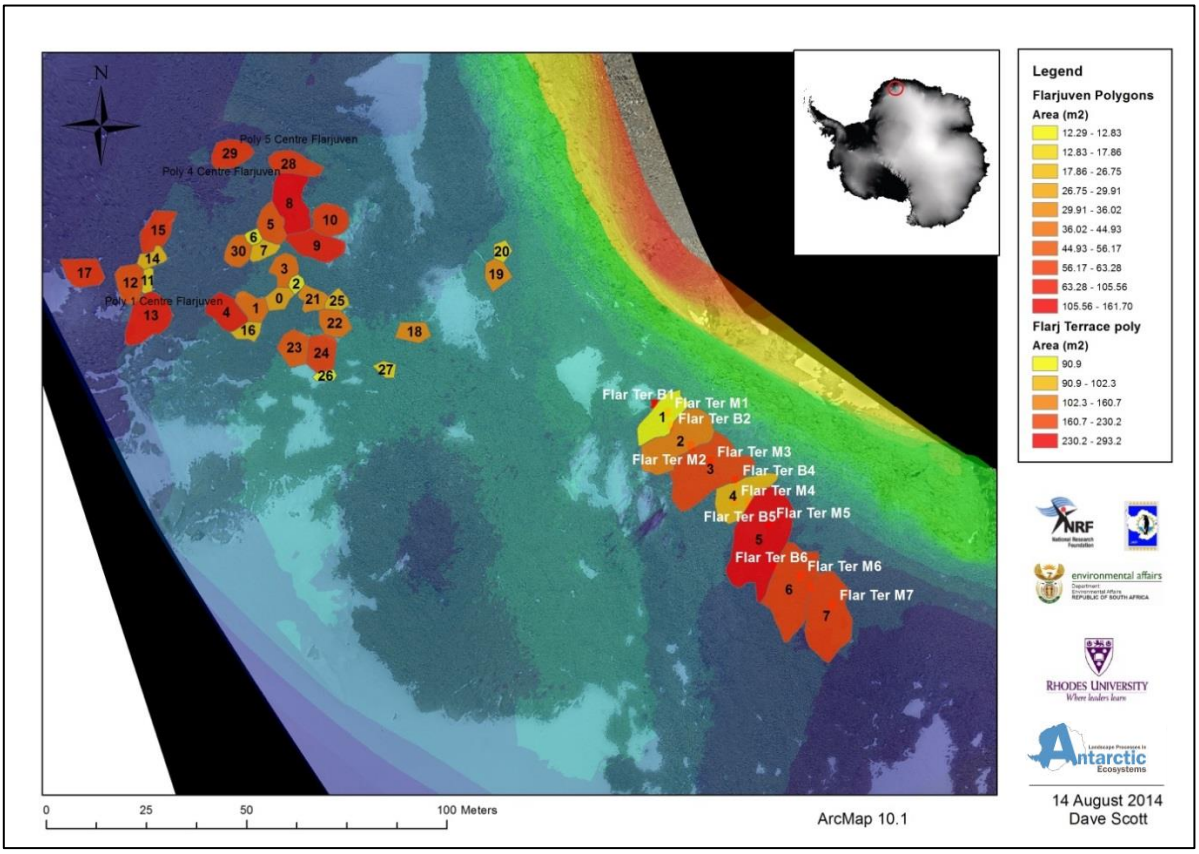

Figure 32: Polygons overlain on a DEM of the Flårjuven study site.

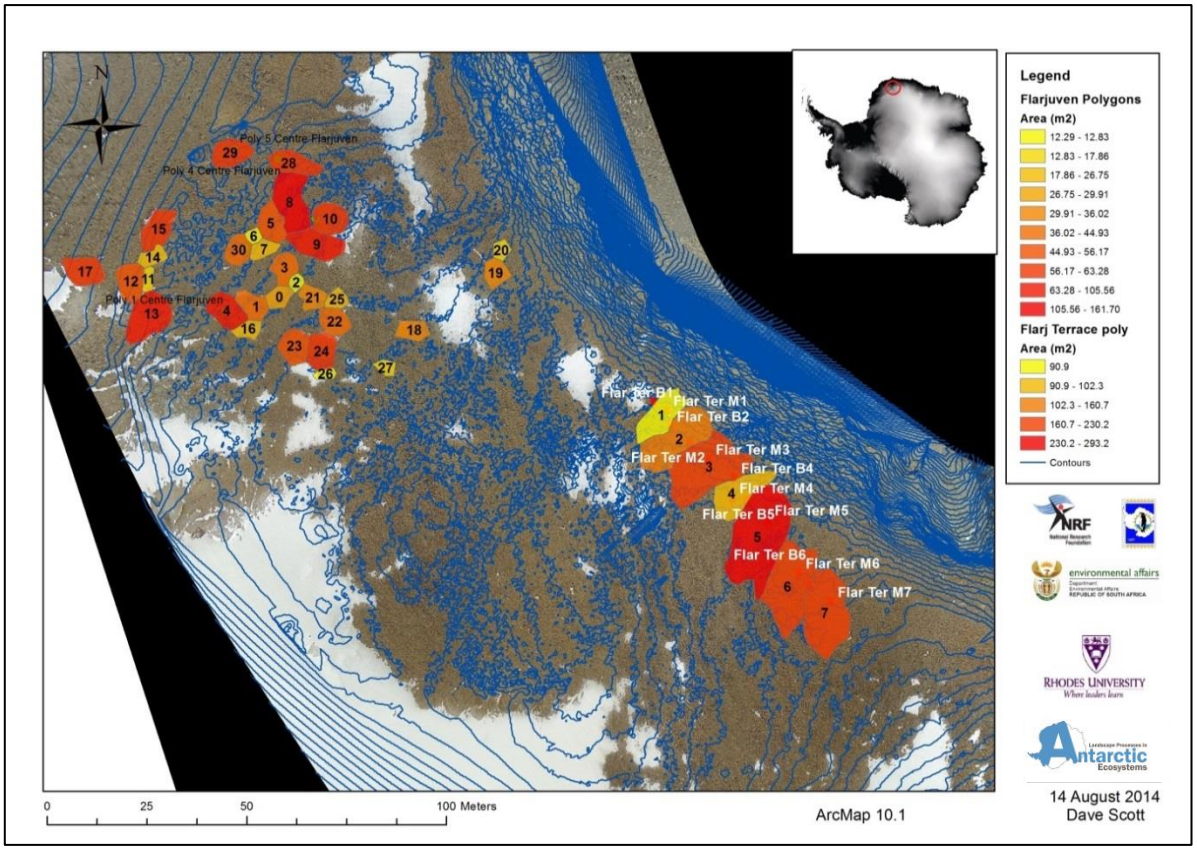

Figure 33: Contour map of the Flårjuven study site.

4.1.2. Ground Thermal Analysis

4.1.2.1. Flårjuven Site 1 (1st logger site)

4.1.2.1.1. 60cm borehole results

The winter and summer months' maximum and minimum recorded temperatures can be seen in Figure 34. The maximum summer air temperature was in 2009 at 2.3°C which was followed by the coldest winter in 2010 reaching a low of -41.38°C. The coldest ground surface temperature was in the winter of 2010 at -40.9°C and the maximum was the summer of 2012 at 18.22°C.

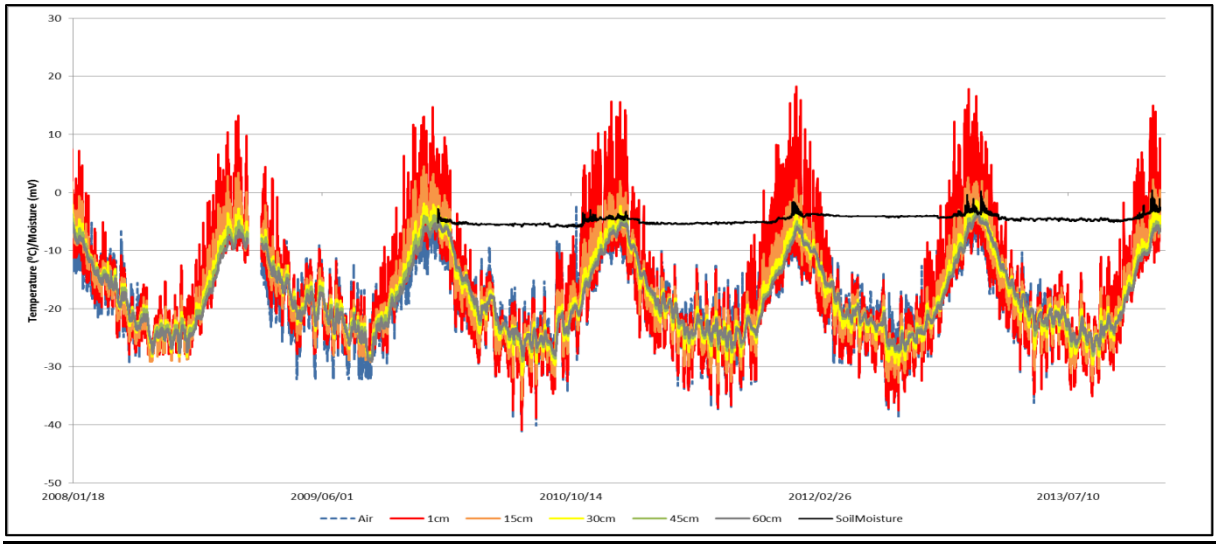

Figure 34: Borehole (60cm) data for the Flårjuven site from January 2008 to January 2014.

A summer period from 16th December 2013 to 9th January 2014 allows for a detailed view of the data (Fig. 35). Specifically, the soil moisture extent (black line) shows that after experiencing a few freeze/thaw cycles the moisture levels began to follow the trend of the 1cm and 15cm high peaks which indicates the direct relation of freeze/thaw cycle to accelerated moisture levels. On the 5th of January 2014 there was a snow fall event (insulating affect) which can be seen on the graph as moisture levels smooth out and then peaks once again toward the end as the freeze/thaw cycles fall into play after the storm.

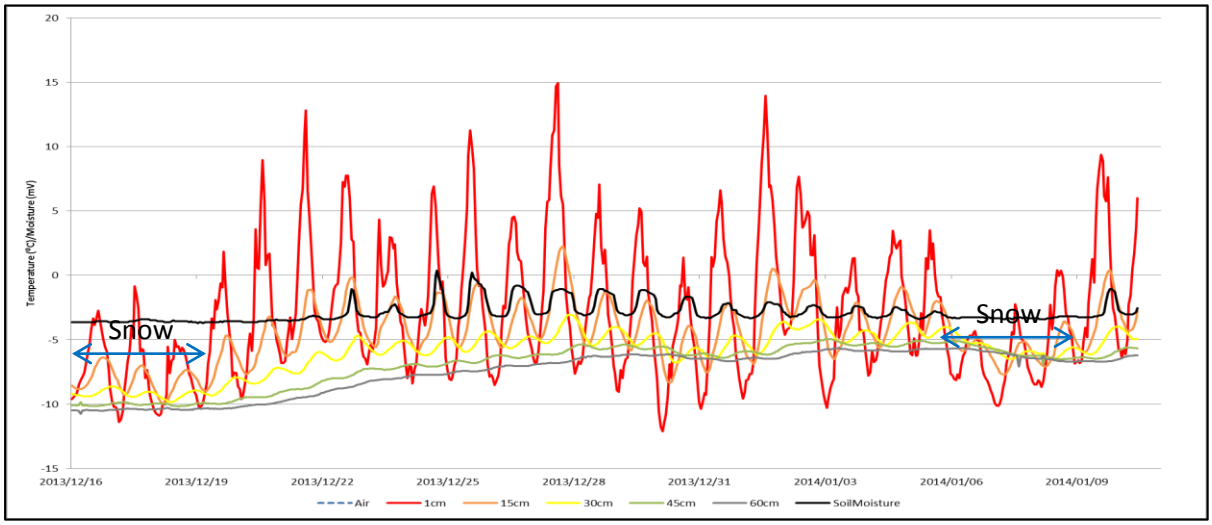

Figure 35: Borehole (60cm) data for the Flårjuven site (logger 1) from 16th December 2013 to 9th January 2014.

The depth profile graph focuses on the zero-degree isotherm and monitors whether it changes over time and if so by how much and in what direction (shallow/deepen) (Fig. 36). The short horizontal red

lines show that the shallowest recorded zero-degree isotherm depth was in 2011 at 22cm below the ground surface and the deepest was in 2010 at 26.5cm below the ground surface.

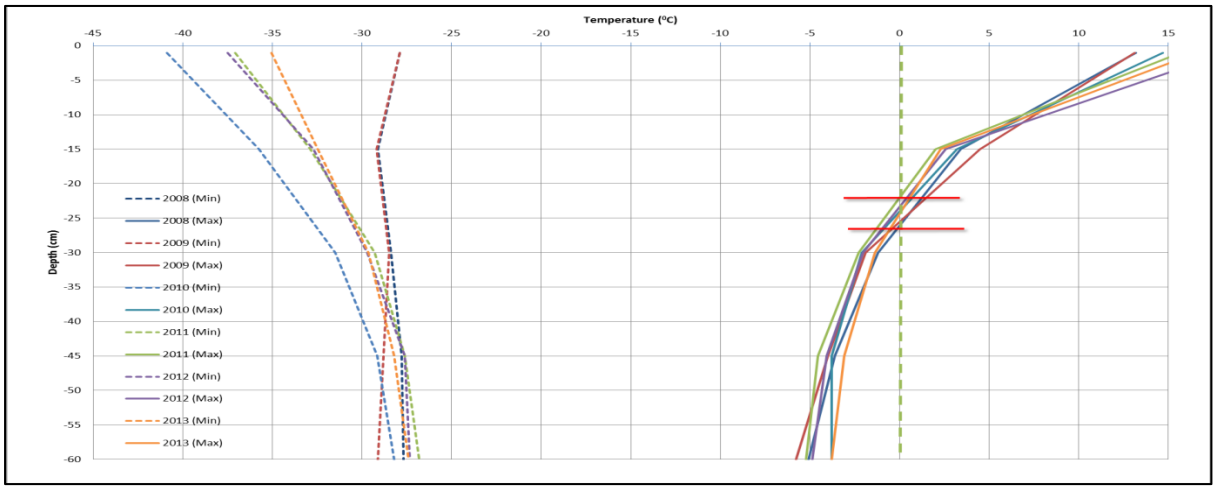

Figure 36: Depth profile for the Flårjuven site (logger 1) for the years 2008 to 2013.

There is little relationship between air temperature and the maximum thaw depth (Fig. 37). The active layer depth does not directly relate to air temperature rises but rather it would be affected more by factors such as cloud cover, snow cover and wind which directly impacts on the amount of solar radiation entering and heating up the ground (Idso *et al*., 1975; Bristow and Campbell, 1984; Bonan, 1989; Zang *et al*., 1997; Julián and Chueca, 2007). Factors such as cumulative degree days are evident in Figure 39, however were not accounted for in this graph.

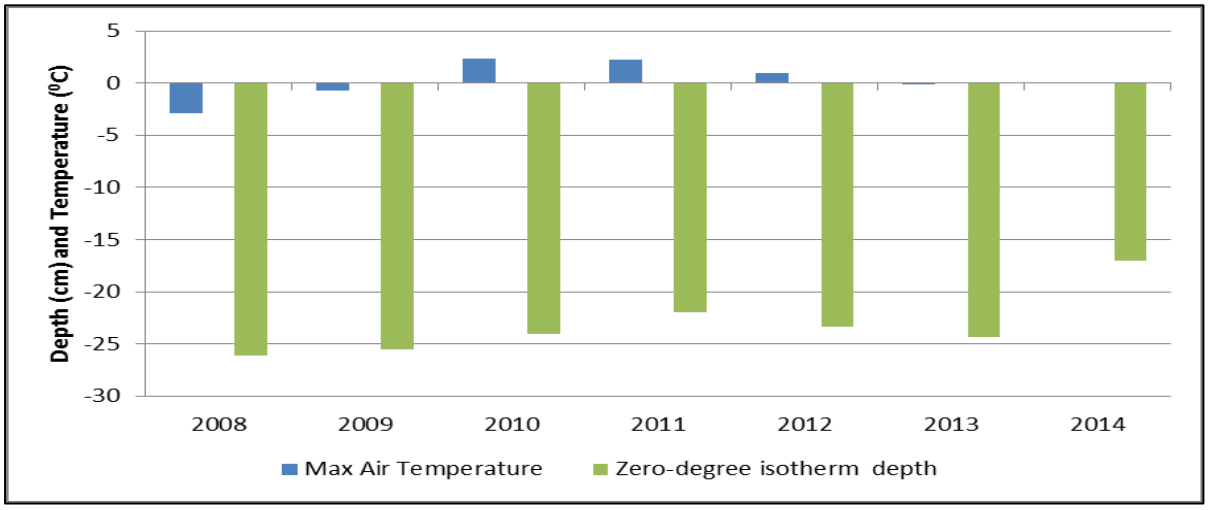

Figure 37: The air temperature data verses the zero-degree isotherm depth for the Flårjuven study site (logger 1) from the years 2008 to 2014. Due to the faulty connection of the air temperature sensor, there is disturbed air temperature data for 2013 and 2014.

4.1.2.2. Flårjuven Site 2 (2nd logger site)

4.1.2.2.1. 60cm borehole results

The winter and summer months' maximum and minimum recorded temperatures can be seen in Figure 38. During the winter months the air temperature fluctuates the most in comparison to the ground temperature data but during the summer period the air temperature drops to the minimum temperature only and the ground surface temperature peaks at the maximum temperatures. The summer air temperature peaked at -0.6°C (9/01/2013) with maximum ground temperature reaching 14°C (24/01/2013). The minimum air temperature was -35°C and on the same date was the coldest recorded ground temperature at -34°C (26/08/2013). Spikes in the soil moisture level can also be seen shortly after the 1cm ground temperature spikes. Regardless of the permanently frozen state, during the winter months fluctuations in temperatures can still be seen.

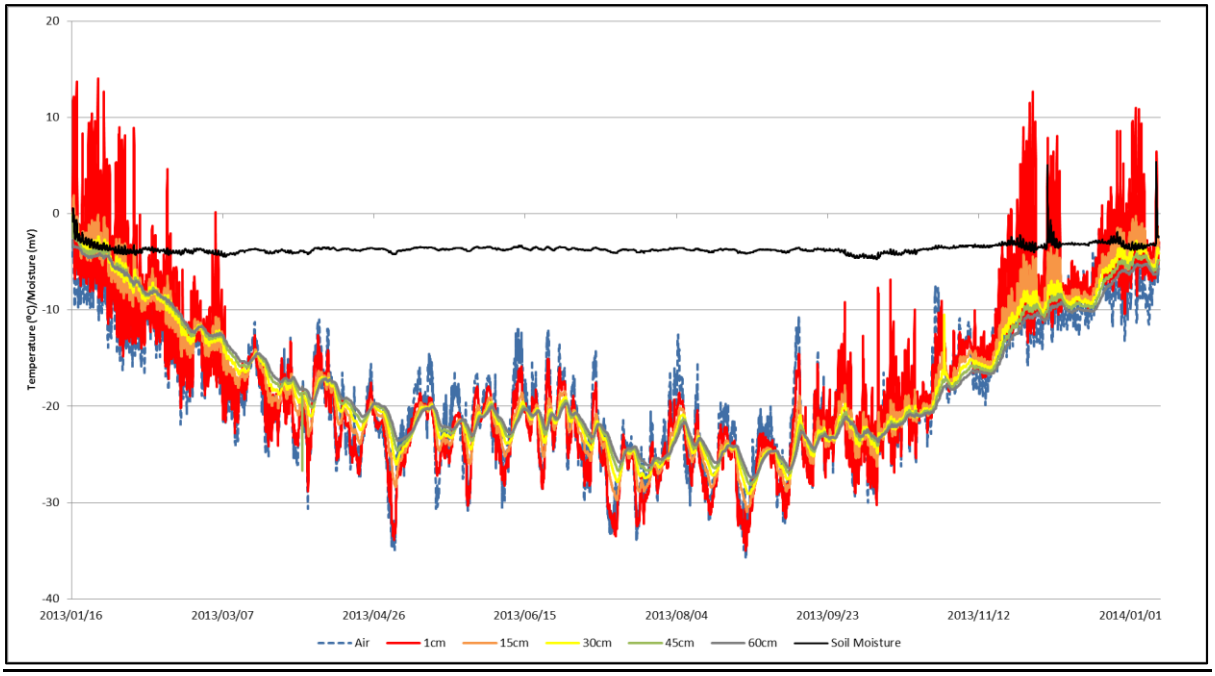

Figure 38: Borehole (60cm) data for the Flårjuven site (logger 2) from January 2013 to January 2014.

A summer period from 16th December 2013 to 9th January allows for a detailed view of the data (Fig. 39). Specifically, the soil moisture extent (black line) shows that after experiencing a few freeze/thaw cycles the moisture level begins to follow the trend of the 1cm and 15cm high peaks which shows the direct relation of freeze/thaw cycles to accelerated moisture levels. Prior to the 22nd December 2013 and on the 5th of January 2014 there was a snow fall event which can be seen on the graph as moisture levels smooth out and then peaks once again toward the end as the freeze/thaw cycles fall into play after the storm. The same events are noticeable at the Flårjuven Site 1 (Fig. 35, pg. 46). Furthermore,

the soil moisture has a really high peak after the snowfall period which suggests the additional moisture obtained from the melting snow.

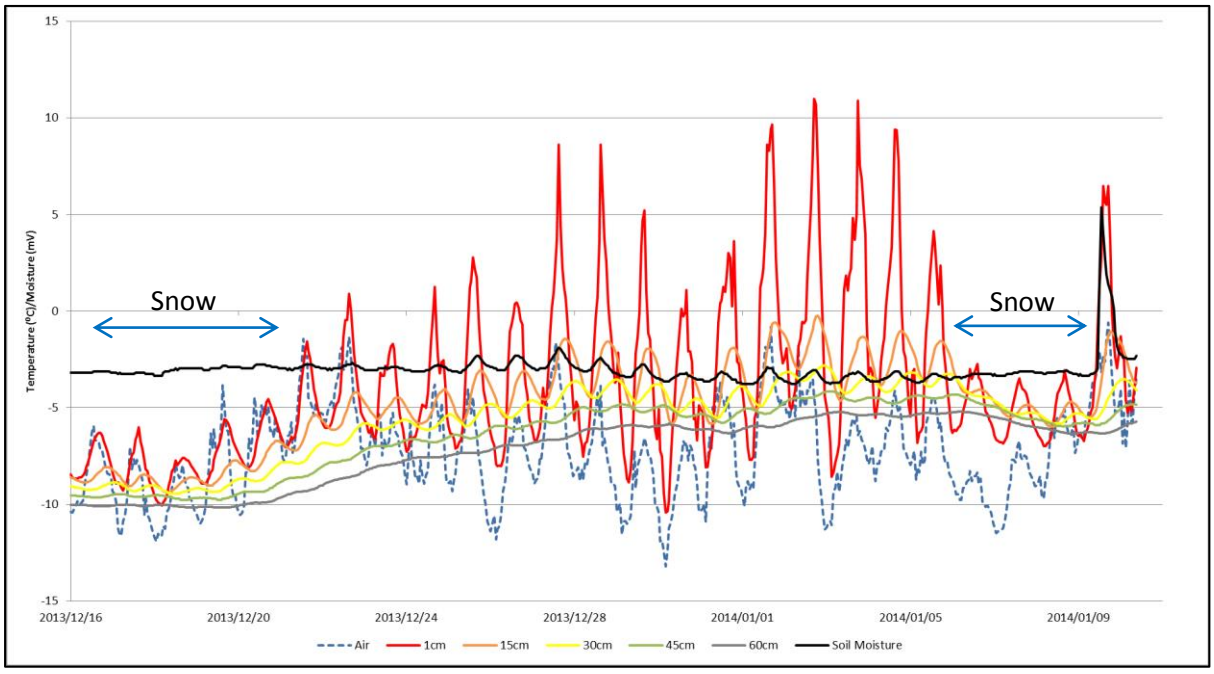

Figure 39: Borehole (60cm) data for the Flårjuven site (logger 2) from 16th December 2013 to 9th January 2014.

The short horizontal red line shows that the zero-degree isotherm was at a maximum depth of 29cm below the ground surface in 2013 (Fig. 40).

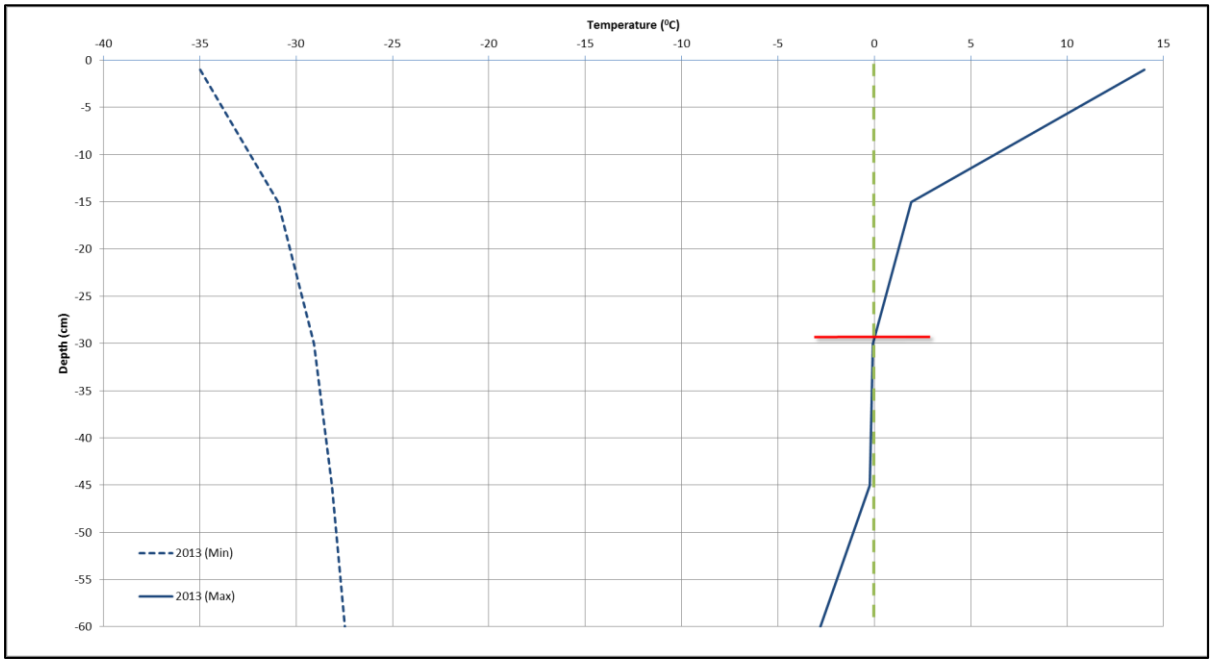

Figure 40: Depth profile for the Flårjuven site (logger 2) for 2013.

Similarly to the graph of the Flårjuven Site 1 (Fig. 37, pg. 48), we cannot draw conclusions based on the relation between air temperature and active layer depth (Fig. 41). However, it must be noted that there is only a full data set for the year of 2013 as 2014 only contains the data for the month of January. Comparing the Flårjuven study site loggers 1 and 2 for the year of 2013 we can see that the air temperature was only -0.1°C at logger 1 with an active layer depth of 24.3cm and at logger 2 the air temperature was -1.3°C with an active layer depth of 29.3cm.

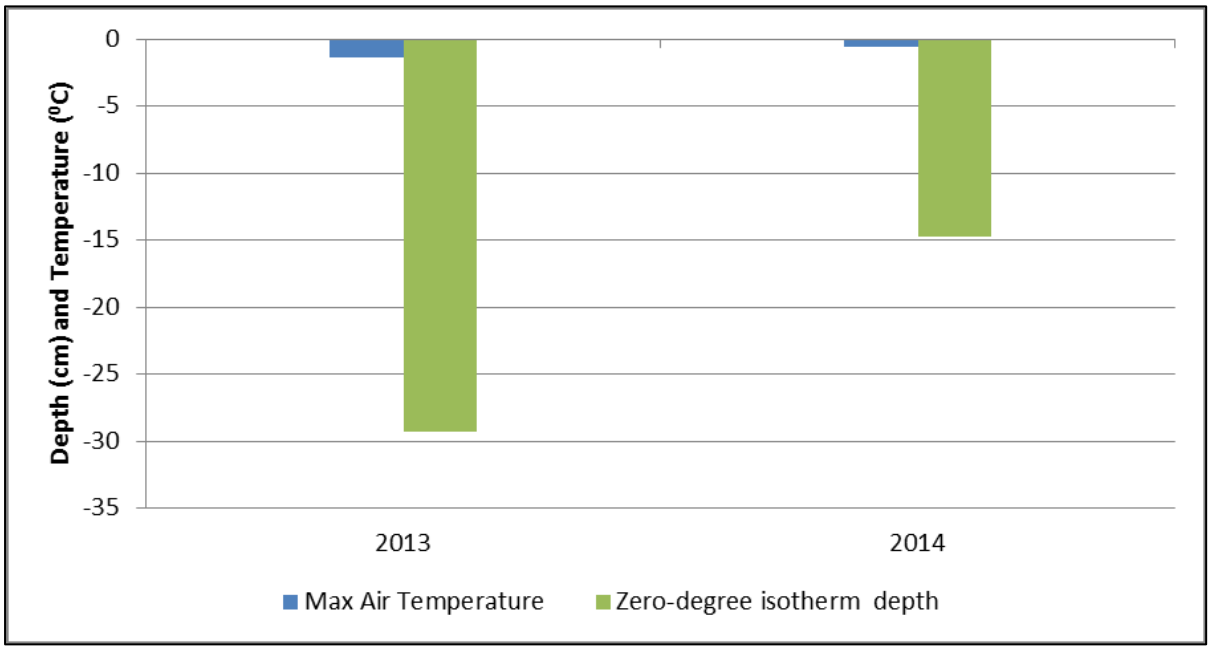

Figure 41: The air temperature data verses the zero-degree isotherm depth for the Flårjuven study site (logger 2) for 2013 and 2014.

4.1.2.2.2. 20cm borehole results

The zero-degree isotherm depth is in the 15cm to 30cm range which could mean that more frequent shallow sensors would be more appropriate for this area (Fig. 36, pg.47 and Fig. 40, pg. 50). The depth of the zero-degree isotherm is presented in black (Fig. 42). It is clear that only during summer (November to February) this site experiences freeze/thaw cycles. Air temperatures fluctuate the most during the winter months in comparison to the ground thermal data but during the summer period the air temperature drops to the minimum temperature only and the ground surface temperature peaks at the maximum temperatures due to reasons mentioned previously. Summer air temperature peaked at -0.6°C (9/01/2013) with maximum ground temperature reaching 13°C (27/12/2013). The minimum air temperature was -35°C (26/08/2013) and on the same date was the coldest recorded ground temperature at -34.2°C. The zero-degree isotherm depth peaks are directly related and proportional to peaks in ground temperature. The maximum depth of the zero-degree isotherm is 20.7cm (27/12/2013) which is the same day as the maximum recorded ground temperature.

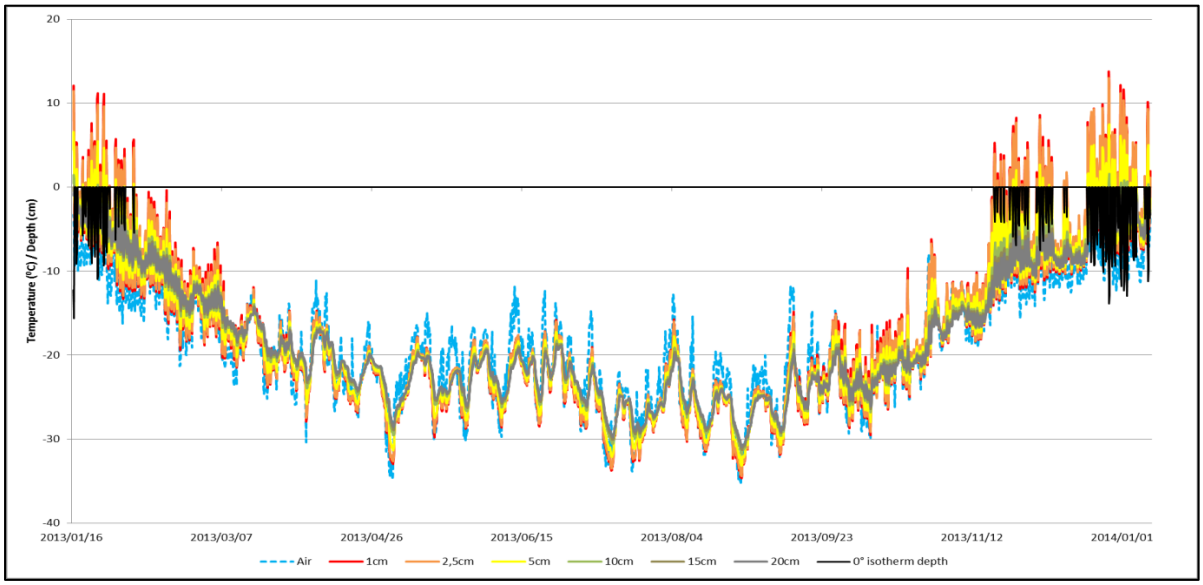

Figure 42: Borehole (20cm) data for the Flårjuven site (logger 2) from January 2013 to January 2014. The graph also shows the zero-degree isotherm depth displayed in black.

A view of this data over the same summer period as site 1 for comparative reasons is presented (Fig. 43). The depth of the zero-degree isotherm can be seen in black. This data shows how the peaks in ground temperature (1cm, 2.5cm) are directly related to the depth of the zero-degree isotherm. Furthermore, it illustrates how the air temperature seems to follow a general trend in peaks with the ground surface temperatures but is not as significantly proportional to the overall zero-degree isotherm depth.

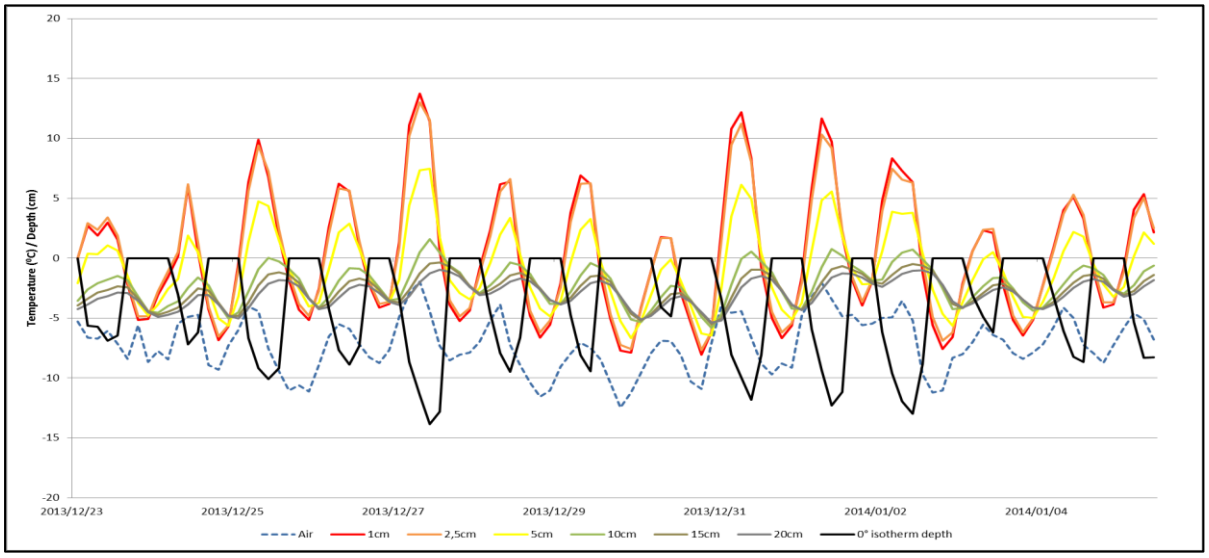

Figure 43: Borehole (20cm) data for the Flårjuven site (logger 2) from 23rd December 2013 to 4th January 2014 (13 day summer period). The graph also shows the zero-degree isotherm depth displayed in black.

4.1.3. Polygon Analysis

An infield analysis was done on five polygons at the Flårjuven study area. A summary of these results can be seen in Table 3. There was a 100% occurrence of snow in the cracks of the five sampled polygons. The mean length of the A-axis was 10.2m with a maximum of 13.1m. Of the polygons sampled, 100% of the A-axis measurements had the same bearing as the hill slope. The mean bearing of the A-axis was 73°. The mean slope gradient was 10.2°, the mean perimeter was 28.4m and the average height of the polygons was 1243m.a.s.l.

Table 3: Polygon field sample data summary from the Flårjuven study area.

	A Axis		**B Axis**				
	Length (m)	**Orientation (magnetic, degrees)**	**Length (m)**	**Orientation (magnetic, degrees)**	**Slope Gradient (degrees)**	**Perimeter (m)**	**Height (m.a.s.l.)**
Mean	10.2	73	6.9	73	10.2	28.4	1243
Max	13.1	112.2	9.4	112.2	13.1	34.4	1247
Min	8.2	50.2	4.3	50.2	8.2	20.2	1242
Standard Deviation	2.2	24.7	1.8	24.7	2.2	5.7	2.2

4.2. Slettfjell

4.2.1. Topographical Analysis

Six perspectives are presented of the Slettfjell study area taken after the 3D model was created from the aerial images (Fig. 44). It was possible to identify many features in the 3D view which could not be obtained from the 2D mosaicked images alone or even from fieldwork analysis. The stripes were the most difficult to determine as their perimeters were not clearly defined from desktop analysis only and therefore it must be noted that the delineated area is not exact. The polygons were easy to delineate as there is direct shading noticeable where the larger rocks form which defines the perimeter. A visual for the area of Slettfjell is given which contains polygon and stripe features (Fig. 45). A total of 196 polygons were digitised, none of which were sampled in the field. The area of the polygons (m^2) is represented in graduated colours, with yellow representing a small area and red representing large polygons. A total of 11 stripes were digitised. The area of the stripes (m^2) is represented in graduated colours, with white representing a small area and green representing large stripes. Statistics were calculated for these polygon and stripe areas (Fig. 46 and 47).

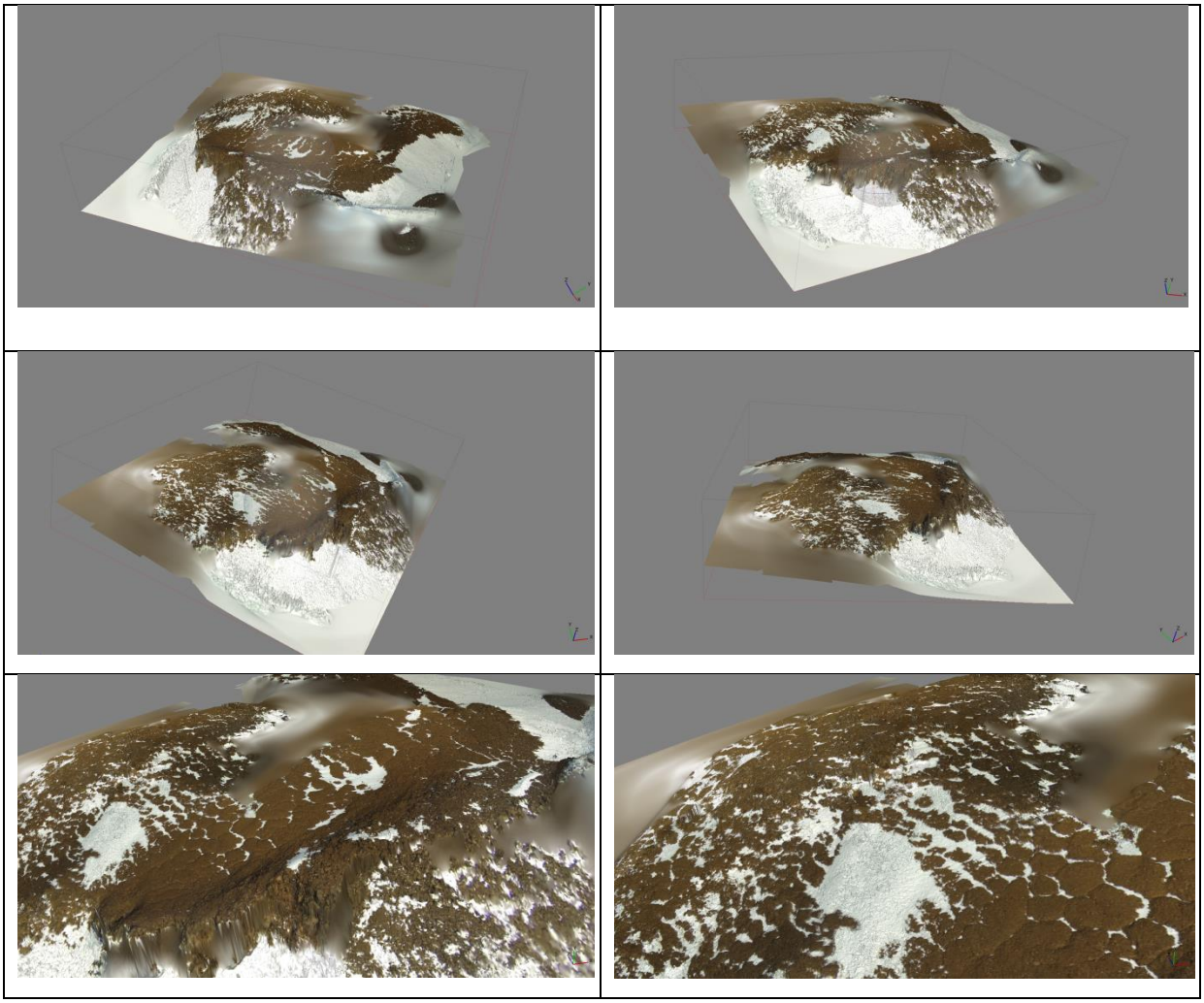

Figure 44: Model representation of the Slettfjell study site showing the topographic area of interest from six perspectives.

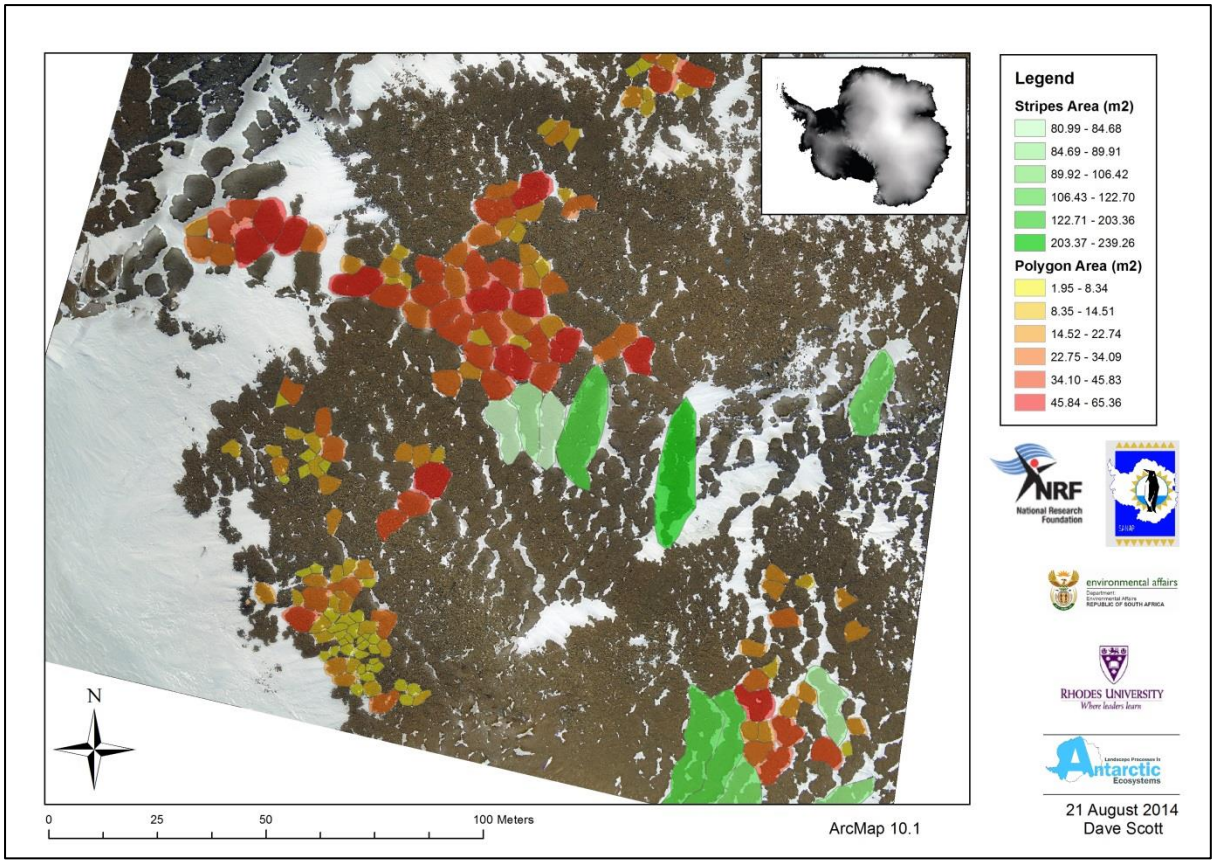

Figure 45: Map showing delineated polygons done in post fieldwork desktop analysis and estimated potential stripe formations (shaded in aggregate white to green). The graduated colours represent size of polygons (m²) with yellow showing small area and red representing large polygons.

The polygon sample size was 196 with a minimum area of 1.95m², a maximum of 65.36m² and a mean area of 20.93m² (Fig. 46). The proposed terrace estimate sample size was 11 with a minimum area of 80.99m², a maximum area of 239.26m² and a mean area of 135.11m² (Fig. 47). The statistics show that there is much variation in the area of the landscape features found on the Slettfjell study site and become the baseline for change over time.

Slettfjell Polygon Area (m²) Statistics

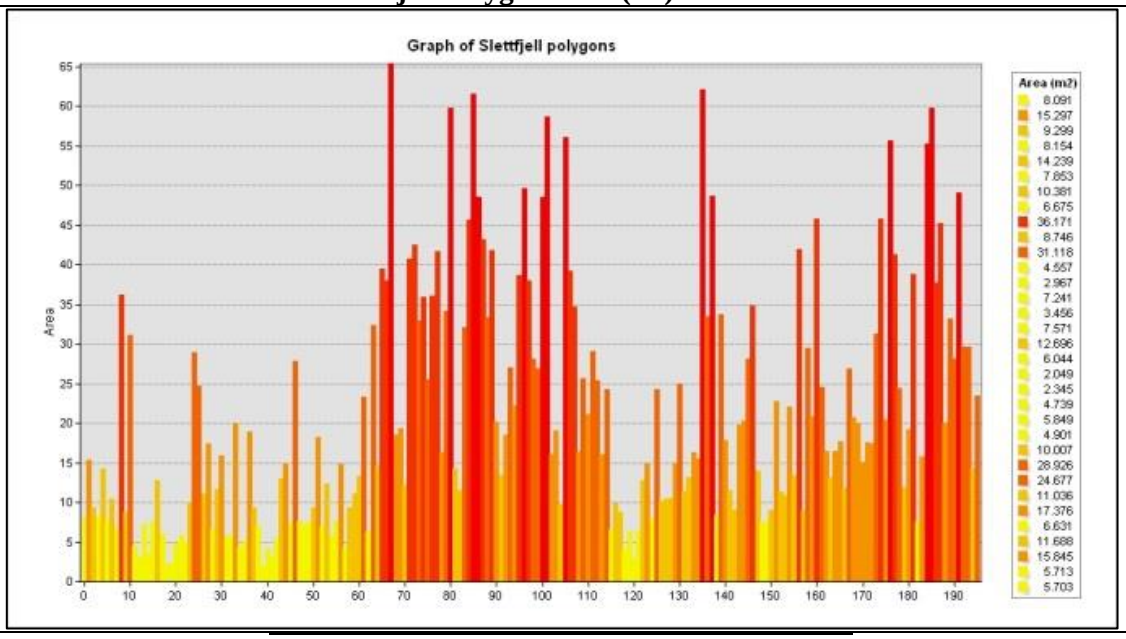

Count:	**196**
Minimum:	1.95
Maximum:	65.36
Sum:	4103.09
Mean:	20.93
Standard Deviation:	14.77

Figure 46: Graph and statistics of the Slettfjell polygon areas determined on ArcMap from aerial photographs.

Slettfjell Stripes Area (m²) Statistics

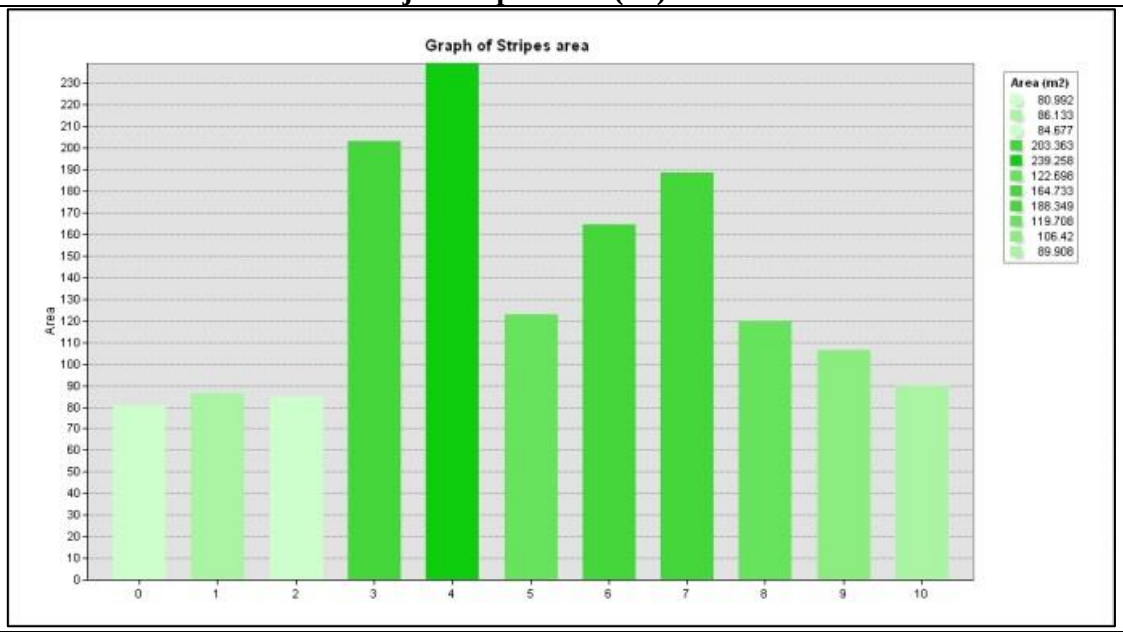

Count:	**11**
Minimum:	80.99
Maximum:	239.26
Sum:	1486.24
Mean:	135.11
Standard Deviation:	52.52

Figure 47: Graph and statistics of the Slettfjell stripe areas determined on ArcMap from aerial photographs.

4.2.2. Ground Thermal Analysis

4.2.2.1. 60cm borehole results

The winter and summer months' maximum and minimum recorded temperatures can be seen in Figure 48. During the winter months the air temperature fluctuates the most in comparison to the ground thermal data but during the summer period the air temperature drops to the minimum temperature only and the ground surface temperature peaks at the maximum temperature. The summer air temperature peaked at 0.42°C (12/12/2013) with maximum ground temperature reaching 5.87°C (31/012/2013). The minimum air temperature was -38.83°C (02/05/2013) and on the same date was the coldest recorded ground temperature at -38.37°C. Spikes in the soil moisture level can also be seen shortly after the 1cm ground temperature spikes however from the 22nd December 2013 it does not seem to follow the usual trend.

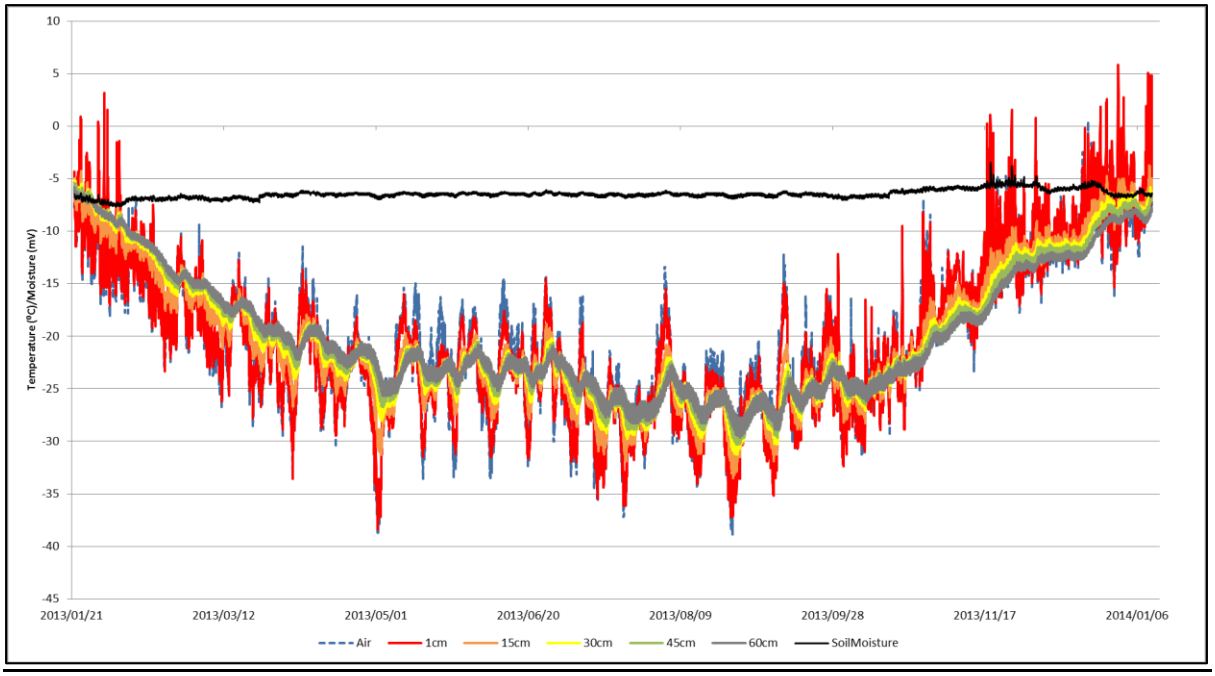

Figure 48: Borehole (60cm) data for the Slettfjell site from January 2013 to January 2014.

A summer period from 16th December 2013 to 9th January 2014 allows for a detailed view of the data (Fig. 49). On the 16th to the 19th of December 2013 there was a cold weather period. Interestingly this appears to be a cold site as the ground temperature only exceeds zero degrees five times during this summer period.

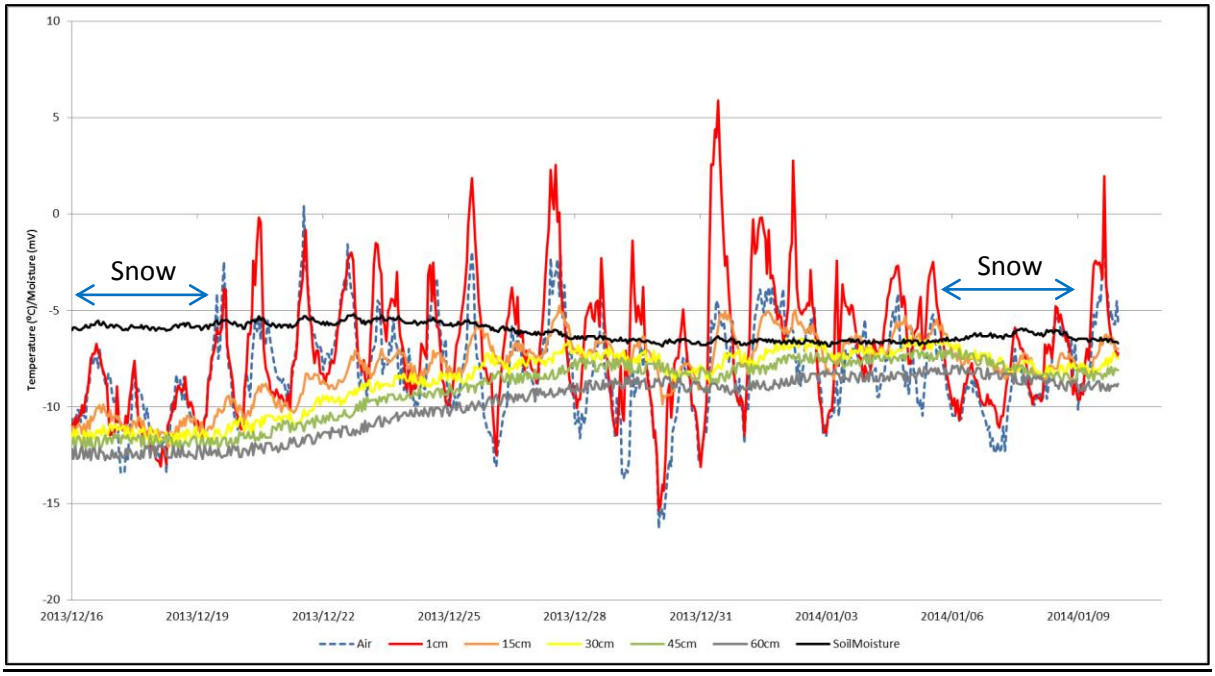

Figure 49: Borehole (60cm) data for the Slettfjell site from 16th December 2013 to 9th January 2014.

The short horizontal red line shows that the zero-degree isotherm was at a maximum depth of 9cm below the ground surface in 2013 and 2014 (Fig. 50). There was an error with the data logger and the 2013 minimum was not displayed on the graph.

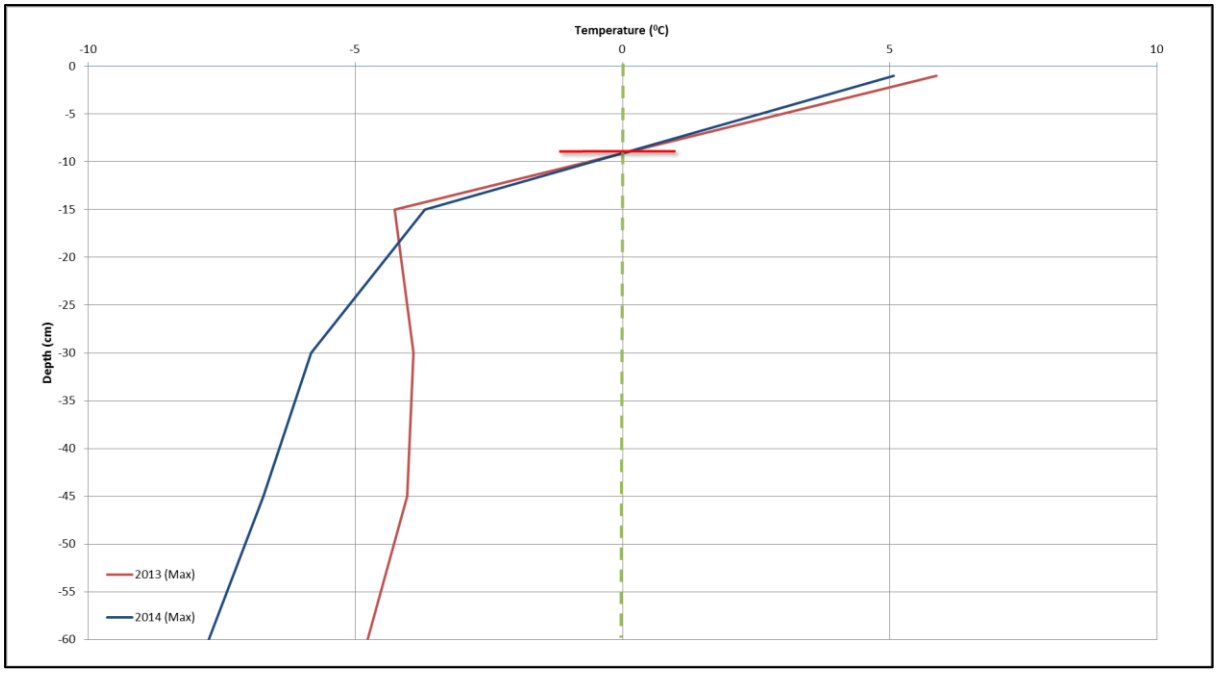

Figure 50: Depth profile graph for the Slettfjell site showing the depth profiles for the years 2013 and 2014.

4.2.2.2. 20cm borehole results

The zero-degree isotherm depth is 9cm below the ground surface which could mean that more frequent shallow sensors would be more appropriate for this area (Fig. 50). It is clear that only during summer (November to February) this site experiences freeze/thaw cycles (Fig. 51). The depth of the zero-degree isotherm is presented in black. Air temperatures fluctuate the most during the winter months in comparison to the ground thermal data but during the summer period the air temperature drops to the minimum temperature only and the ground surface temperature peaks at the maximum temperatures due to reasons mentioned previously. Summer air temperature peaked at -1.16°C (9/01/2013) with maximum ground temperature reaching 10.76°C (10/01/2014). The minimum air temperature was -37.94°C (26/08/2013) and the coldest recorded ground temperature at -37.44°C (09/09/2013). The zero-degree isotherm depth peaks are directly related and proportional to peaks in ground temperature. The maximum depth of the zero-degree isotherm was 9.24cm (10/01/2014).

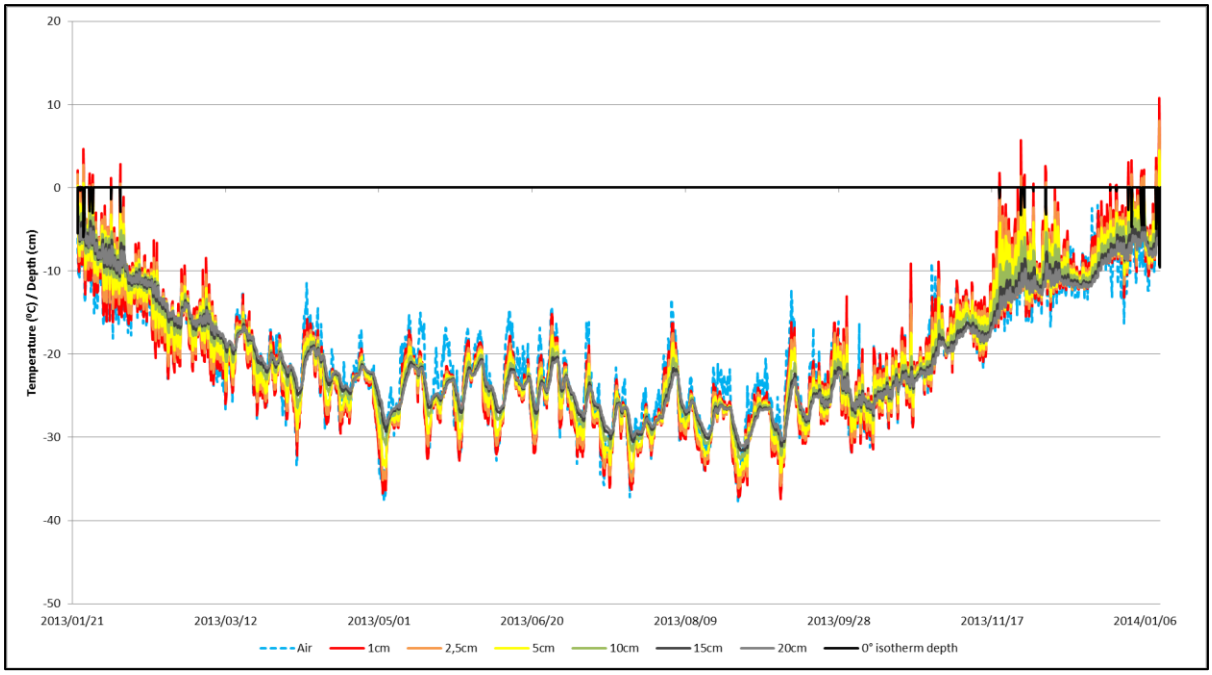

Figure 51: Borehole (20cm) data for the Slettfjell site from January 2013 to January 2014. The graph also shows the zero-degree isotherm depth displayed in black.

A view of this data over a summer period is presented (Fig. 52). The depth of the zero-degree isotherm can be seen in black. This data shows direct relationship in ground temperature maximums (1cm, 2.5cm) to the depth of the zero-degree isotherm. Furthermore, it illustrates how the air temperature data seems to follow a general trend in peaks with the ground surface temperatures but is not as significantly proportional to the overall zero-degree isotherm depth. On the 6th there was a snow storm event which dampened the effects of temperature and radiation on the active layer for three days and can be seen by the horizontal black line on the graph. The same event was noticed at the Flårjuven site (Fig. 39, pg. 50).

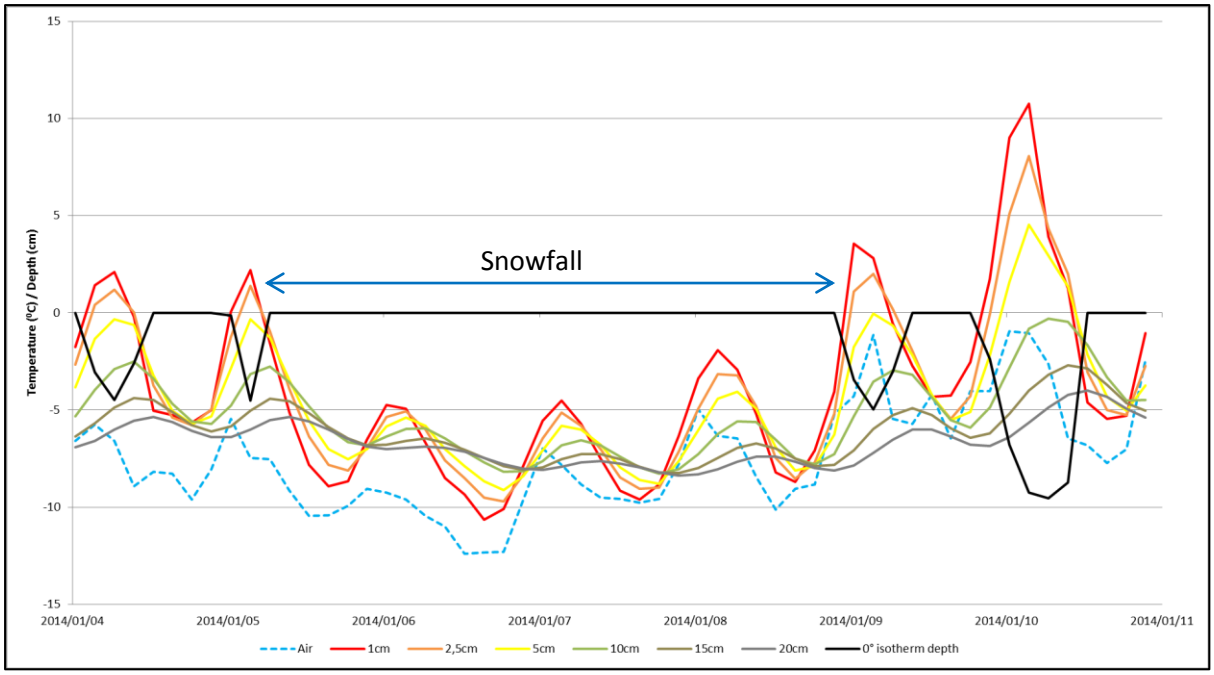

Figure 52: Borehole (20cm) data for the Slettfjell site from 4th January 2014 to 11th January 2014 (8 day summer period). The graph also shows the zero-degree isotherm depth displayed in black.

4.3. Valterkulten

4.3.1. Topographical Analysis

Four perspectives are presented of the Valterkulten study area taken after the 3D model was created from the aerial images (Fig. 53). It was possible to identify many features in the 3D view which could not be obtained from the 2D mosaicked images alone or even from field analysis. The terraces were the most difficult to determine as their perimeters were not clearly defined from desktop analysis and therefore it must be noted that the delineated area is not exact. Further investigation is advised as these terrace features may be ground creep due to freeze/thaw cycles. A visual for the area of Valterkulten is given which contains polygon and terrace features (Fig. 54). A total of nine polygons were digitised, none of which were sampled in the field. The area of the polygons (m^2) is represented in graduated colours, with white representing a small area and green representing large polygons. A total of 11 terraces were digitised. The area of the stripes (m^2) is represented in graduated colours, with yellow representing a small area and red representing large terraces. Statistics were calculated for these polygon and terrace areas (Fig. 55 and 56).

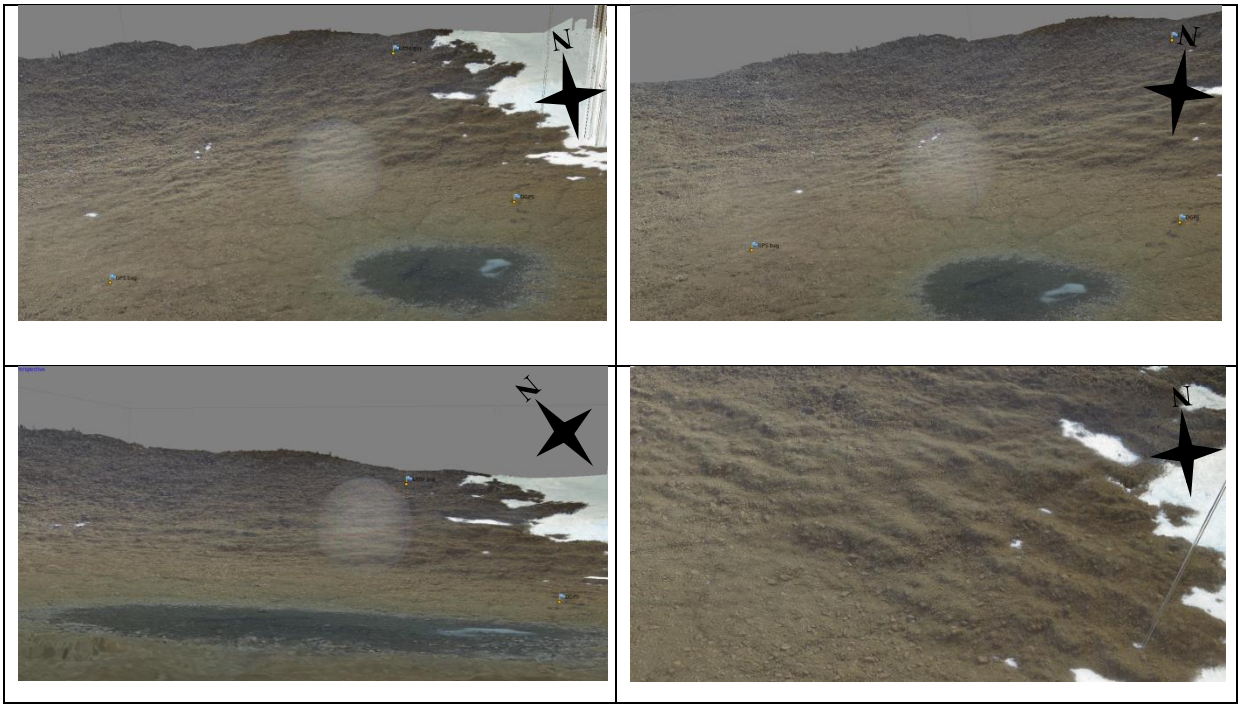

Figure 53: Model representation of the Valterkulten study site showing the topographic area of interest from four perspectives.

Topographic contour lines were created from a DEM of the Valterkulten study site (Fig. 54). These contours were then adjusted with data collected by the DGPS to ensure a more accurate profile. The polygons and terraces are displayed in graduated colours based on size. The Valterkulten logger is situated in a bowl 20m from a melt water pond. The terraces are found on the Southern facing slopes of 34^0 and the polygons are found on the flattened base of the bowl. Due to the topography and the formation of a bowl, it would be clear that the site is somewhat protected from wind. The difference in altitude from the pond to the top of the Northern slope is around 80m.

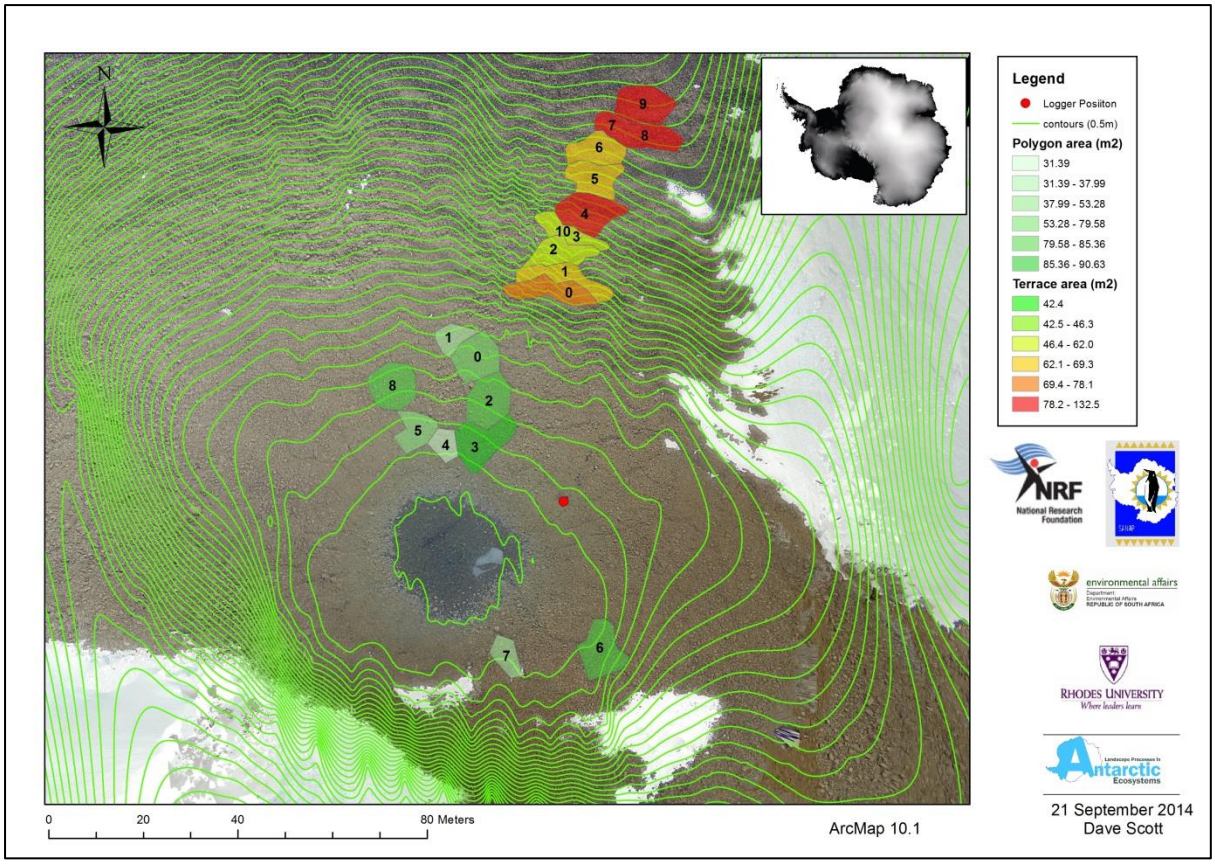

Figure 54: Contour map showing delineated polygons and terraces done in post fieldwork desktop analysis. The colours represent area (m²) with the aggregation of green to red representing terraces and white to green representing polygons.

The polygon sample size was nine with a minimum area of 31.39m², a maximum of 90.63m² and a mean area of 64.63m² (Fig. 55). The terrace sample size was 11 with a minimum area of 22.95m², a maximum of 91.94m² and a mean area of 63.68m² (Fig. 56). The statistics show that there is much variation in the size of the landscape features found on the Valterkulten study site and become the baseline for change over time.

Valterkulten Polygon Area (m²) Statistics

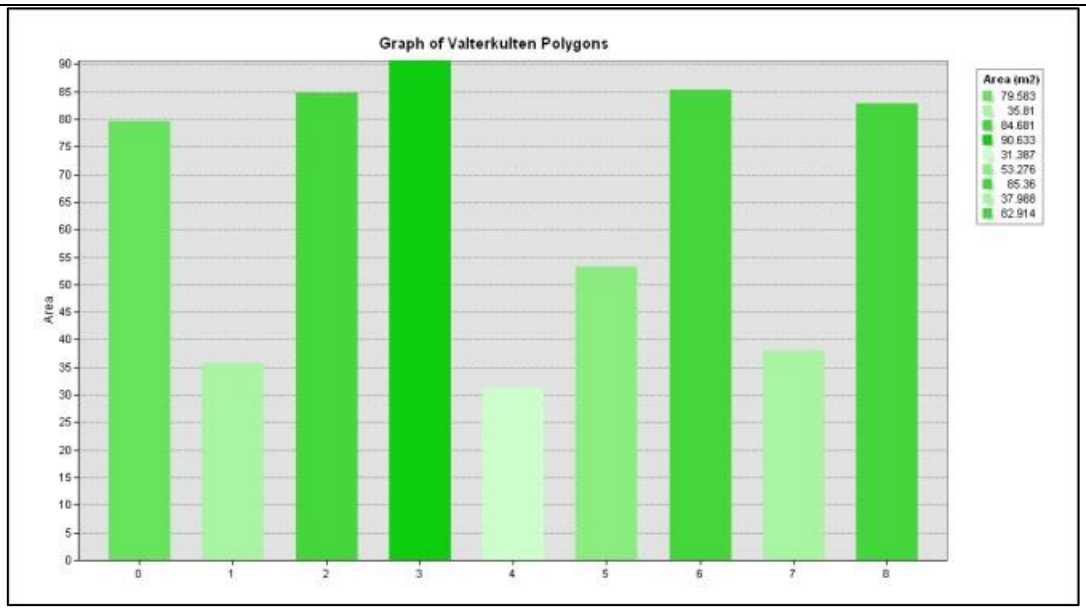

Count:	**9**
Minimum:	31.39
Maximum:	90.63
Sum:	581.63
Mean:	64.63
Standard Deviation:	23.19

Figure 55: Graphs and statistics of the Valterkulten polygon areas determined on ArcMap from aerial photographs.

Valterkulten Terrace Area (m²) Statistics

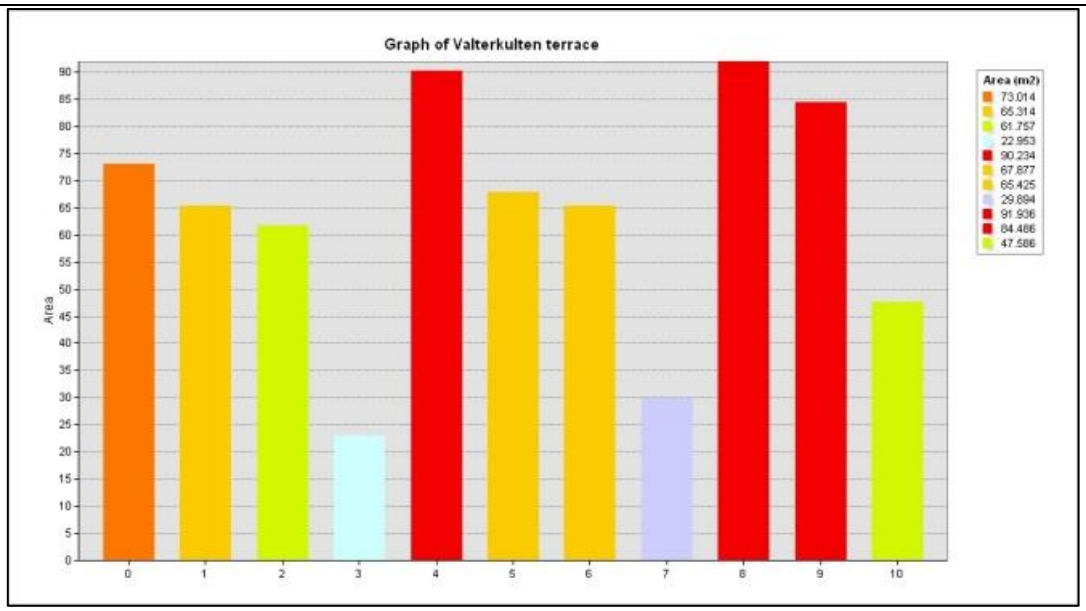

Count:	**11**
Minimum:	22.95
Maximum:	91.94
Sum:	700.48
Mean:	63.68
Standard Deviation:	21.55

Figure 56: Graph and statistics of the Valterkulten terrace areas determined on ArcMap from aerial photographs.

4.3.2. Ground Thermal Analysis

4.3.2.1. 60cm borehole results

The winter and summer months' maximum and minimum recorded temperatures can be seen in Figure 57. During the winter months the air temperature fluctuates the most in comparison to the ground thermal data but during the summer period the air temperature drops to the minimum temperature only and the ground surface temperature peaks at the maximum temperatures due to reasons previously mentioned. Summer air temperature peaked at 3.65°C (31/12/2013) with maximum ground temperature reaching 21.33°C (27/12/2013). The minimum air temperature was -33.42°C (14/07/2013) and on the same date was the coldest recorded ground temperature at -35.45°C. Spikes in the soil moisture level can also be seen shortly after the 1cm ground temperature spikes; however from the 22nd December 2013 it does not follow the usual trend.

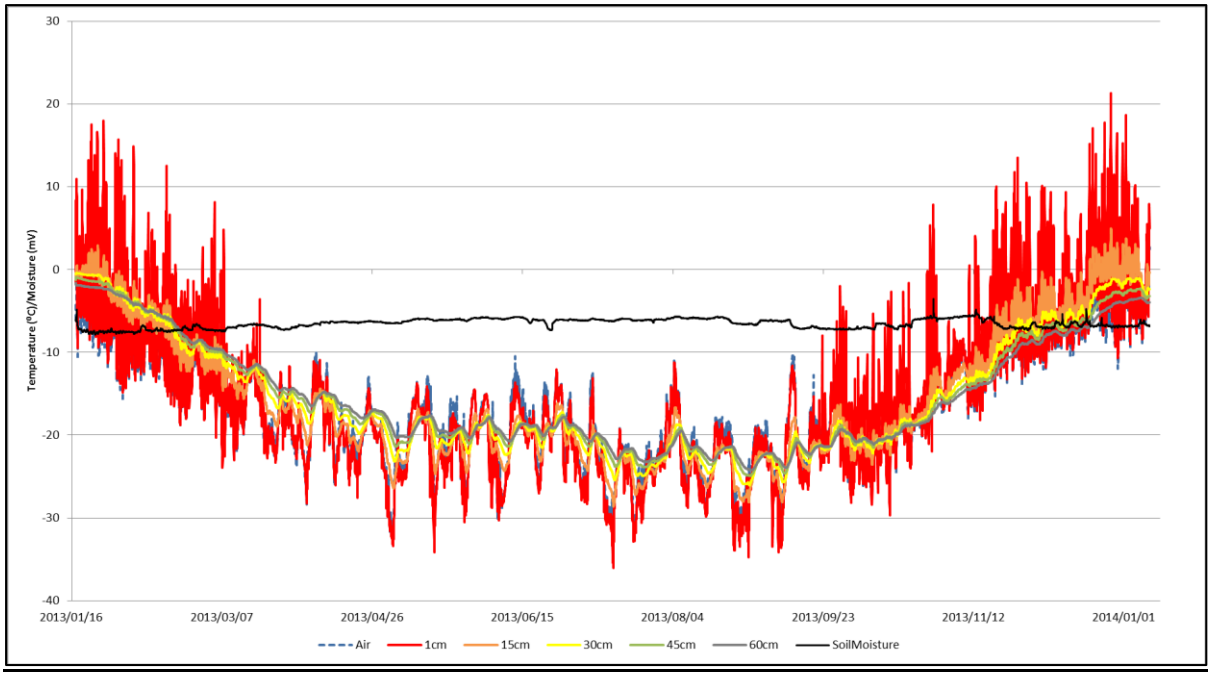

Figure 57: Borehole (60cm) data for the Valterkulten site from January 2013 to January 2014.

A summer period from 16th December 2013 to 9th January allows for a detailed view of the data (Fig. 58). Similarly to the Flårjuven and Slettfjell site, the snow event is evident on the graph from the 6th January 2014 as all the data peaks are heavily dampened.

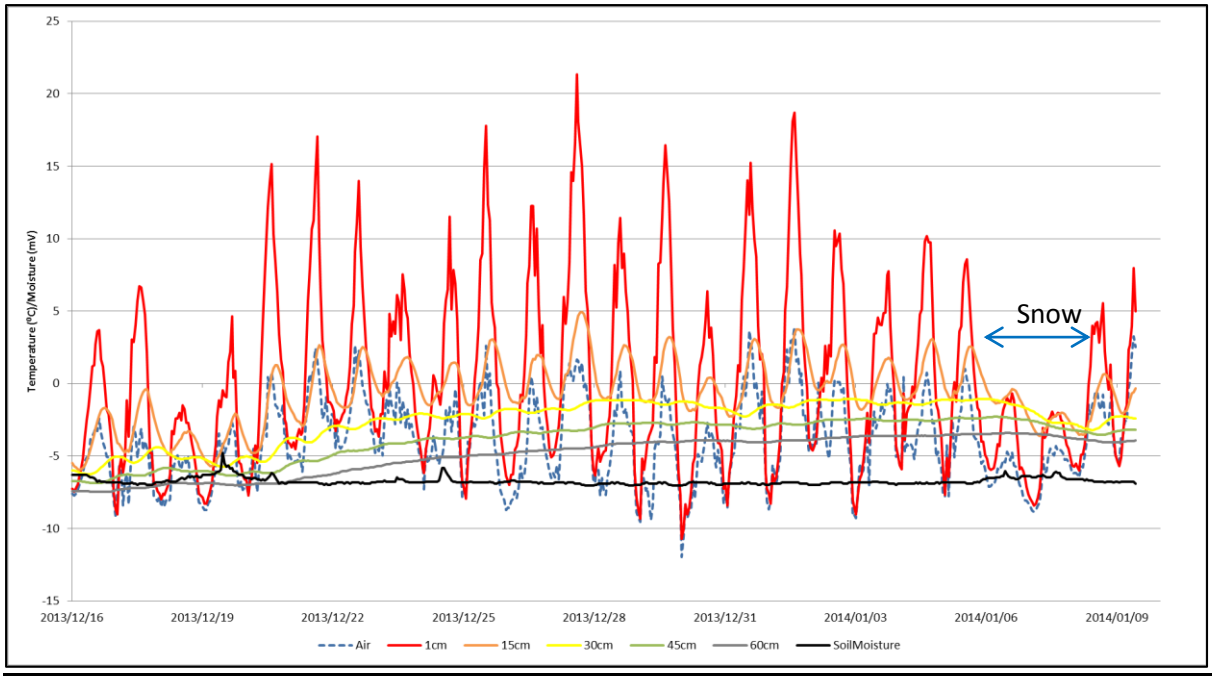

Figure 58: Borehole (60cm) data for the Valterkulten site from 16 December 2013 to 9 January 2014.

The short horizontal red line shows that the zero-degree isotherm was at a maximum depth of 29cm below the ground surface in 2013 (Fig. 59).

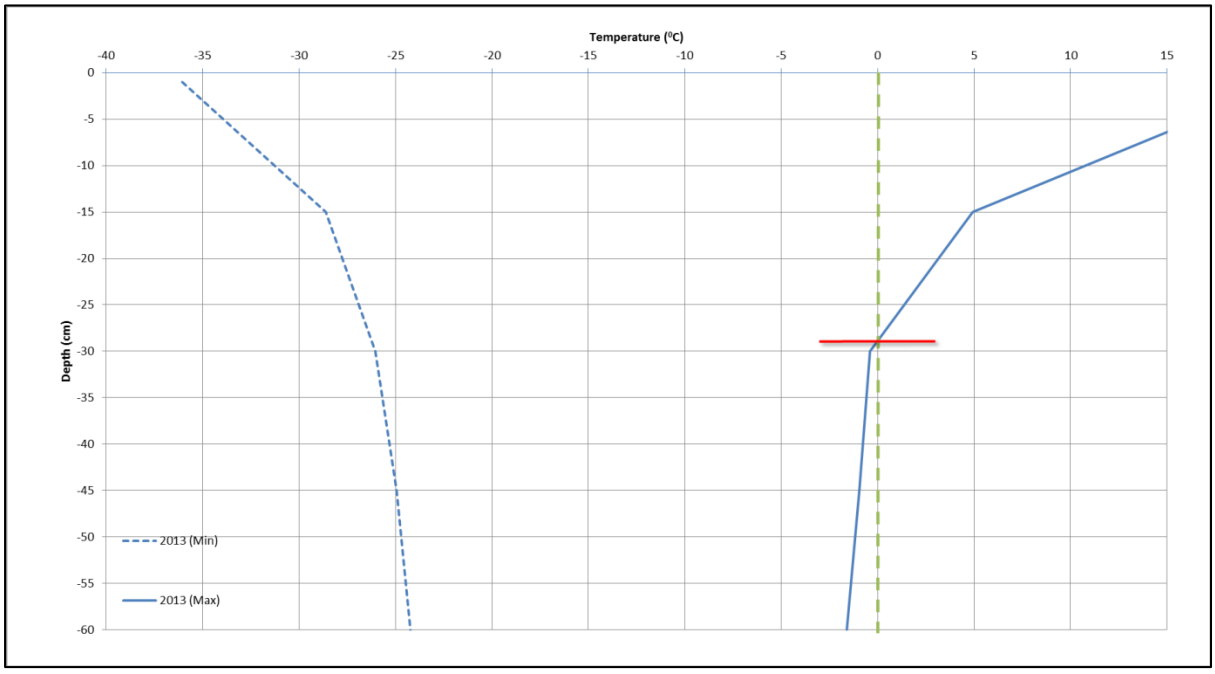

Figure 59: Depth profile graph for the Valterkulten site showing the depth profiles for 2013.

4.3.2.2. 20cm borehole results

The zero-degree isotherm depth is 29cm below the ground surface which could mean that more frequent shallow sensors may not be more appropriate for this area (Fig. 59). The site only experiences cycles over the zero-degree isotherm during summer (November to February) (Fig. 60). Air temperatures fluctuate the most during the winter months in comparison to the ground thermal data but during the summer period the air temperature drops to the minimum temperature only and the ground surface temperature peaks at the maximum temperatures due to reasons mentioned previously. The summer air temperature peaked at 3.65°C (31/12/2013) with the ground temperature reaching 21.49°C (27/12/2013). The minimum air temperature was -33.42°C (14/07/2013) and the coldest recorded ground temperature at -33.86°C (15/07/2013). The maximum depth of the zero-degree isotherm was 20.71cm (27/12/2013).

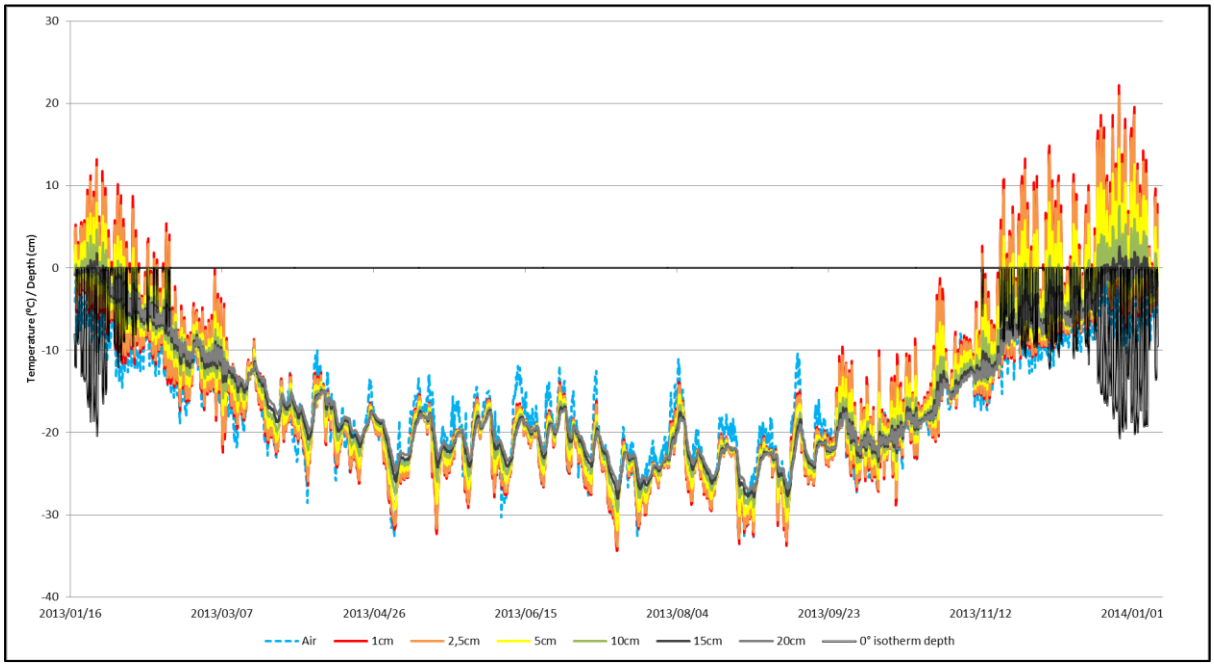

Figure 60: Borehole (20cm) data for the Valterkulten site from January 2013 to January 2014. The graph also shows the zero-degree isotherm depth displayed in black.

A view of this data over a summer period is presented (Fig. 61). The depth of the zero-degree isotherm can be seen in black. This data shows how the peaks in ground temperature (1cm and 2.5cm) are directly related to the depth of the zero-degree isotherm. Furthermore, it illustrates how the air temperature seems to follow a general trend in peaks with the ground surface temperatures but is not as significantly proportional to the overall zero-degree isotherm depth.

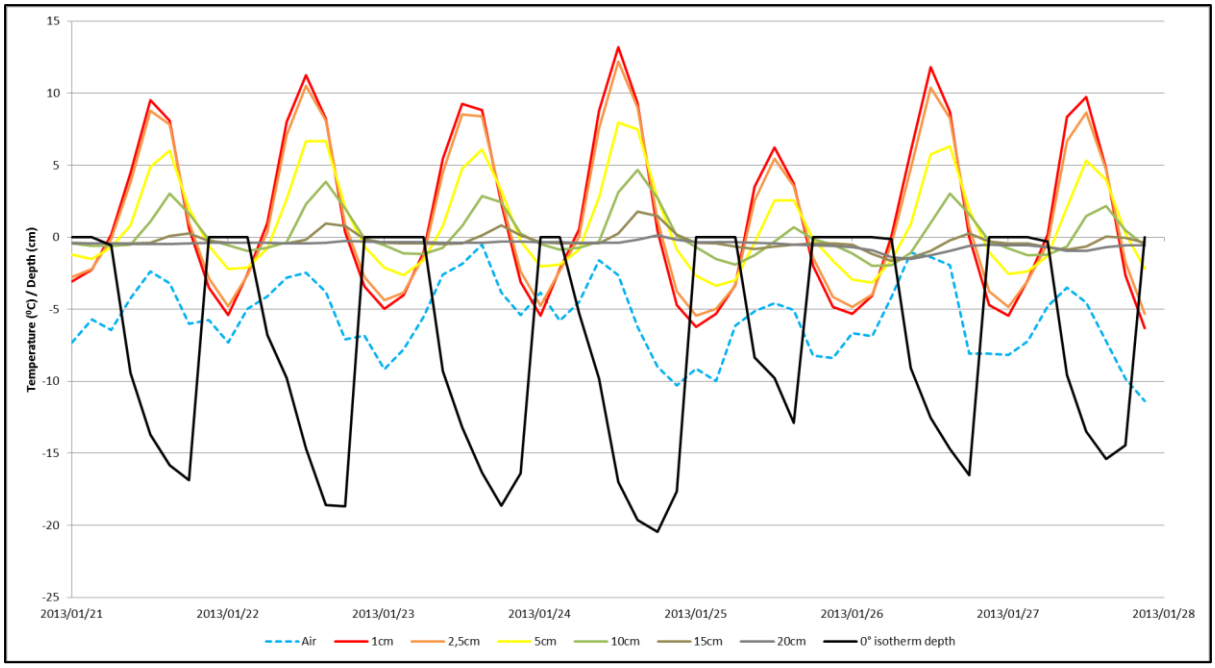

Figure 61: Borehole (20cm) data for the Valterkulten site from 21st January 2013 to 28th January 2013 (8 day summer period). The graph also shows the zero-degree isotherm depth displayed in black.

4.4. Robertskollen

The Robertskollen site had two areas of topographic interest. The borehole logger is situated on site 1 where there is sorted and non-sorted patterned ground. Site 2 boasts a high concentration of sorted and non-sorted patterned ground but also biotic life.

4.4.1. Topographical Analysis

Four perspectives are presented of the Robertskollen study area (1) and eight perspectives are presented for the Robertskollen study area (2) taken after the 3D model was created from the aerial images (Fig. 62 and 63). Although Robertskollen was the warmest of the sites due to its low altitude, the only topographic landscape features of interest were sorted and non-sorted ground. The main observations for this area are the noticeable melt water collection and large amount of lichen, moss and algal growth.

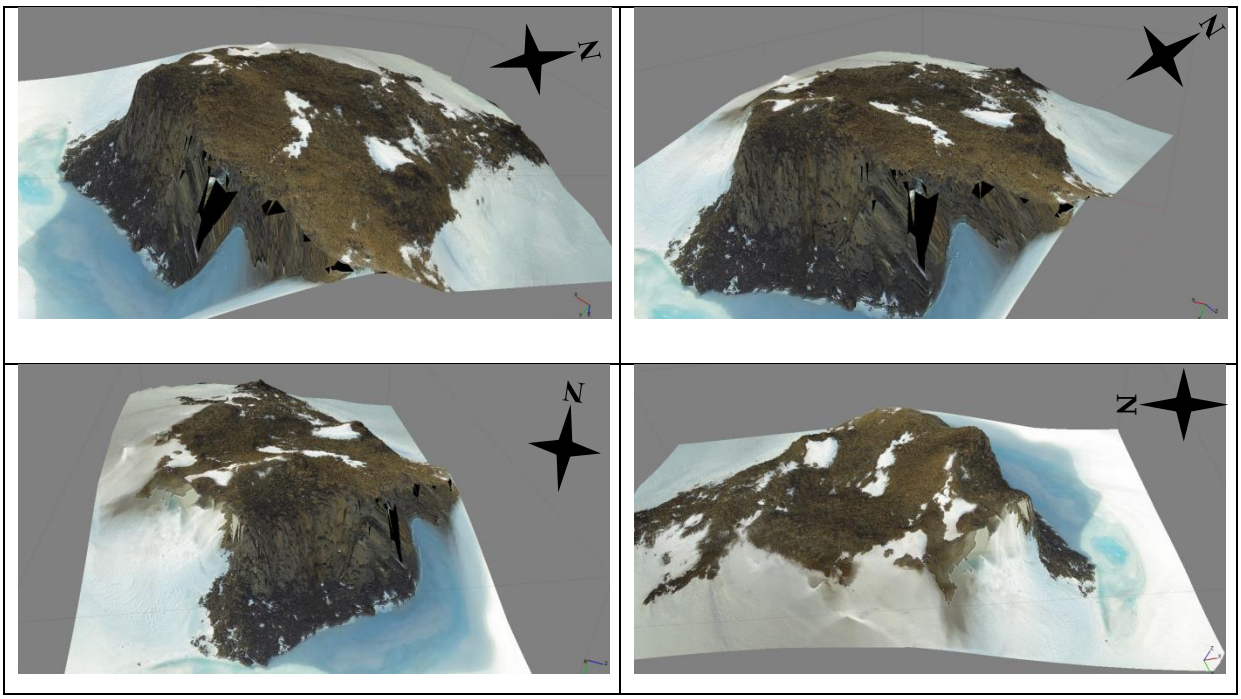

Figure 62: Model representation of the Robertskollen study site (1) showing the topographic area of interest from four perspectives.

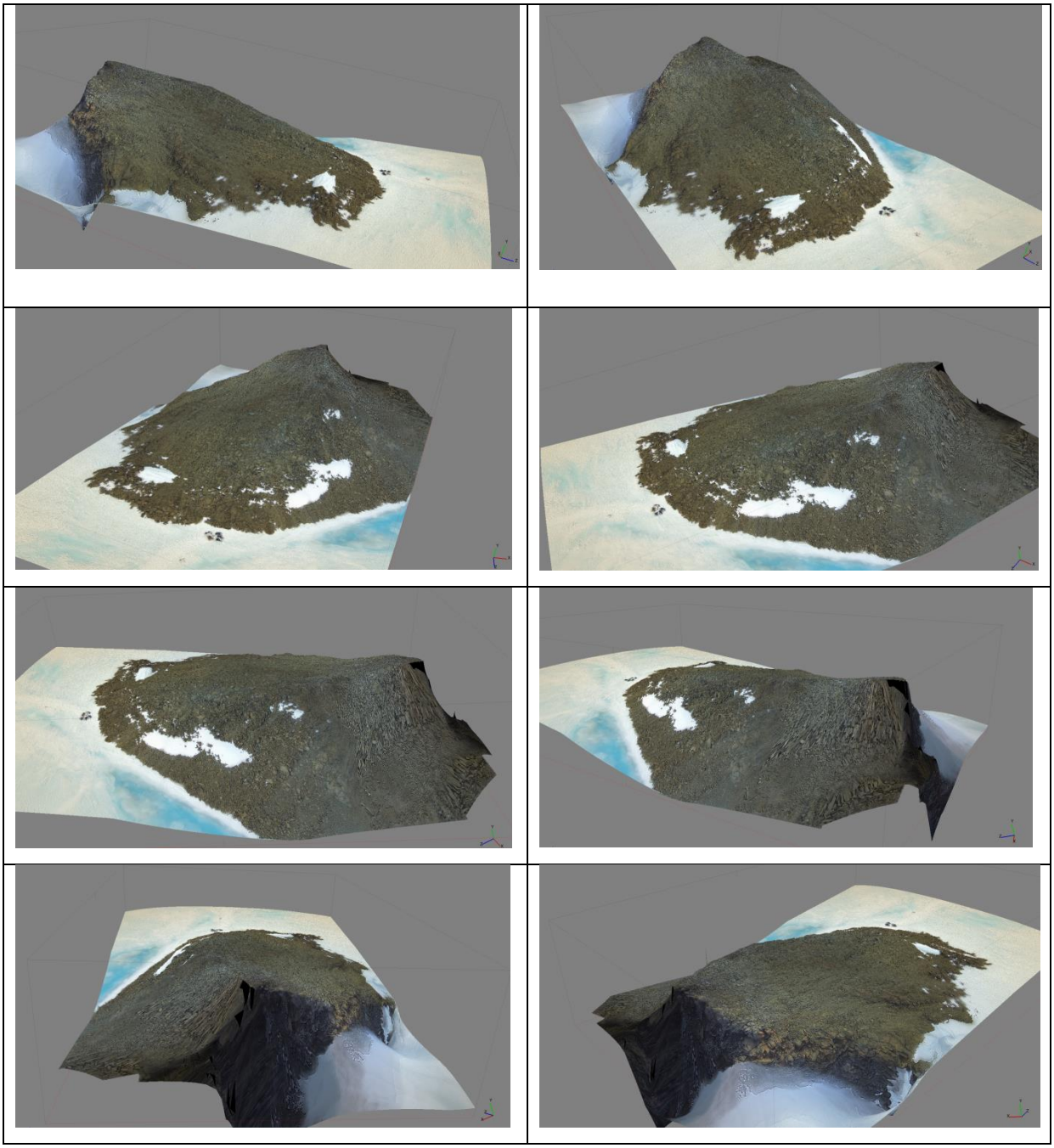

Figure 63: Model representation of the second Robertskollen study site (2) showing the topographic area of interest from eight perspectives.

Hillshading was used to create a map from the DEM for the Robertskollen study site (1) (Fig. 64). On the south eastern side of the site there is a cliff line with an altitude change of around 100m. Moving from South to North there is a reasonably steep gradient which flattens out towards the middle of the site and then slowly increases once again towards the North.

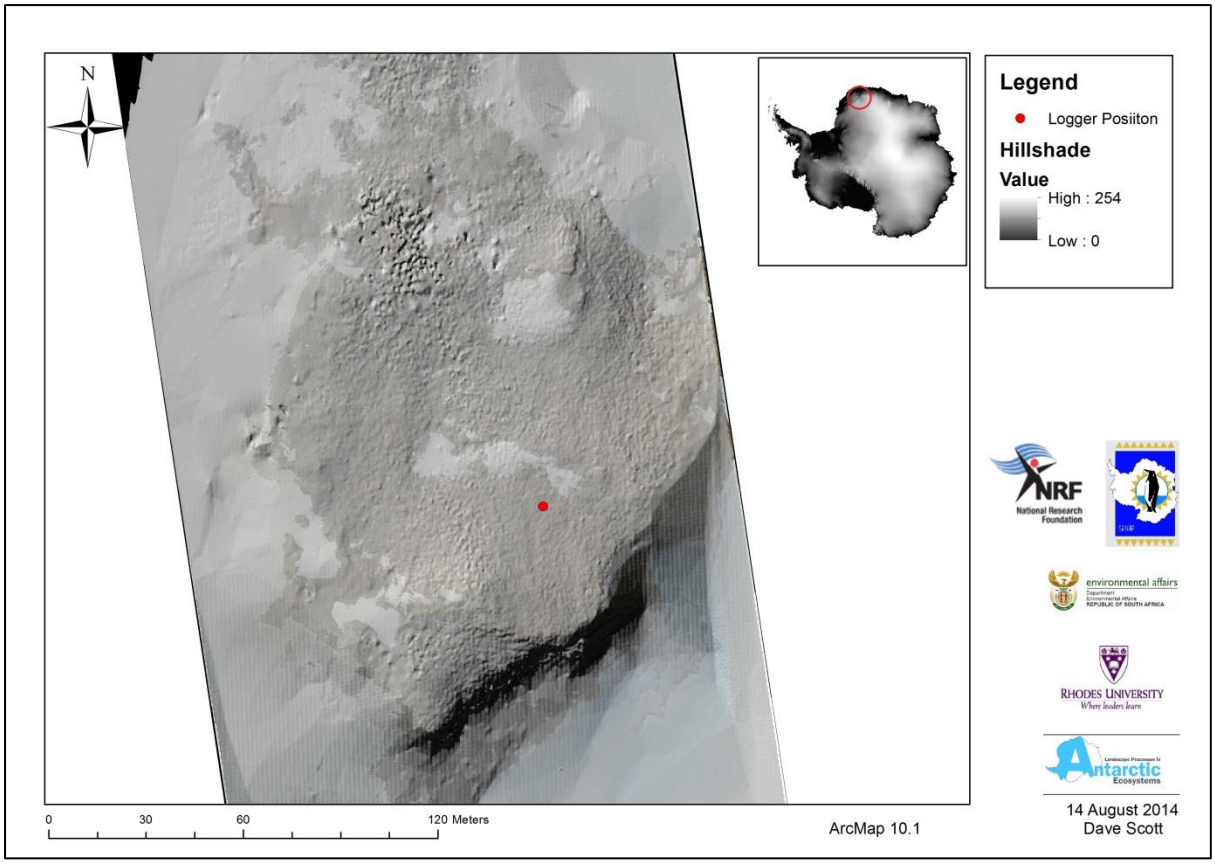

Figure 64: Map showing hillshading of the Robertskollen study area (1).

4.4.2. Ground Thermal Analysis

4.4.2.1. 60cm borehole results

The winter and summer months' maximum and minimum recorded temperatures can be seen in Figure 65. During the winter months the air temperature fluctuates the most in comparison to the ground thermal data but during the summer period the air temperature drops to the minimum temperature only and the ground surface temperature peaks at the maximum temperatures. Summer air temperature peaked at 0.68°C (10/01/2014) with maximum ground temperature reaching 16.47°C (01/01/2013). The minimum air temperature was -32.06°C (14/07/2013) and on the same date was the coldest recorded ground temperature at -31.02°C. Peaks in the soil moisture level can also be seen shortly after the 1cm ground temperature peaks; however, from the 22 December 2013 it does not seem to follow the usual trend.

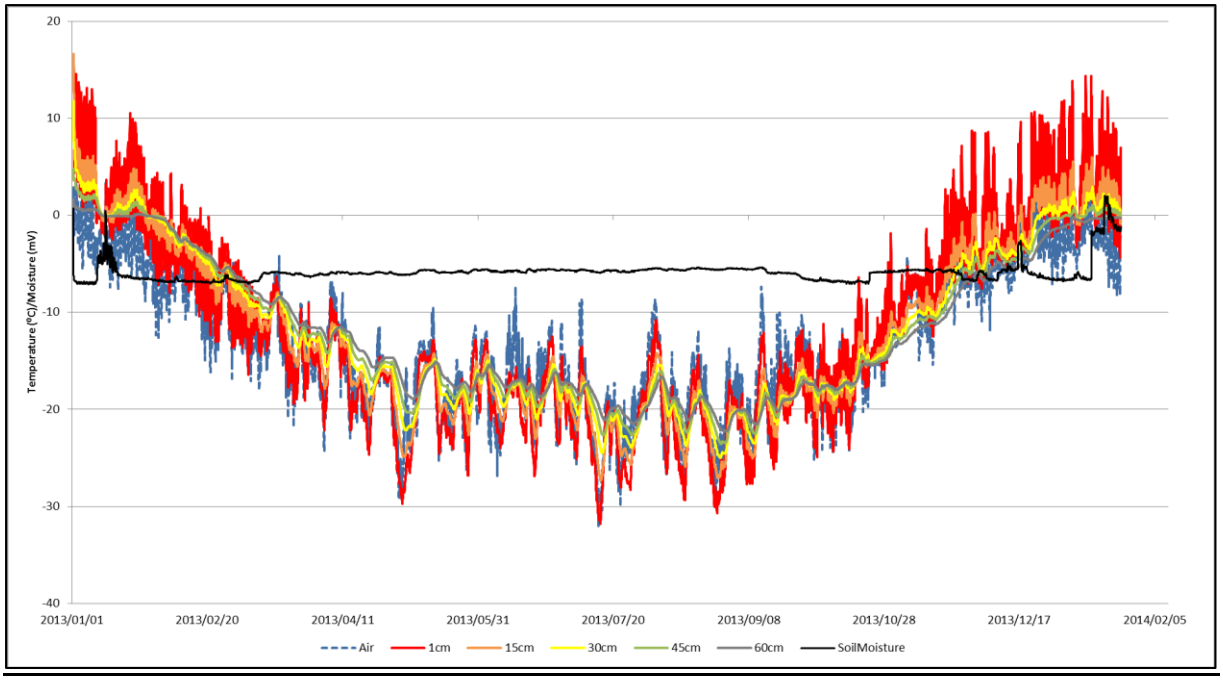

Figure 65: Borehole (60cm) data for the Robertskollen site from January 2013 to January 2014.

A summer period from 16th December 2013 to 9th January 2014 allows for a detailed view of the data (Fig. 66). On the 18th, 19st and 20th of December 2013 and the 6th to the 8th of January 2014 all the data shows a depression which represents a snow storm/cloud cover events. The graph clearly shows the difference between the air temperature and ground temperatures.

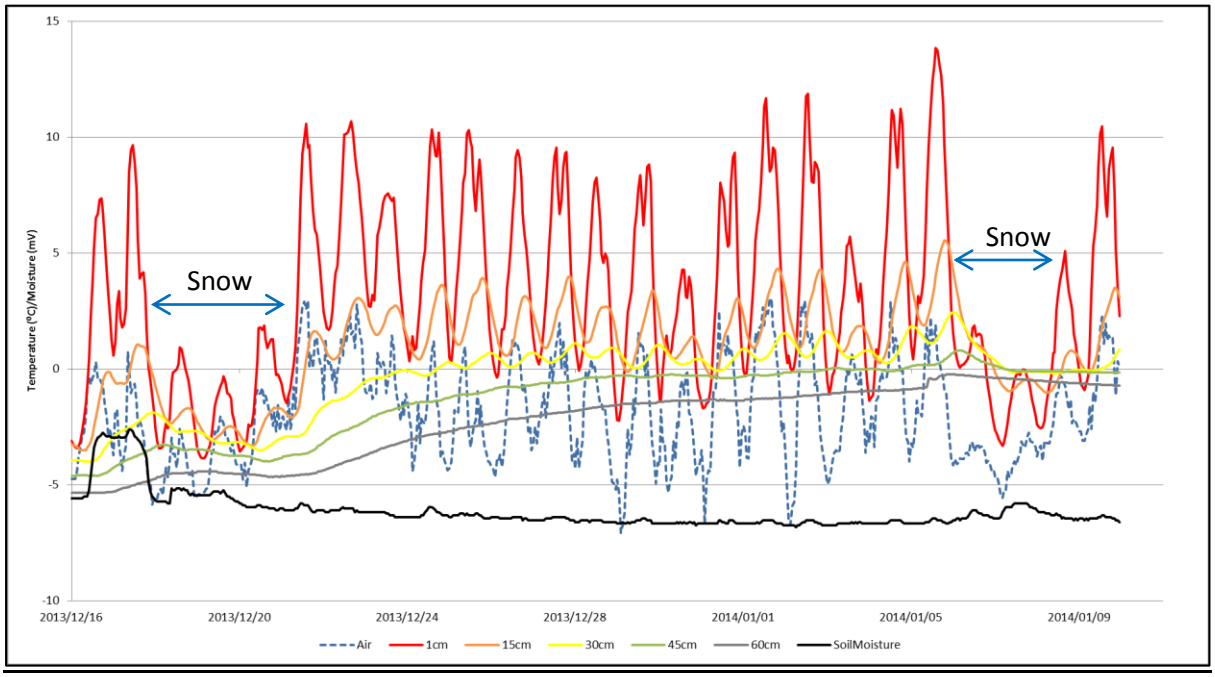

Figure 66: Borehole (60cm) data for the Robertskollen site from 16th December 2013 to 9th January 2014.

The graph and data is limited for such a warm site like Robertskollen as the 2013 depth falls below the 60cm mark (estimated at 66cm) (Fig. 67).

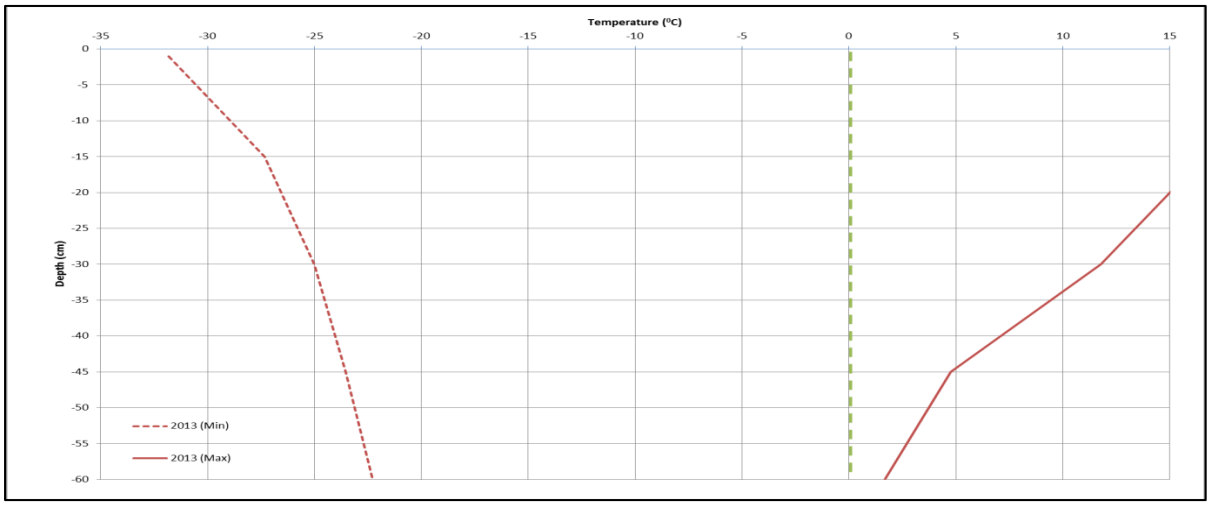

Figure 67: Depth profile graph for the Robertskollen site showing the depth profile for 2013.

4.4.2.2. 20cm borehole results

The zero-degree isotherm depth is was estimated at 66cm below the ground surface which could mean that more frequent shallow sensors are irrelevant for this area (Fig. 67). Robertskollen is an exceptionally warm study site and therefore as seen in Figure 67 and 68, the calculated zero-degree isotherm depth is limited by the data. The depth of the zero-degree isotherm was often cut short at the 40cm mark due to the lack of data (black lines). It is clear that only during summer (November to February) this site experiences cycles over the zero-degree isotherm. Air temperature fluctuates the most only during the winter months in comparison to the ground thermal data but during the summer period the air temperature drops to the minimum temperature only and the ground surface temperature peaks at the maximum temperatures due to reasons mentioned previously. Summer air temperature peaked at 5.94°C (10/01/2014) and on the same day was the maximum ground temperature reaching 22.84°C. The minimum air temperature was -31.02°C (14/07/2013) and on the same day was the coldest recorded ground temperature at -33.67°C.

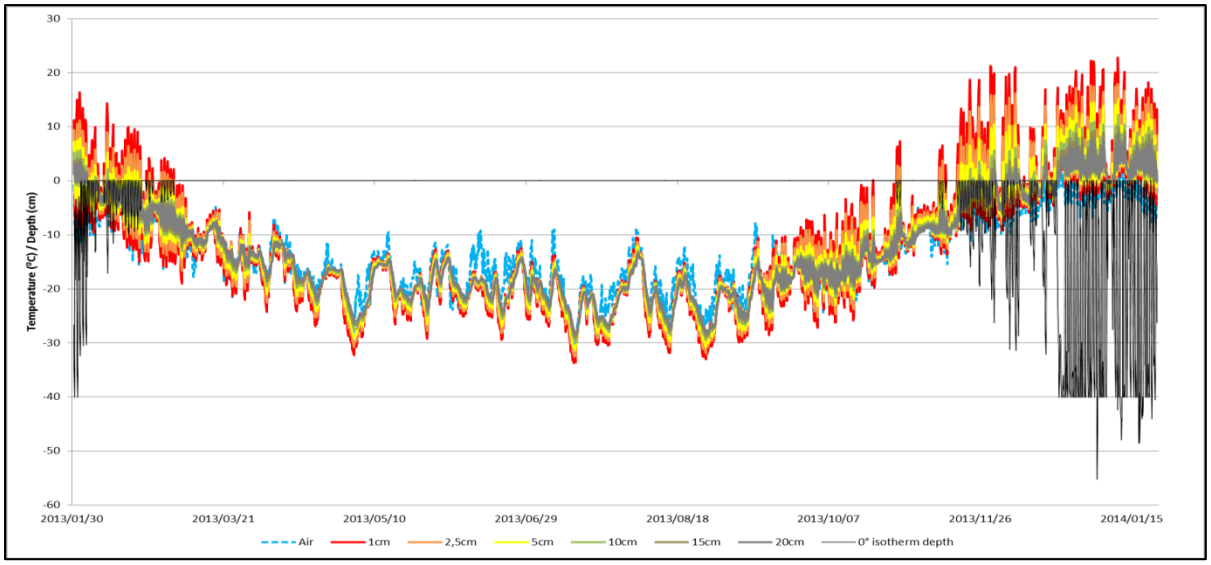

Figure 68: Borehole (20cm) data for the Robertskollen site from January 2013 to January 2014. The graph also shows the zero-degree isotherm depth displayed in black.

A view of this data over a summer period is presented (Fig. 69). The depth of the zero-degree isotherm can be seen in black. This data shows how the peaks in ground temperature (1cm and 2.5cm) are directly related to the depth of the zero-degree isotherm. Furthermore, it illustrates how the air temperature seems to follow a general trend in peaks with the ground surface temperatures but is not as significantly proportional to the overall zero-degree isotherm depth. Similarly to the previous study sites, on the 6th there was a snow storm event which dampened the effects of temperature and radiation on the active layer for three days and can be seen by the horizontal black line on the graph.

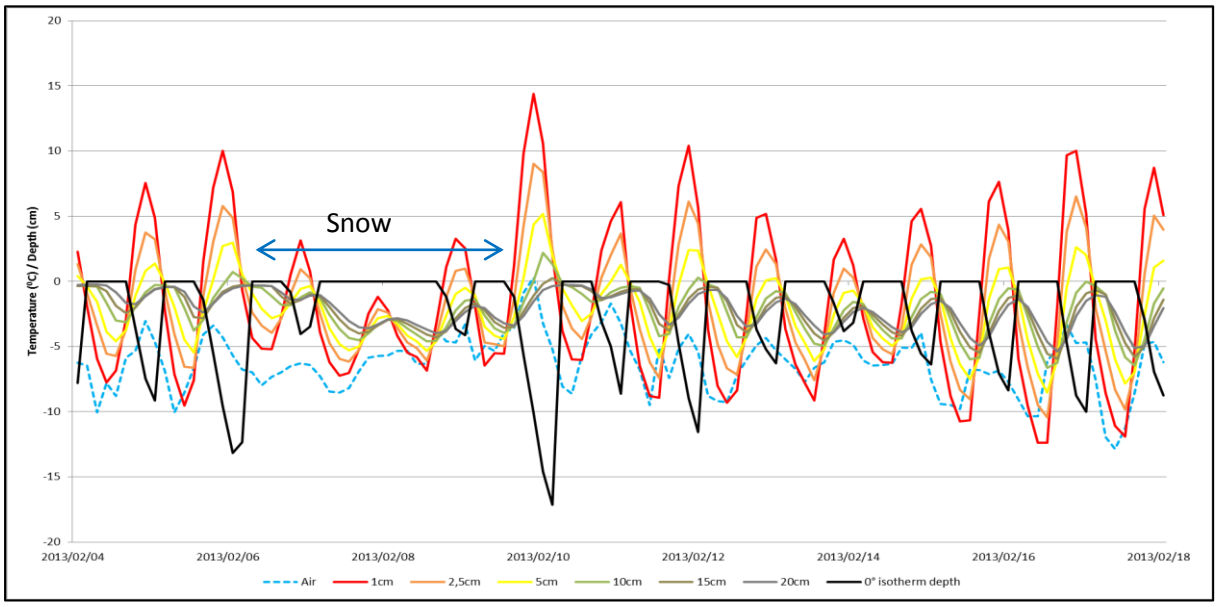

Figure 69: Borehole (20cm) data for the Robertskollen site from 4th February 2013 to 18th February 2013 (15 day summer period). The graph also shows the zero-degree isotherm depth displayed in black.

4.5. Vesleskarvet

4.5.1. Topographical Analysis

Eight perspectives are presented of the Vesleskarvet study area taken after the 3D model was created from the aerial images (Fig. 70). Vesleskarvet is a blockfield site situated on a windswept nunatak. The only features of interest at this site found were sorted and unsorted ground found during fieldwork. Unlike the other sites, a helicopter was used to take aerial images with two GoPro cameras mounted to the frame and Cannon 600D SLR cameras were manned on either side of the helicopter for high quality images. All four cameras were set to one second time lapse intervals. Control points (flags) were set in place before the flight and therefore allowed for the software to georeference the DEM. On the boarder of the model and cliff line areas there was a lack of image overlay which can be seen by the black triangles (Fig. 70).

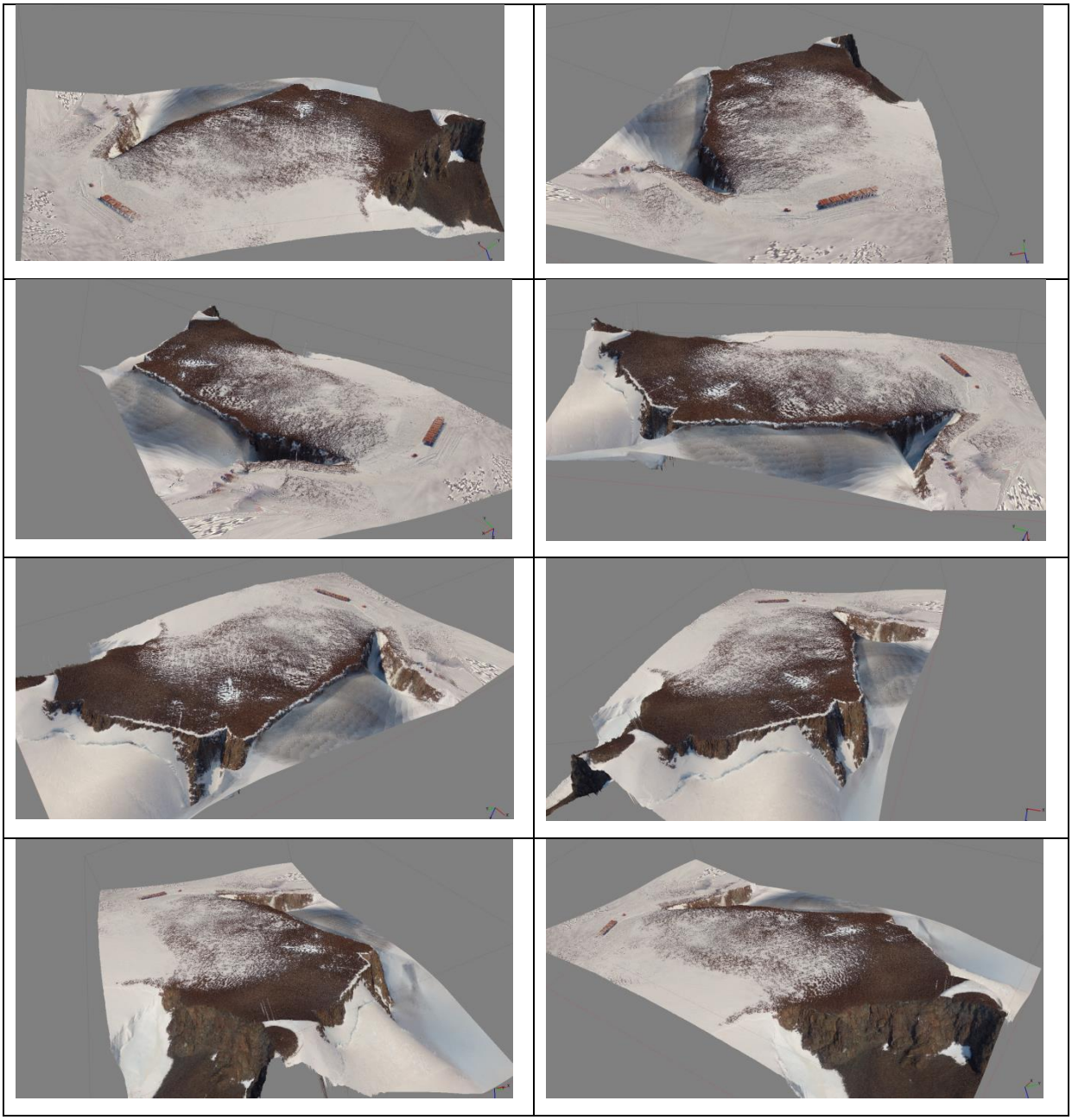

Figure 70: Model representation of the Vesleskarvet logger study area showing the topographic area of interest from four perspectives.

4.5.2. Ground Thermal Analysis

4.5.2.1. 60cm borehole results

The winter and summer months' maximum and minimum recorded temperatures can be seen in Figure 71. During the winter months the air temperature fluctuates the most in comparison the ground temperatures data but during the summer period the air temperature drops to the minimum temperature only and the ground surface temperature peaks at the maximum temperatures due to reasons mentioned previously. Summer air temperature peaked at 6.77°C (22/12/2010) with maximum ground temperature reaching 14.28°C (2013/01/06). The minimum air temperature was -40.78°C (07/07/2010) and on the same date was the coldest recorded ground temperature at -39.66°C. Spikes in the soil moisture level can also be seen shortly after the 1cm ground temperature spikes. The trend line shows a general increase in temperature over the five years of data collected. Due to data logger errors there is no data for the top three sensors for 2013.

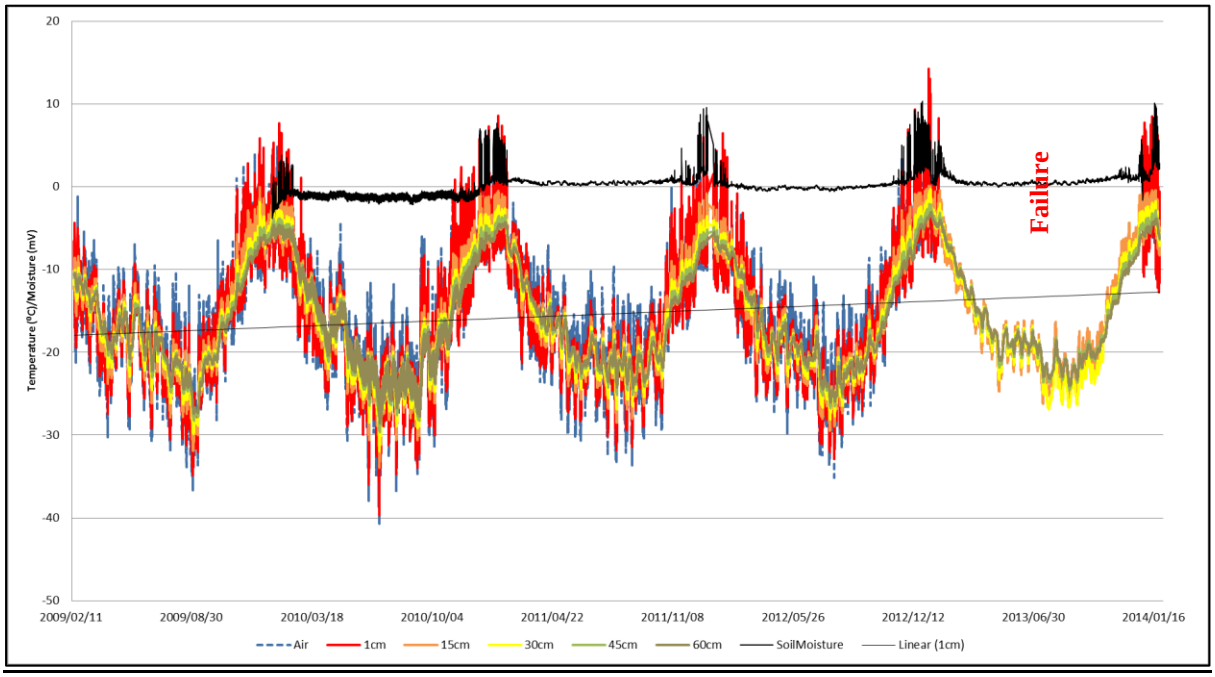

Figure 71: Borehole (60cm) data for the Vesleskarvet site from January 2009 to January 2014.

A summer period from 16th December 2013 to 9th January allows for a detailed view of the data (Fig. 72). On the 6th of January 2014 there was a snowstorm event which is shown by a depression on the graph. The graph clearly shows the difference between the air temperature and ground temperatures. Furthermore the lag effect can be seen in 1cm peak after the air temperature peak.

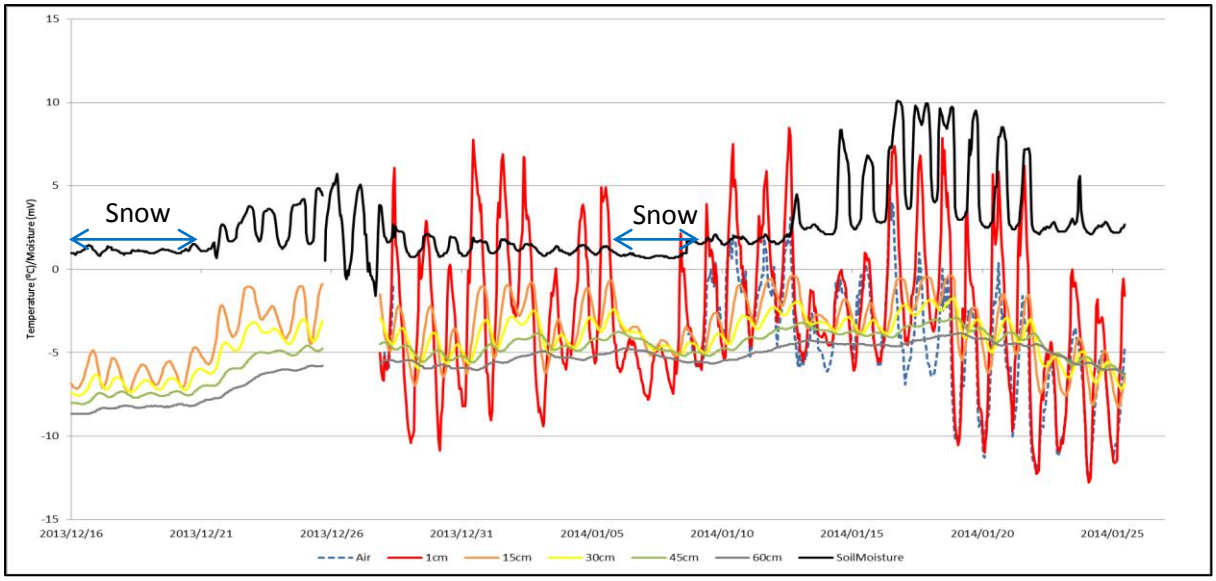

Figure 72: Borehole (60cm) data for the Vesleskarvet site from 16th December 2013 to 25 January 2014.

The short horizontal red line shows that the zero-degree isotherm was at a depth of 14.5cm below the ground level for all the recorded years (Fig. 73). This is unique from the other sites, as the depth has fluctuated over the years with a general trend in deepening of the zero-degree isotherm. The 2013 minimum data is missing due to data logger errors.

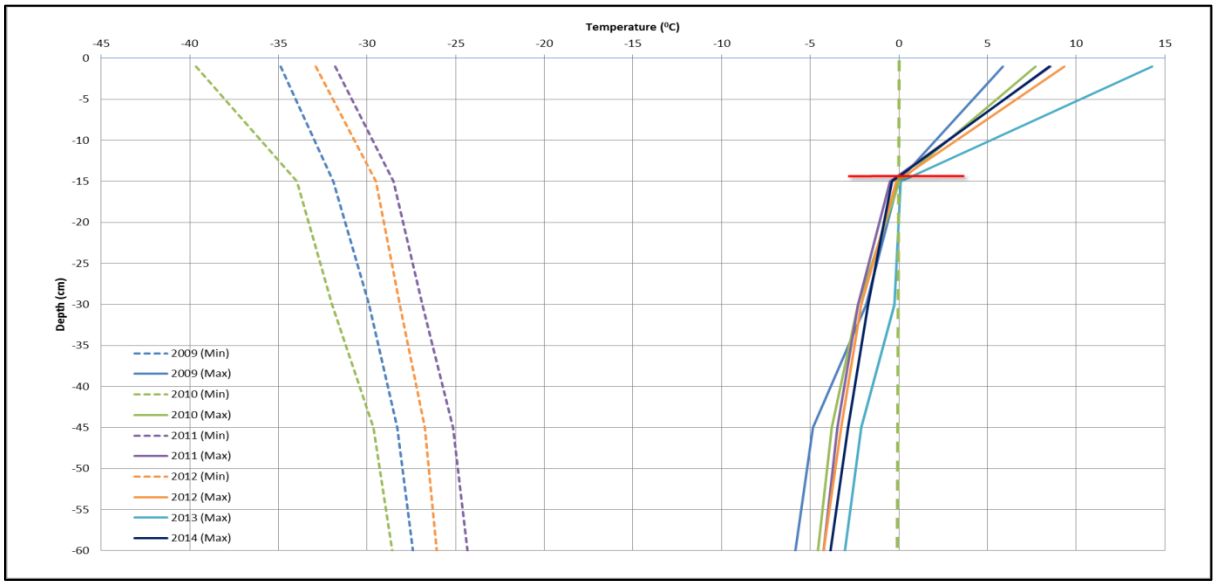

Figure 73: Depth profile graph for the Vesleskarvet site showing the depth profiles for the years 2009 to 2014.

The air temperature comparison to zero-degree isotherm depth graph is presented and similarly to Flårjuven it can be seen that there is no relation between the two (Fig. 74). A general increasing in zero-degree depth can be seen over the years with 2013 having an exceptionally high recording, which is similar to that of the Troll site readings.

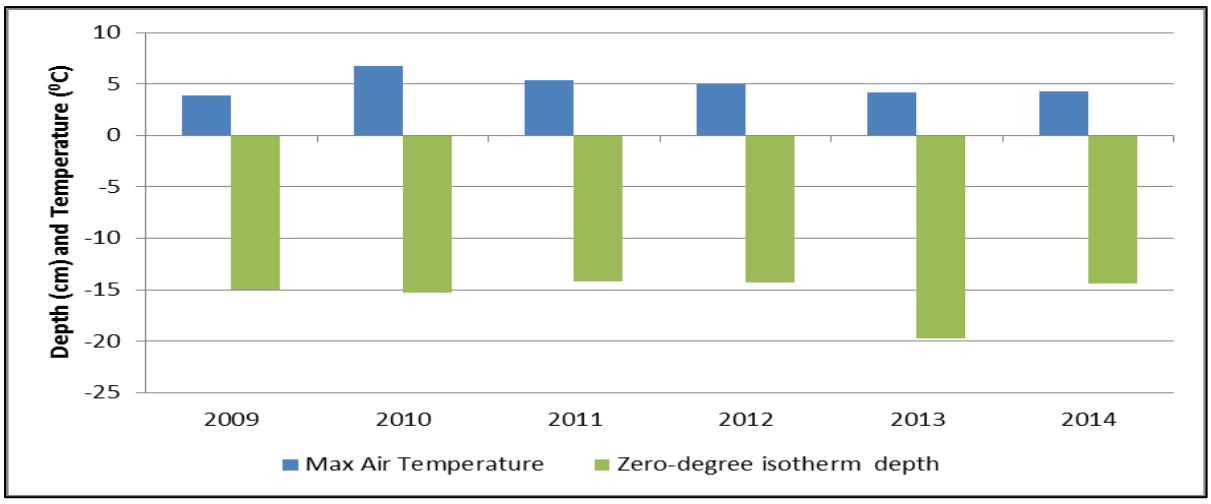

Figure 74: The air temperature data comparison to the zero-degree isotherm depth for the Vesleskarvet study site from the years 2009 to 2014.

4.5.2.2. 20cm borehole results

The zero-degree isotherm depth is 14.5cm below the ground surface (Fig. 75) which could mean that more frequent shallow sensors would be more appropriate for this area. The depth of the zero-degree isotherm is presented in black (Fig. 75). It is clear that only during summer (November to February) this site experiences cycles over the zero-degree isotherm. Summer ground temperature peaked at 14.01°C (01/01/2014). The zero-degree isotherm depth peaks are directly related and proportional to peaks in ground temperature. The maximum depth of the zero-degree isotherm was 17.26cm on the 5th of January 2014 which is a deeper depth than the 60cm borehole data has presented. Closer spacing of the sensors (5cm spacing) has shown to be important for colder sites.

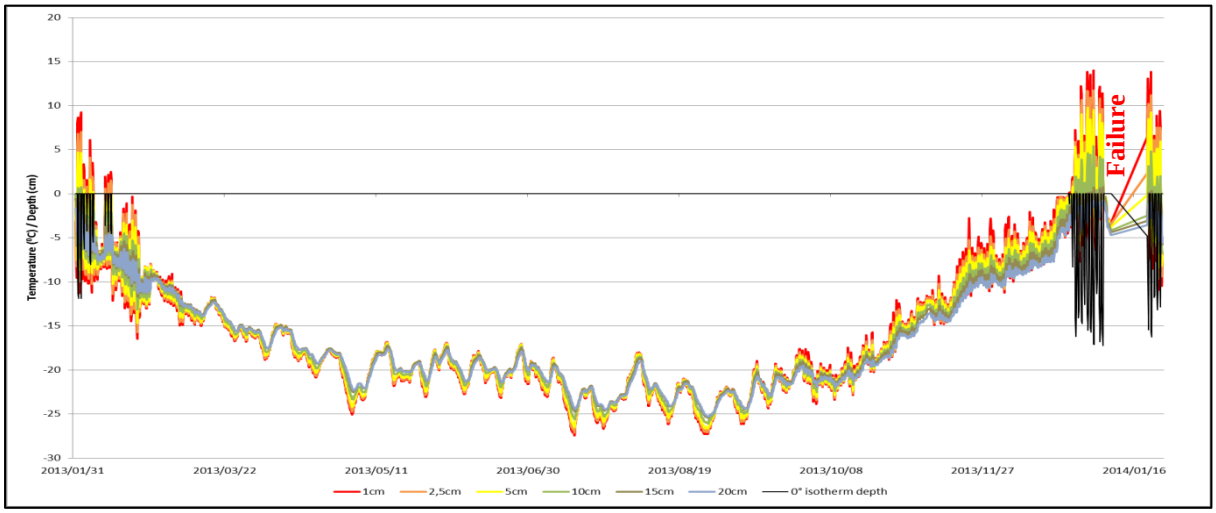

Figure 75: Borehole (20cm) data for the Vesleskarvet from January 2013 to January 2014. The graph also shows the zero-degree isotherm depth displayed in black.

4.6. Troll

Troll contains two areas of interest for this study. Site 1 has a borehole dating back to 2007 but this area has been potentially affected by the construction of buildings and therefore cannot accurately represent the area. The second borehole site was setup in a more represented area for the site (further up the slope).

4.6.1. Topographical Analysis

Four perspectives are presented of the Troll study area (logger site) and three perspectives are presented for the North East polygon area taken after the 3D model was created from the aerial images (Fig. 76 and 77). It was possible to identify the polygon features in the 3D view which could not be obtained from the 2D mosaicked images alone. Unfortunately this was the trial and error site for the UAV operations and control points were not set in place before the flights. However, it was possible to obtain rough GPS coordinates from Google Earth and although this model is not accurate, it was still possible to calculate relative polygon areas. The Troll site contains the highest concentration of polygon formations and they are easy to delineate through 3D mapping.

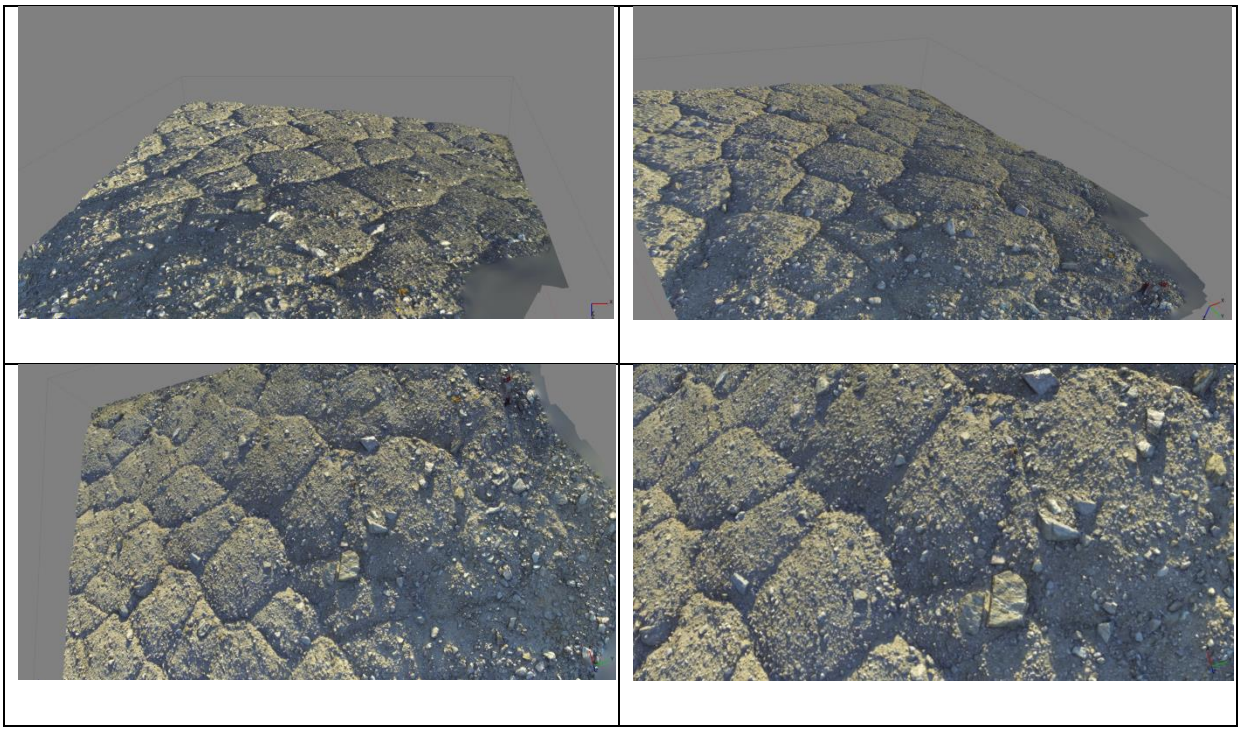

Figure 76: Model representation of the Troll logger study area showing the topographic area of interest from four perspectives.

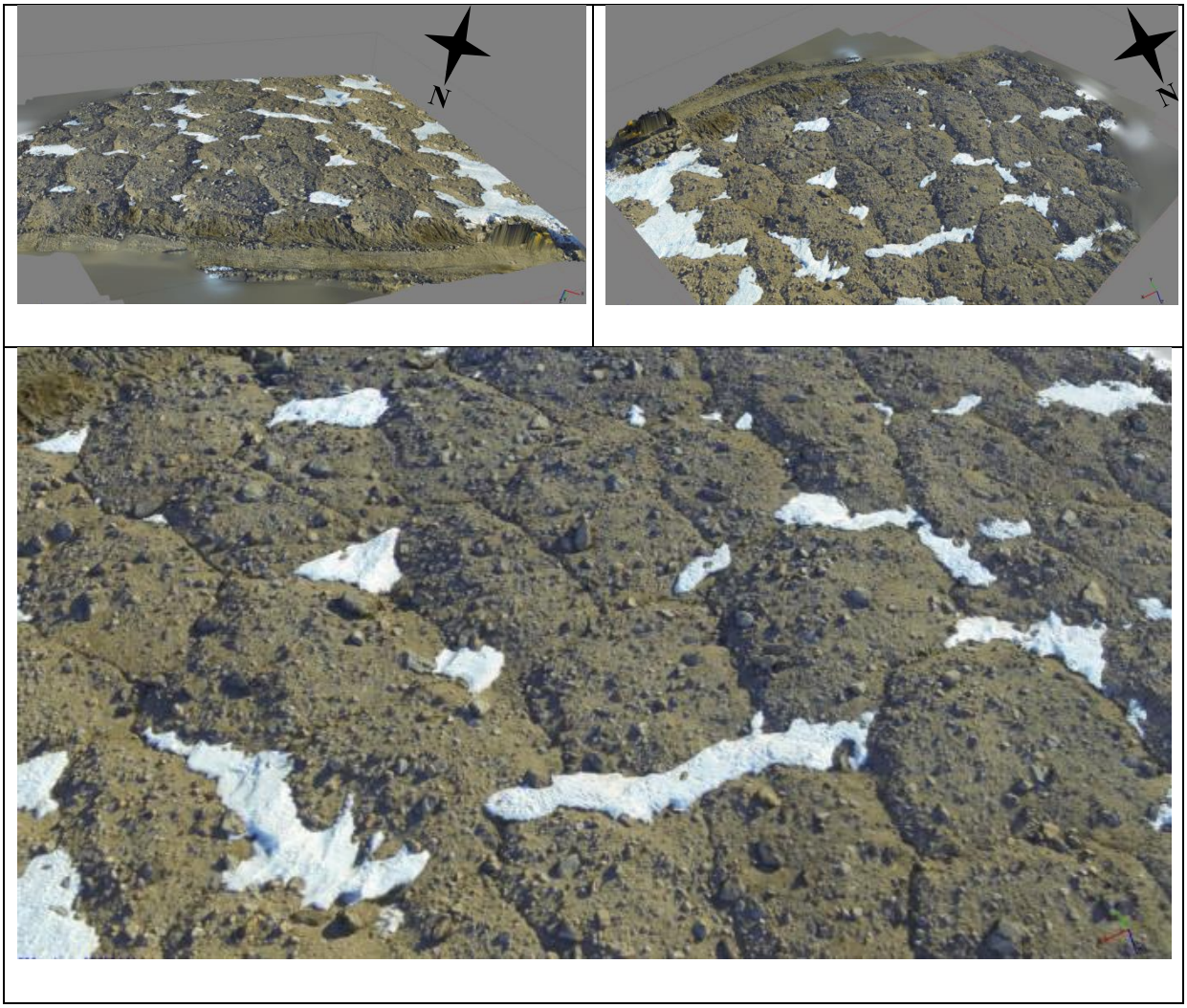

Figure 77: Model representation of the Troll NE study area showing the topographic area of interest from three perspectives.

The polygon formations are easy to delineate as there is direct shading noticeable where the larger rocks form which defines the perimeter. A visual for the area of Troll can be seen in Figure 78 which contains polygon features. A total of 44 polygons were digitised, none of which were sampled in the field. The graduated colours represent the area of the polygons (m^2) with green representing a small area and red representing large polygons.

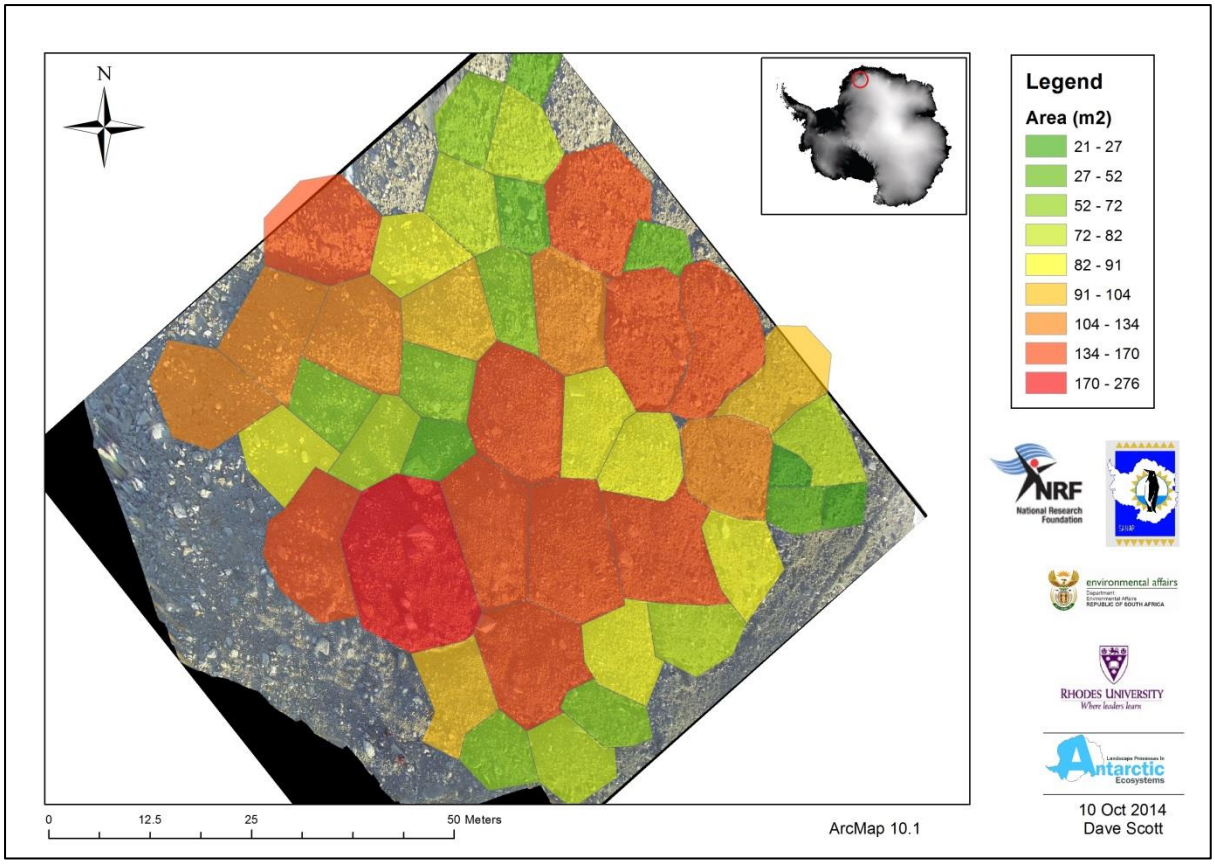

Figure 78: Map showing delineated polygons for the Troll site done in post fieldwork desktop analysis. The graduated colours represent area of polygons (m²) with green showing small area and red representing large polygons.

The polygon sample size was 44 with a minimum area of 21.79m², a maximum area of 276.53m² and a mean area of 101.26m² (Fig. 79). The statistics show that there is much variation in the size of the landscape features found on the Troll study site and become the baseline for change over time.

Troll Polygons Area (m²) Statistics

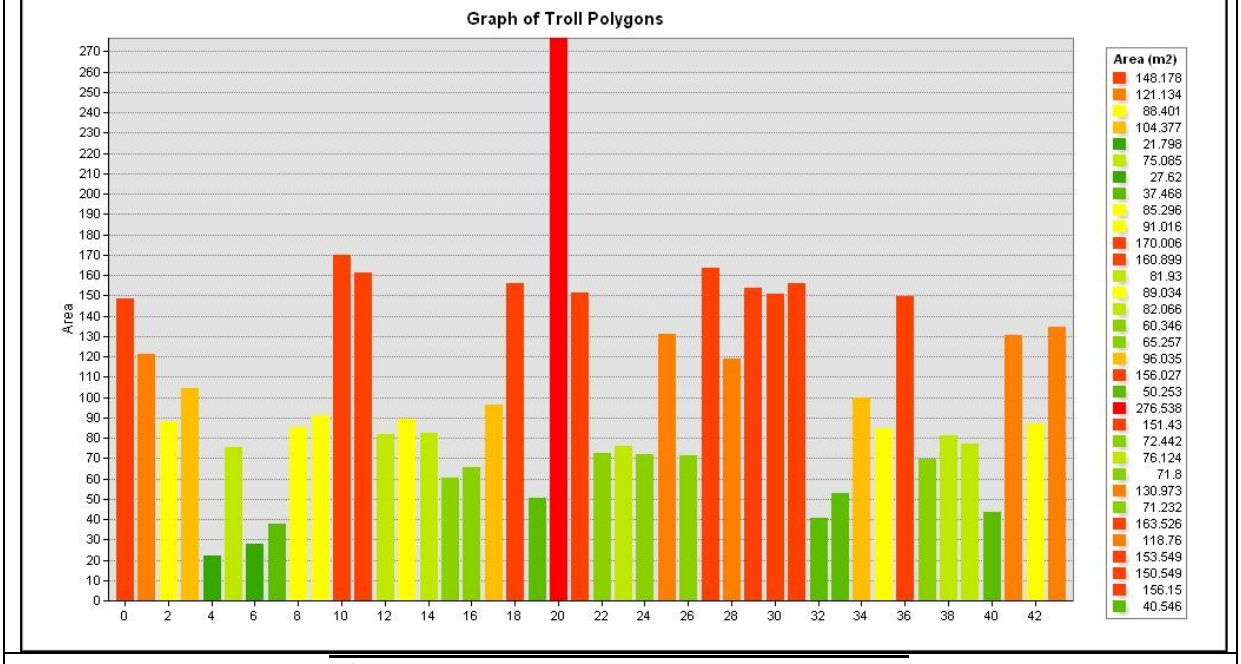

Count:	**44**
Minimum:	21.79
Maximum:	276.53
Sum:	4455.58
Mean:	101.26
Standard Deviation:	48.44

Figure 79: Graph and statistics of the Troll polygon areas determined on ArcMap from aerial photographs.

4.6.2. Ground Thermal Analysis

4.6.2.1. Troll Site 1 (1st logger site)

4.6.2.1.1. 2m borehole results

The winter and summer months' maximum and minimum recorded temperatures can be seen in Figure 80. During the winter months the air temperature fluctuates the most in comparison to the ground thermal data but during the summer period the air temperature drops to the minimum temperature only and the top ground temperature peaks at the maximum temperatures due to reasons mentioned previously. The summer air temperature peaked at 8.76°C (10/11/2014) with maximum ground temperature reaching 6.16°C (06/01/2013). The minimum air temperature was -49.29°C (23/06/2008) and the coldest recorded ground temperature at -36.14°C (26/07/2012). Spikes in the soil moisture level can also be seen shortly after the 1cm ground temperature spikes. The trend line shows a general increase in temperature over the seven years of data collected. Due to data logger errors there is no data for the second half of 2009 and 2013.

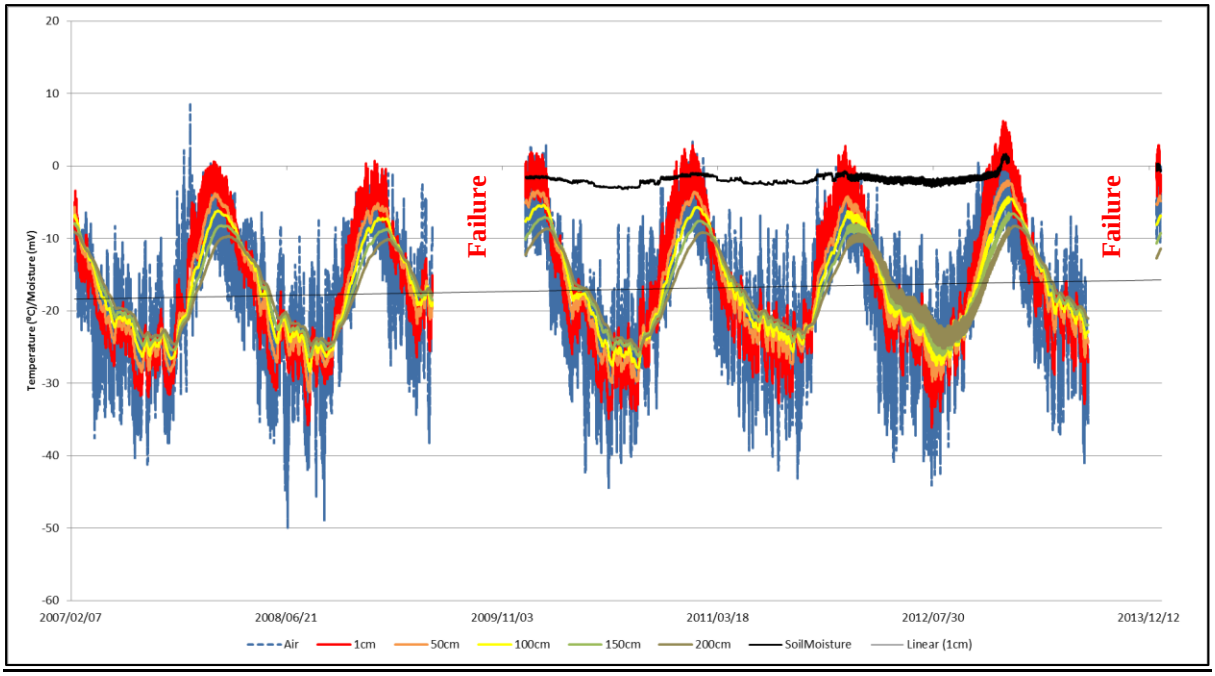

Figure 80: Borehole (60cm) data for the Troll site (Logger 1) from January 2007 to January 2014.

A summer period from 29th December 2013 to 8th January 2014 allows for a detailed view of the data (Fig. 81). On the 6th of January 2014 there was a snowstorm event which is shown by a depression on the graph. The graph clearly shows the difference between the air temperature and ground temperatures. Furthermore the lag effect can be seen in the 1cm peak after the air temperature peak.

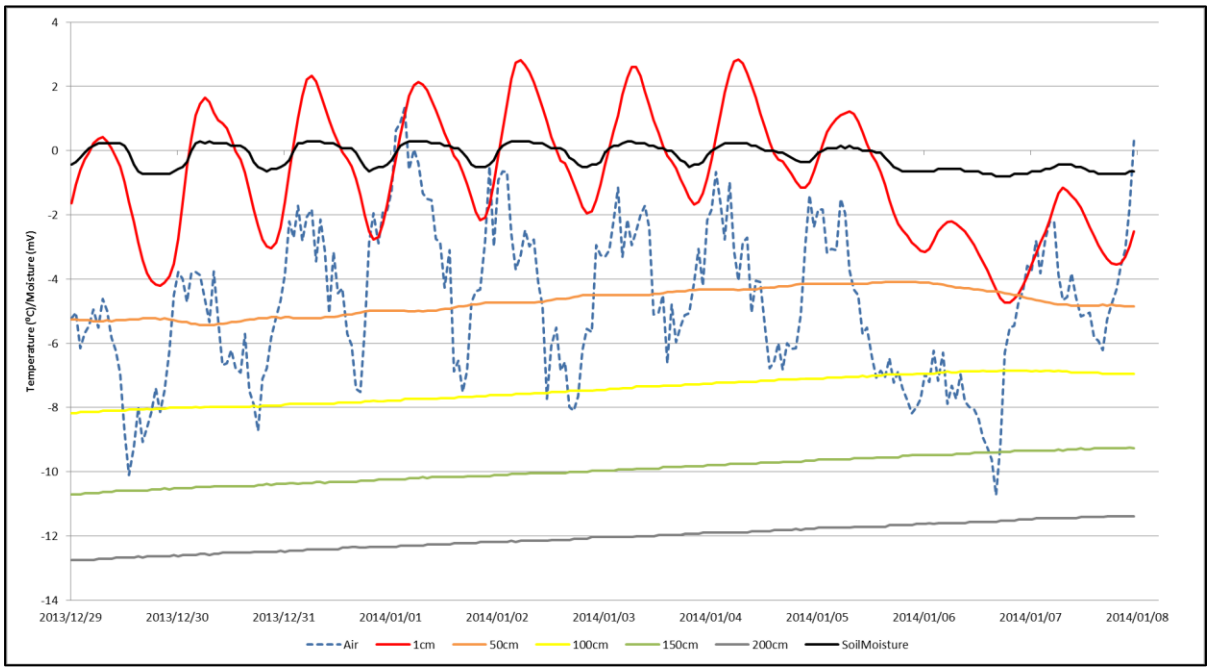

Figure 81: Borehole (60cm) data for the Troll site (logger 1) from 29th December 2013 to 8th January 2014.

The short horizontal red lines show that the zero-degree isotherm was shallowest in 2007 at only 1.2cm below the ground surface and in 2012 it was at its maximum depth of 25cm (Fig. 82).

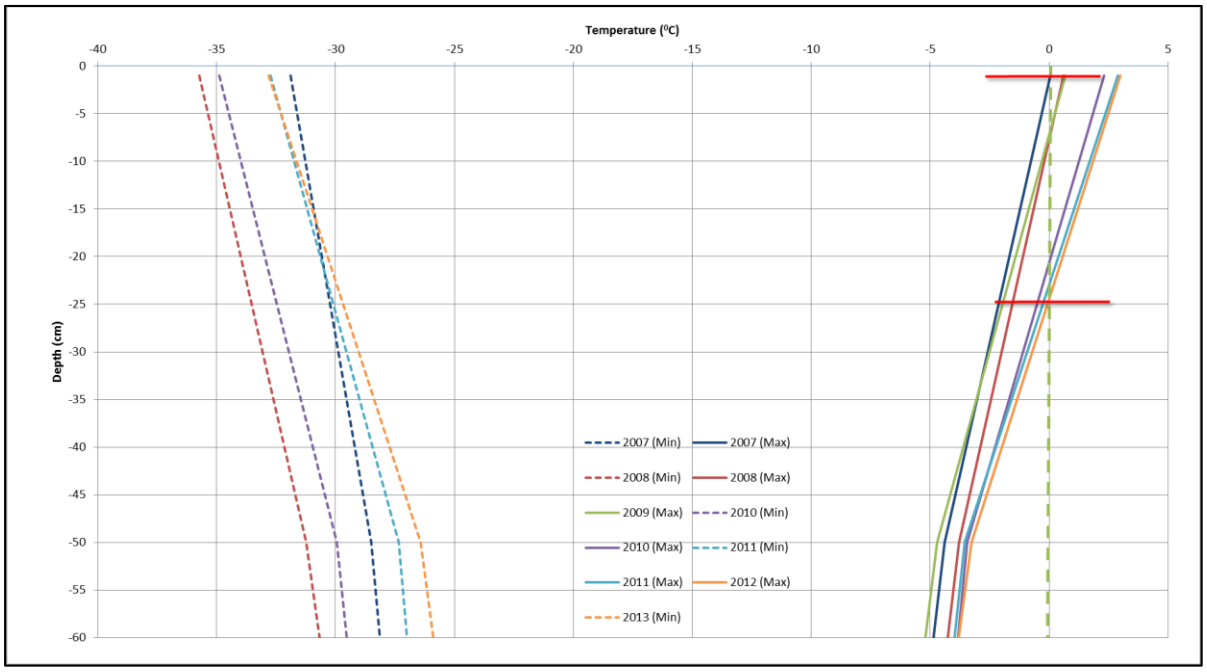

Figure 82: Depth profile graph for the Troll site (logger 1) showing the depth profiles for the years 2007 to 2014.

The air temperature comparison to the zero-degree isotherm depth graph is presented and similarly to Flårjuven it can be seen that there is no relation between the two (Fig. 83). A depth increase in zero-degree can be seen over the years with 2013 having an exceptionally high recording.

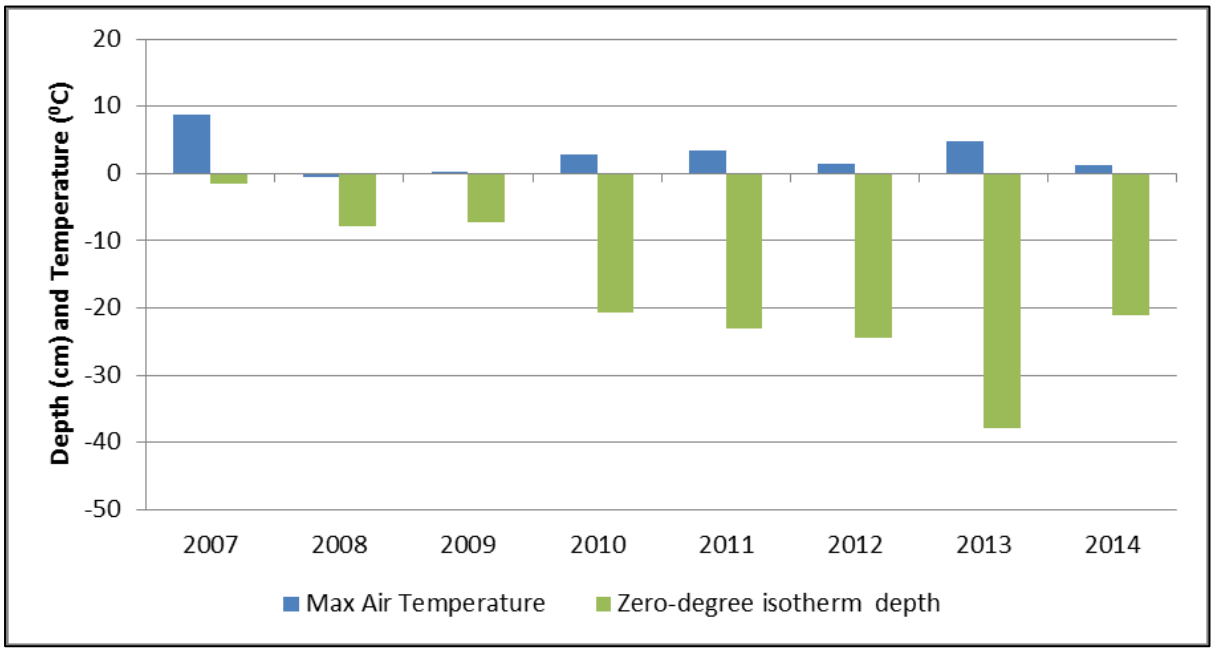

Figure 83: The air temperature data comparison to the zero-degree isotherm depth for the Troll study site (logger 1) from the years 2007 to 2014.

4.6.2.2. Troll Site 2 (2nd logger site)

4.6.2.2.1. 2m borehole results

The winter and summer months' maximum and minimum recorded temperatures can be seen in Figure 84. During the winter months the air temperature fluctuates the most in comparison to the ground thermal data but during the summer period the air temperature drops to the minimum temperature only and the ground surface temperature peaks at the maximum temperatures due to reasons mentioned previously. Interestingly in comparison to the other sites this graph shows that the ground temperature doesn't reach the maximum temperatures which are contradictory to the other data. Summer air temperatures peaked at 4.64°C (01/01/2014) with maximum ground temperature reaching -0.95°C (04/01/2014). The minimum air temperature was -40.45°C (15/07/2013) and the coldest recorded ground temperature at -31.65°C (29/08/2013). The soil moisture appears to be faulty as displayed by the jumping of the data and due to it not following any trend.

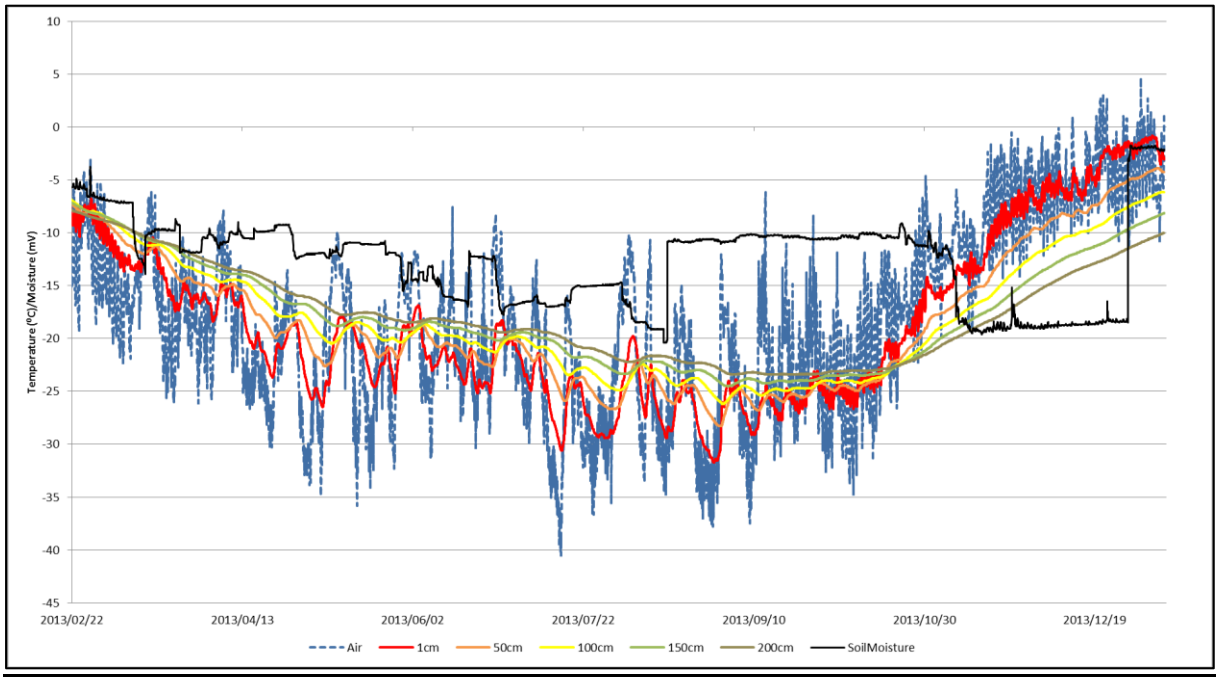

Figure 84: Borehole (60cm) data for the Troll site (logger 2) from January 2013 to January 2014.

A summer period from 16th December 2013 to 9th January 2014 allows for a detailed view of the data (Fig. 85). On the 6th of January 2014 there was a snowstorm event which is shown by a depression on the graph. The graph clearly shows the difference between the air temperature and ground temperatures. Furthermore the lag effect can be seen in the 1cm peak after the air temperature peak.

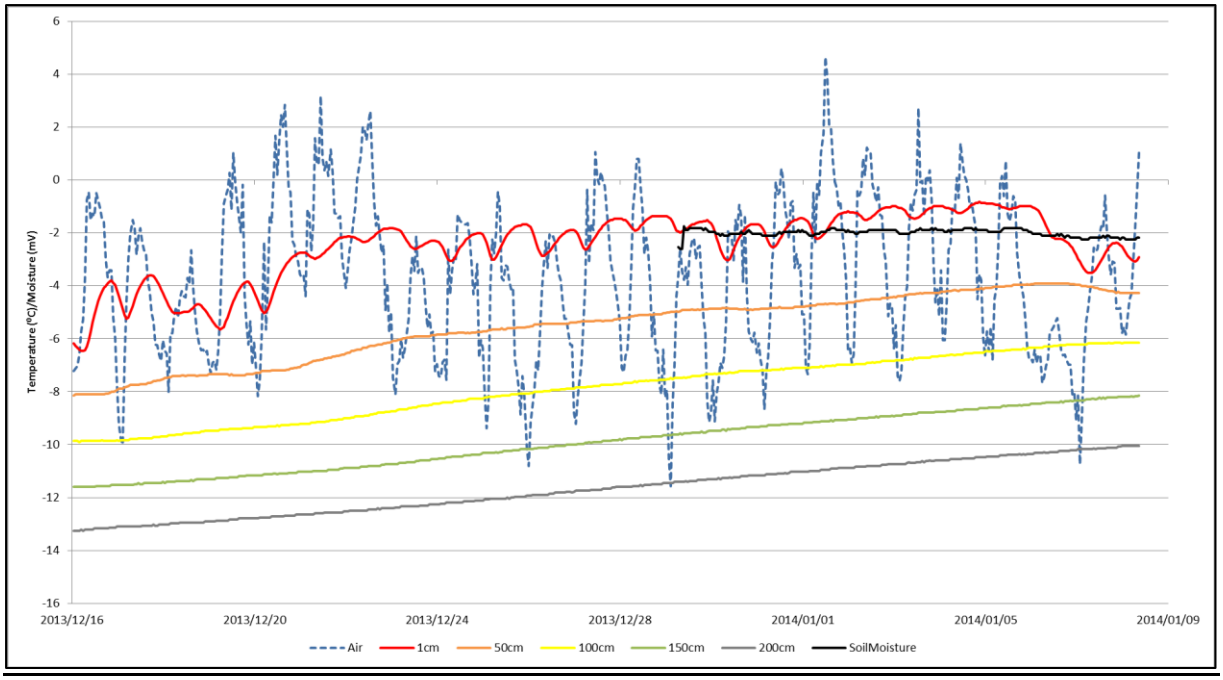

Figure 85: Borehole (60cm) data for the Flårjuven site (logger 2) from 16th December 2013 to 9th January 2014.

4.6.2.3. 20cm borehole results

Two 20cm borehole loggers were installed near the 2m borehole logger sites. One logger was set inside a polygon crack with the other in the centre of the polygon. The zero-degree isotherm falls into the 2cm to 25cm depth range (Fig. 82, pg. 88) which could mean that more frequent shallow sensors would be more appropriate for this area. The depth of the zero-degree isotherm is presented in black (Fig. 86). It is clear that only during summer (November to February) this site experiences cycles over the zero-degree isotherm. Air temperatures fluctuate the most during the winter months in comparison to the ground thermal data but during the summer period the air temperature drops to the minimum temperature only and the ground surface temperature peaks at the maximum temperatures due to reasons mentioned previously. The summer air temperature peaked at 3.17°C (21/12/2013) with maximum ground temperature reaching 20.8°C in the centre and 22.46°C in the crack (28/12/2013). The minimum air temperature was -40.9°C (15/07/2013) with minimum ground temperature reaching -40.21°C in the centre and -41.07°C in the crack (15/07/2013). The zero-degree isotherm depth peaks are directly related and proportional to peaks in ground temperature. The maximum depth of the zero-degree isotherm was 23.21cm in the centre and 18.13cm in the crack of the polygon (22/01/2013).

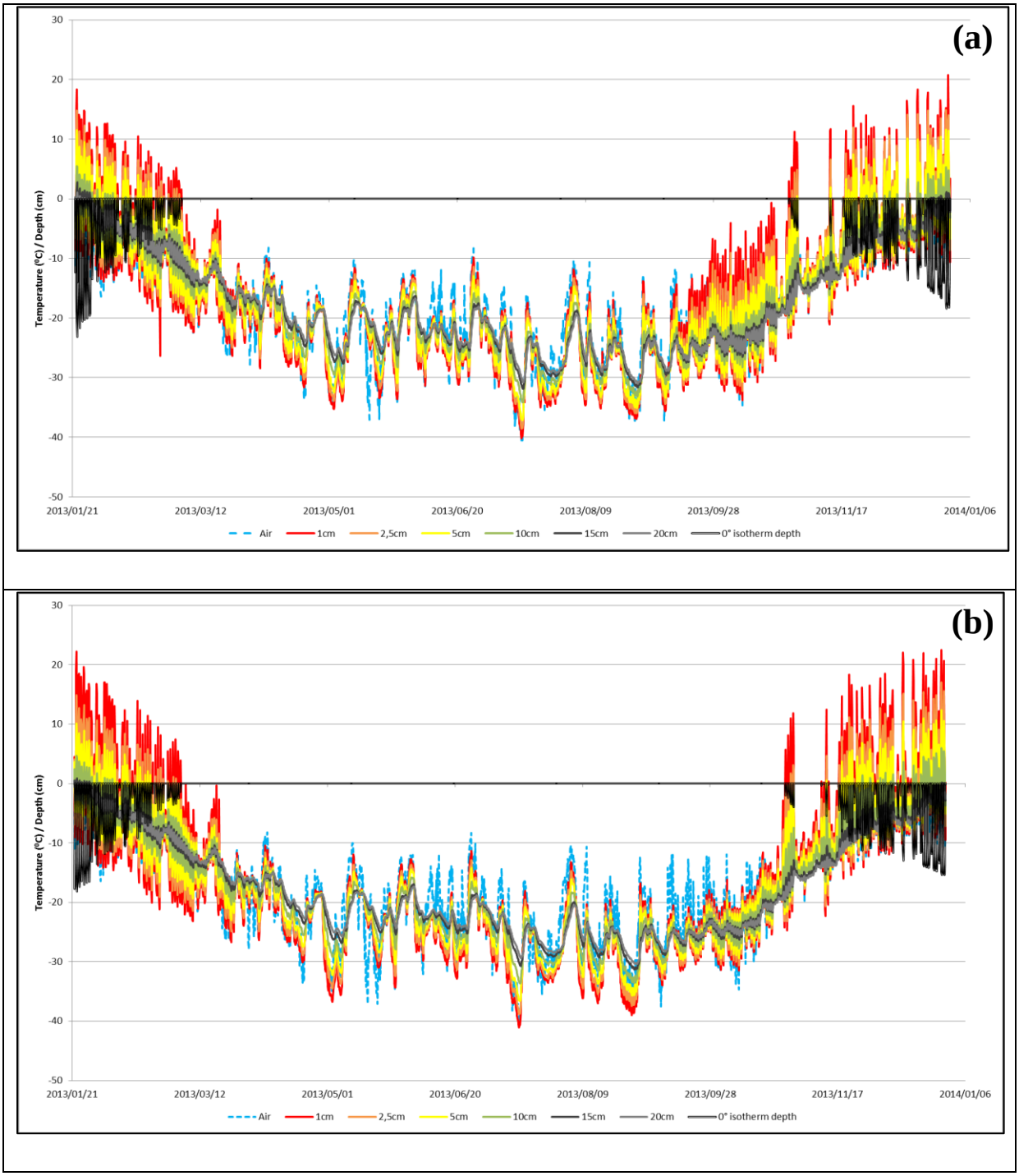

Figure 86: Borehole (20cm) data for both the Troll site, centre (a) and crack (b), from January 2013 to January 2014. The graphs also show the zero-degree isotherm depth displayed in black.

A view of high frequency logging of the crack and centre is presented for a two day period (Fig. 87). The polygon centre data is shown in a solid line and the crack data is shown in a dotted line. The 1cm, 2.5cm and 10cm depth data reaches a higher temperature in the crack but at a depth of 15cm and 20cm it is the centre which shows the higher temperature. At a depth of 5cm the temperature of both

the crack and centre seem to be similar. In an overall view, the centre of the polygon tends to peak before the crack.

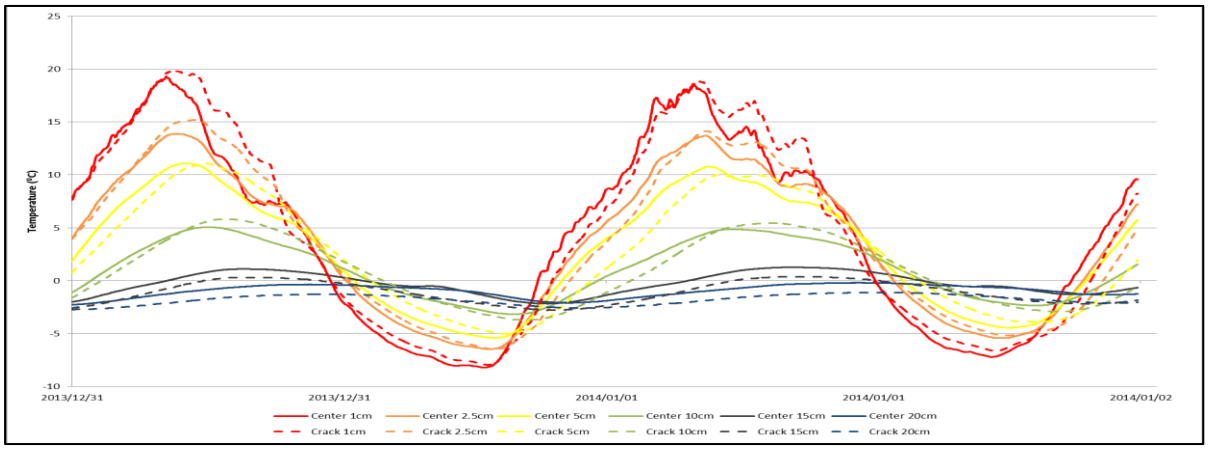

Figure 87: High frequency data for the duration of two days at the Troll study area showing the superimposed crack and centre 20cm borehole data.

4.6.3. Polygon Analysis

Field analysis was done on 30 randomly selected polygons at the Troll study area. A summary table of these results can be seen in Appendix D. A shortened version is presented in Table 4. There was an 83.33% occurrence of snow in the cracks of the 30 sampled polygons. The mean length of the A-axis was 15.03m with a maximum of 30m. Of the polygons sampled, 50% of the A-axis measurements fell had the same bearing as the hill slope. The mean bearing of the A-axis was 161.8°. The mean slope gradient was 13.72°, the mean perimeter was 40.21m and the average height of the polygons was 1704.38m.a.s.l. Finally, the soil moisture was higher in the centre than in the cracks. Soil samples were also collected from the crack and the centre of each polygon and the results are presented in Appendix F. Figure 88 shows the average particle size distribution results for the Troll polygon crack and centre samples. The particle size is smaller in the centre than in the crack of these polygon samples.

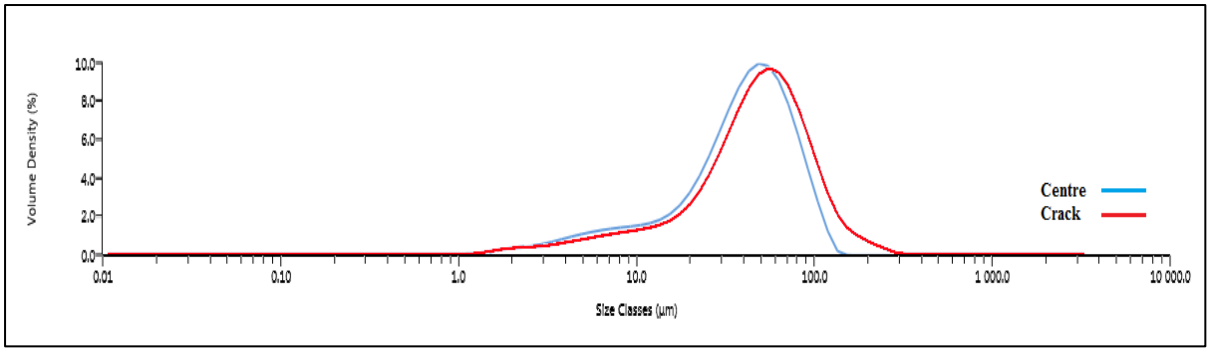

Figure 88: Average particle size distribution graph for the Troll polygon crack and centre samples.

Table 4: Polygon field sample data summary for the Troll study area.

	A Axis		B Axis					Soil Moisture	
	Length (m)	**Orientation (magnetic, degrees)**	**Length (m)**	**Orientation (magnetic, degrees)**	**Slope Gradient (degrees)**	**Perimeter (m)**	**Height (m.a.s.l.)**	**Centre**	**Crack**
Mean	15.03	147.62	11.31	192.42	13.72	40.21	1704.38	2047.33	1638.17
Max	30	350	20	355	27	66.20	2100	2210	2140
Min	7.20	0	5	0	8	18.30	1175	2010	1123
Standard Deviation	5.09	146	3.94	163.60	4	11.93	345.93	36.67	442.37

CHAPTER 5: Discussion and Conclusion

To better understand the circumstances where polygons, terraces, and sorted and non-sorted ground occurs, study area comparisons will be presented in this section. Firstly, available imagery for WDML and the use of an Unmanned Aerial Vehicle (UAV) in Antarctica will be discussed and potential issues highlighted. Furthermore, a discussion over camera types and aerial vehicle types will be presented. Thermal data comparisons are in the form of figures and tables for ease of interpretation. All of the sites contained data for 2013 and therefore this year will be used for comparative purposes across all of the sites. However, in order to understand potential variables in the years; Flårjuven, Troll and Vesleskarvet will be used as they contain up to seven years of recorded thermal data. Landscape features similarities across sites will be compared. Finally, recommendations for future work and concluding remarks are presented.

5.1. Landscape Analysis

One of the techniques used to study landscape features was by use of an Unmanned Aerial Vehicle (UAV). An assessment of current available imagery is needed for comparitive purposes. Authors have expressed the need for ongoing monitoring and a setup of baseline data and this is where this project is designed to fill that gap (Bockheim, 1995; Bockheim and Hall, 2002; Bockheim et al., 2008; Hallet et al., 2011; Guglielmin, 2012).

5.1.1. Available imagery

There is a lack of aerial data for most of the areas of interest for this project. Landsat images and comparative photographs are used to demonstrate the need for a better form of aerial photography for the WDML area (Fig. 89). This is where the UAV fits in. Available imagery is of a very low quality as shown in Figure 89 and the UAV was built to mitigate this issue. The UAV was specifically designed and built to deal with the cold climatic conditions and be able to hover and land in tight areas. Although limited by its flying time due to six battery powered motors the UAV was able to cover most of the study sites with 12 minutes of flying time (three flights), capturing up to 720 pictures (240 pictures per flight). With an autonomous UAV and precise planning of the area, coverage and overlap (80%) on each image could be calculated precisely. However, for the purpose of mapping landscape features in WDML, a manually operated UAV proved to be sufficient. Computer modelling software is advanced enough to not need to worry about the exact angle and altitude each photograph was taken from.

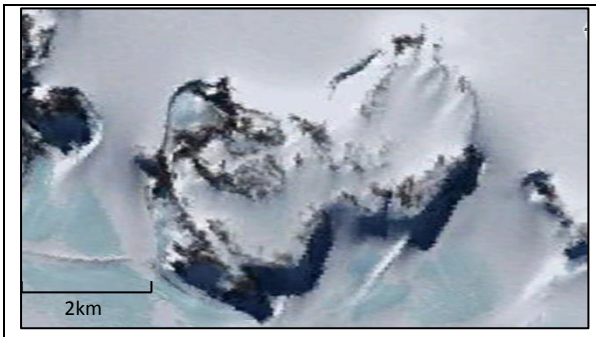

Figure 1a: A Landsat image of the Flårjuven study area showing pixilation even from an estimated height of 8.5km.

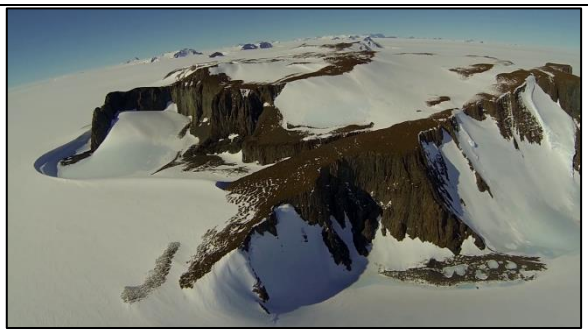

Figure 1b: A single image of the site taken from a helicopter (Scott, DA).

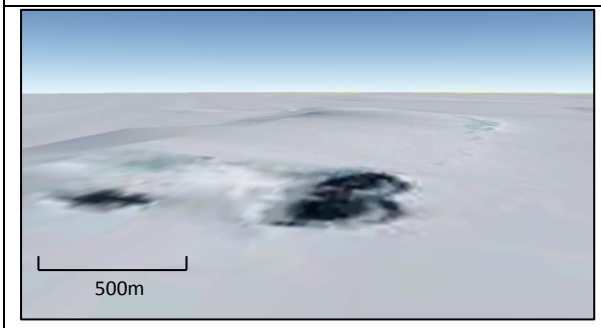

Figure 2a: A Landsat image of the Robertskollen study area from a side angle view showing a large amount of pixilation from an oblique view distance of around 4km away and an altitude of 1km. Even from this distance there is a complete lack of feature detail and no height aspect.

Figure 2b: A photograph (Scott, DA) of the Robertskollen study area from a similar angle. This image illustrate that the Google Earth models dramatically lack detail for the majority of WDML. The only areas where they are vaguely useful are at one of the six study areas, Troll.

Figure 3a: A Landsat image of the Troll study area. This is the area of WDML which has the highest details in free aerial photographs yet still lacks any useable data for the purpose of this project. Even from an altitude of 200m the image is pixelated and can only be used for determining which areas contains land features such as polygons.

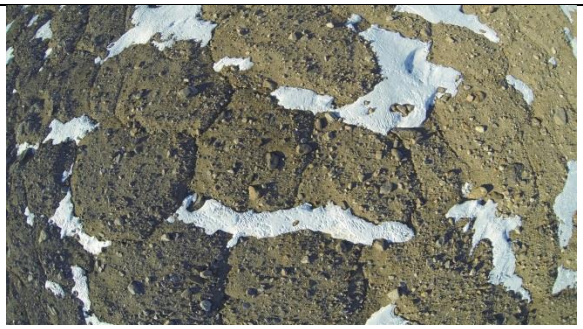

Figure 3b: A photograph of the Troll study area from a similar angle. This shows how much detail can be collected from a single aerial photograph. Multiple images like this can create a much more thorough understanding of the study area for post field study desktop analysis.

Figure 89: Satellite images compared to UAV derived imagery.

5.1.2. Comparing GoPro to Digital Single-lens reflex camera modelling

One of the major concerns of this investigative study was what effect the fish-eye lense of the GoPro camera would have on the 3D modelling outcome. To achieve the forth objective, which was to develop and utilise new technologies to document landforms, an assessment of aerial photographic equipment was needed. A helicopter was used to take aerial photographs of the Vesleskarvet site. Mounted to the helicopter were two GoPro cameras, one facing 45° forward and the other directly downward. Furthermore, a Cannon 600D DSLR camera was manned on either side of the helicopter for high quality images and also pointed downwards. All four cameras were set to one second time lapse intervals. Control points (flags) were set in place before the flight in order to allow for georeferencing. The differences in two model outputs between using only the GoPro cameras (left) and then only the DSLR cameras (right) is presented in Figure 90. The output models are very similar; however the DSLR outputs tends to have more defined model borders. The colour output is much clearer in the DSLR model and the objects have better definition. Both models show black areas where there was not enough overlap in aerial images or the topography was steep but the GoPro model shows large pixel errors in some of the areas of low overlap. The overall quality of the DSLR camera model is more defined and therefore recommended for future studies. Relating this test to the use of the UAV, a point and shoot camera would provide a similar output to the DSLR model as it is the fisheye lens of the GoPro which creates pixel errors in the models. For high accuracy a GoPro camera should not be used. A point and shoot camera would be good substitute for a GoPro as it provides high quality images yet still is light in weight.

GoPro model	**SLR model**
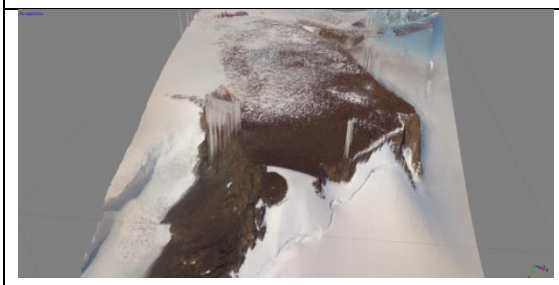	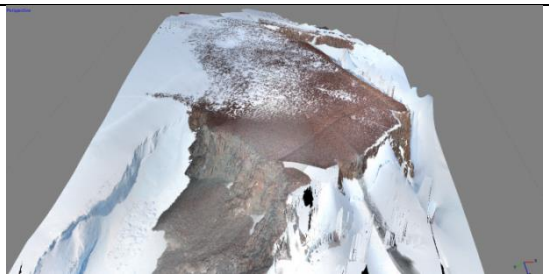
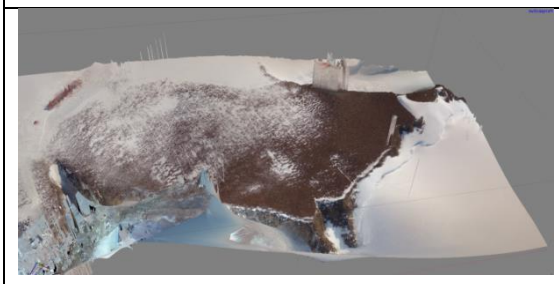	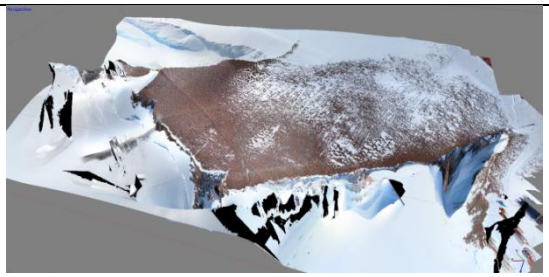

Figure 90: Comparison of GoPro to DSLR 3D modelling.

5.1.3. Comparing UAV to a helicopter for aerial photography

A UAV was used for taking aerial images in the project mainly due to the cost effectiveness of the vehicle. The advantages and disadvantages of a UAV and Manned Aerial Vehicle (MAV) are presented in Table 5. The main outcome is the cost effectiveness of the UAV; however it is limited by wind speed and payload. Furthermore, it is recommended to cover large study areas with a MAV for reducing data collection time.

Table 5: The advantages and disadvantages of a UAV over a MAV.

Aerial Vehicle	Advantages	Disadvantages
UAV	• Cheaper to fly • Easy to transport • No licensing needed • Quick to setup • Basic flight planning needed • Easy to fly an area again • No danger to human health	• Limited by wind speed • Limited payload • Limited by battery life • Limited camera size • Limited on-board equipment (e.g. LiDAR) • Training is required • Limited altitude and flight distances • Potential impact on wildlife • Regulations for UAVs are being set in place by the Antarctic community (SCAR, 2014).
Helicopter	• Long flight duration • Relatively unlimited payload • Can fly in strong wind conditions • Can cover large areas in a single flight • Effective on reducing time	• Extremely expensive to hire • Pilot required • Flight planning essential • Limited minimum altitude • Human risk factor • Potential impact on wildlife

5.2. Consolidation

The air temperature drops to the minimum recorded temperature during the winter months whereas in the summer months it is the ground surface temperatures which form the high peaks on the graph (1cm, 15cm, and 30cm). During the summer months the effect of the solar radiation on the ground temperatures is far greater than the effect of the ambient air temperature (Idso *et al*., 1975; Bristow and Campbell, 1984; Bonan, 1989; Zang *et al*., 1997; Julián and Chueca, 2007). Factors such as cloud cover, snow cover and wind also directly influence the amount of solar radiation entering and heating up the ground and direct temperatures (Idso *et al*., 1975; Bristow and Campbell, 1984; Bonan, 1989; Zang *et al*., 1997; Julián and Chueca, 2007). The Earth's energy mechanism where the incoming solar energy is obscured by several factors is a direct link to these thermal readings (Trenberth *et al*., 2009).

The atmosphere, clouds and the surface of the earth reflects solar radiation (Trenberth *et al*., 2009). Depending on cloud cover and land cover these factors may vary significantly.

The summary table of the study sites thermal data, features, zero-degree isotherm depth and freeze-thaw cycle count for all the sites and borehole depths are presented in Table 6 (pg. 103-104). Polygon features are common among all the sites except Vesleskarvet and Robertskollen. Robertskollen has the minimum altitude at 468m.a.s.l. and Vesleskarvet at 848m.a.s.l. whereas all the other sites are above 1000m.a.s.l. with Slettfjell situated the highest at 1472m.a.s.l. The maximum recorded air temperature was at Troll at 8.76°C (10/11/2014) with the second highest maximum being 6.77°C (22/12/2010) at Vesleskarvet. The air temperature has proven to have less significance with respect to zero-degree isotherm depth. Therefore, the ground temperature is of more importance for these sites. Robertskollen is the site with the most biological growth and has the maximum recorded ground temperature at 22.84°C (10/01/2014) which is also linked to altitude, followed by Troll at 22.46°C (28/12/2013) and Valterkulten at 21.49°C (27/12/2013). The number of cycles over the zero-degree isotherm was calculated at both borehole depths which showed similar results. In order to compare all the sites, the relative freeze/thaw event counts (the number of times the temperature crossed the zero-degree isotherm) from the year 2013 were used. The sites are listed below in descending order based on number of relative cycle events:

1. Troll - 11.01 (Depth - 25cm)
2. Robertskollen - 10.99 (Depth - 66cm)
3. Valterkulten - 8.90 (Depth - 29cm)
4. Flårjuven - 4.98 (Depth - 29cm)
5. Vesleskarvet - 1.87 (Depth - 17.26cm)
6. Slettfjell - 0.73 (Depth - 9.24cm)

Troll has the highest number of cycles over the zero-degree isotherm yet it does not have the deepest zero-degree isotherm level. Furthermore, it contains the highest concentration of polygon formations in WDML. Robertskollen has a similar number of cycles over the zero-degree isotherm to that of Troll; however, it also has the deepest zero-degree isotherm layer (deepest thaw level). Robertskollen therefore has ideal conditions for polygons, terraces, steps, stripes and sorted and non-sorted ground formation (high cycle event count and deep thawing); however, only a few sorted and non-sorted patterns are found there. This suggests that formations are not related to the depth of the zero-degree isotherm but rather to the frequency of the cycles in relation to the sediment type and date of ground exposure (deglaciation) of the site.

The number of cycles over the zero-degree isotherm of all the sites and loggers is presented in Figure 91. It is suggested that the zero-degree isotherm is not the exact temperature at which freeze/thaw

cycles take place but only an estimate. Robertskollen experiences the most cycles over the zero-degree isotherm and Slettfjell has the least when comparing the deep borehole data. Interestingly when comparing the shallow borehole data it can be seen that the Troll crack has the most frequent cycles. Furthermore, moisture content of the ground affects the pattern formations. All the shallow loggers show a higher number of cycles over the zero-degree isotherm than their associated deep loggers, with the exception of the Robertskollen site, which show the complexity at shallow depths. Furthermore, this links it to the habitat of biotic life in these cold regions as the freeze/thaw cycles create microhabitat environments. Therefore, it can be concluded that the shallow boreholes capture more cycle occurrences and are a more useful depths for most of the study areas. For warm areas such as the Robertskollen site it is recommended that two metre borehole loggers are installed in order to capture a detailed understanding of the active layer.

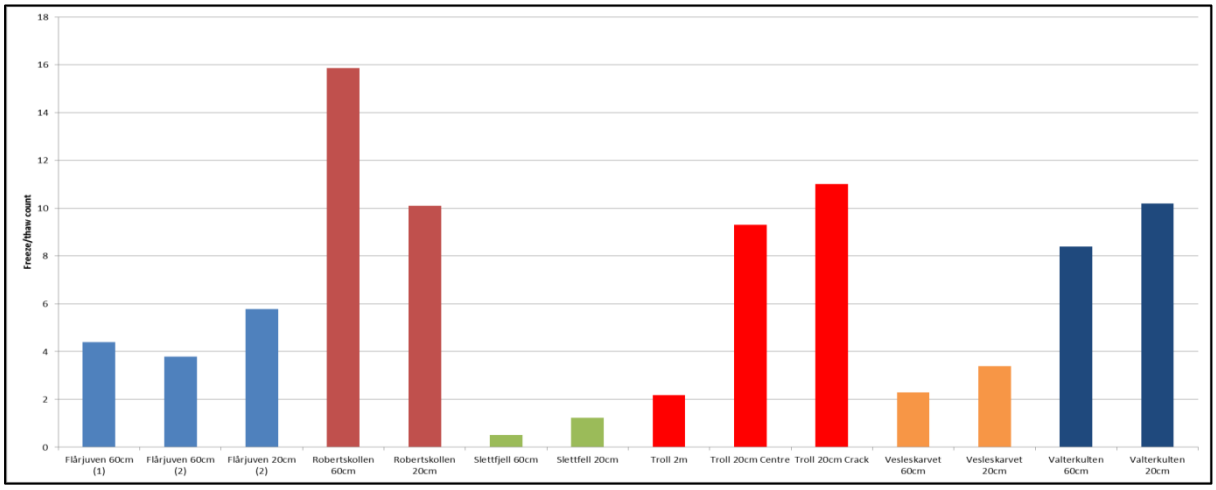

Figure 91: The relative freeze/thaw cycle count from all the sites and borehole depths.

It is argued by many authors that factors such as wind, cloud cover and snow cover directly impact the amount of solar radiation entering and heating up the ground (Idso *et al*., 1975; Bristow and Campbell, 1984; Bonan, 1989; Zang *et al*., 1997; Julián and Chueca, 2007). The results have shown that the air temperature has less influence than ground surface temperatures on the active layer dynamics. However, it is important to note that a more in-depth study into this field with regards to solar radiation and influencing factors could be a worthwhile follow-up study as many aspects have not been taken into consideration. The sites vary dramatically with regards to zero-degree isotherm depth and it is noted that the age of the sediments (more fines) and exposure date does not contribute to the depth of the active layer but more to the features found in the landscape. Although careful study into the sediment, rock type, and age was not the focus, general observations were sufficient. The Slettfjell site which has the shallowest active layer also has one of the most concentrated polygon feature areas of WDML. The quantity of features found is therefore directly linked to the particle size of the sediments (Hallet *et al*., 2011).

Table 6: Summary table of the study sites thermal data, features, zero-degree isotherm depth and freeze-thaw cycle count.

Study area	Borehole	Features	m.a.s.l	Date	Max Air (°C)	Min Air (°C)	Max 1cm (°C)	Min 1cm (°C)	Depth (cm)	Average Permafrost temperature (°C)	Distance to ice shelf	Freeze/thaw count (2013)
Flårjuven (1st logger)	Deep	• Sorted and non-sorted patterns • Polygons	1278	2008-2014	2.3°C (9/01/2010)	-41.38°C (7/07/2010)	18.22°C (10/01/2012)	-40.9°C (7/07/2010)	26.5cm	-18.1	174km	4.44
Flårjuven (2nd logger)	Deep	Sorted and non-sorted patterns • Polygons and terraces	1380	2013-2014	-0.6°C (9/01/2013)	-35°C (26/08/2013)	14°C (24/01/2013)	-34°C (26/08/2013)	29cm	-17.7	174km	3.19
Flårjuven (2nd logger site)	Shallow	• Sorted and non-sorted patterns • Polygons and terraces	1380	2013-2014	-0.6°C (9/01/2013)	-35°C (26/08/2013)	13°C (27/12/2013)	-34.2°C (26/08/2013)	20.7cm (27/12/2013)	-18.0	174km	4.98
Slettfjell	Deep	• Sorted patterns • Polygons and stripes	1472	2013-2014	0.42°C (12/12/2013)	-38.83°C (02/05/2013)	5.87°C (31/12/2013)	-38.37°C (02/05/2013)	9cm	-19.9	190km	0.33
Slettfjell	Shallow	• Sorted patterns • Polygons and stripes	1472	2013-2014	0.42°C (12/12/2013)	-38.83°C (02/05/2013)	10.76°C (10/01/2014)	-37.44°C (09/09/2013)	9.24cm (10/01/2014)	-20.3	190km	0.73
Valterkulten	Deep	• Non-sorted patterns • Polygons and terraces	1021	2013-2014	3.65°C (31/12/2013)	-33.42°C (14/07/2013)	21.33°C (27/12/2013)	-35.45°C (14/07/2013)	29cm	-15.3	161km	7.42
Valterkulten	Shallow	• Non-sorted patterns • Polygons and terraces	1021	2013-2014	3.65°C (31/12/2013)	-33.42°C (14/07/2013)	21.49°C (27/12/2013)	-33.86°C (15/07/2013)	20.71cm (27/12/2013)	-15.6	161km	8.90
Robertskollen	Deep	• Sorted and non-sorted patterns. • High concentration of lichen, moss and algae.	468	2013-2014	5.94°C (10/01/2014)	-32.06°C (14/07/2013)	16.47°C (01/01/2013)	-31.81°C (15/07/2013)	66cm est.	-11.8	120km	10.99

Robertskollen	Shallow	• Sorted and non-sorted patterns. • High concentration of lichen, moss and algae.	468	2013-2014	5.94°C (10/01/2014)	-32.06°C (14/07/2013)	22.84°C (10/01/2014)	-33.67°C (14/07/2013)	66cm est.	-12.9	120km	9.02
Vesleskarvet	Deep	• Sorted patterns	848	2009-2014	6.77°C (22/12/2010)	-40.78°C (07/07/2010)	14.28°C (2013/01/06)	-39.66°C (2013/01/06)	14.5cm	-16.0	140km	1.87
Vesleskarvet	Shallow	• Sorted patterns	848	2013-2014	*Err*	*Err*	14.01°C (02/01/2014)	-27.46°C (15/07/2013)	17.26cm	-16.3	140km	1.80
Troll (1st logger)	Deep (1)	• Non-sorted patterns • Polygons	1283	2007-2014	8.76°C (10/11/2014)	-49.29°C (23/06/2008)	6.16°C (06/01/2013)	-36.14°C (26/07/2012)	1.2cm-25cm	-17.0	220km	9.05
Troll (2nd logger)	Deep (2)	• Non-sorted patterns • Polygons	1290	2013-2014	4.64°C (01/01/2014)	-40.45°C (15/07/2013)	0.95°C (04/01/2014)	-31.73°C (29/08/2013)		-17.7	220km	
Troll	Shallow - Centre	• Non-sorted patterns • Polygons	1297	2013-2014	3.17°C (21/12/2013)	-40.9°C (15/07/2013)	20.8°C (28/12/2013)	-40.21°C (15/07/2013)	23.21cm (22/01/2013)	-17.5	220km	9.30
Troll	Shallow - Crack	• Non-sorted patterns • Polygons	1296	2013-2014	3.17°C (21/12/2013)	-40.9°C (15/07/2013)	22.46°C (28/12/2013)	-41.07°C (15/07/2013)	18.13cm (22/01/2013)	-17.6	220km	11.01

The number of cycles over the zero-degree isotherm (freeze/thaw) per year for the Flårjuven site (a), Troll site (b) and the Vesleskarvet site (c) are presented in Figure 92. On the Flårjuven graph (a) it can be seen that 2008, 2009 and 2011 had a very similar amount of freeze/thaw events (over the 0°C mark) at 3.51, 3.55 and 3.81 respectively. The year of 2010 had a high of 5.03 events and 2012 had the all-time high of 5.38, with 2013 dropping down to 4.44. At the Troll site (b) there is an obvious increasing trend in the freeze/thaw cycle occurrence showing a steep rise in the trend line. The data showed almost zero freeze/thaw cycles in 2007 (a cold year), yet there has been a steady increase over the years to 2.81 in 2012 and 9.05 in 2013. Finally at the Vesleskarvet site (c) in 2009 there was an occurrence of 0.93 and then in 2010 and 2012 there was a freeze/thaw cycle value of 2.11 and 2.08 respectively. The year 2012 reached a high of 2.7 and then dropped down to 1.87 relative freeze/thaw events in 2013. The trend line of Vesleskarvet is almost identical to that of Flårjuven. The trend lines show that there is an increase in freeze/thaw cycle events and it can then be concluded that for all these sites the environment has been warming up over the last seven years. Unfortunately the data for the rest of the sites only dates back to 2013 and therefore cannot be used to work out short term trends. However, all six sites are in the same geographical zone and it could be presumed that they have similar trend lines and, therefore, suggest that warming is taking place. The trend lines show change, however, the sample size is very small and therefore may be considered insignificant.

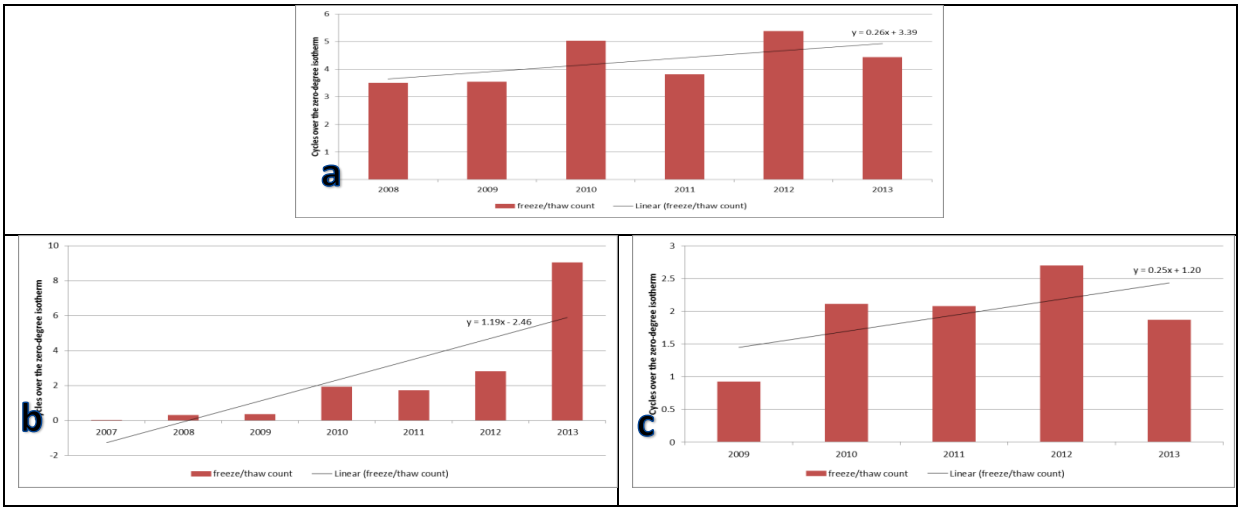

Figure 92: The relative freeze/thaw cycle count per year for the Flårjuven site (a), Troll site (b) and the Vesleskarvet site (c).

5.3. Periglacial landforms

Post fieldwork analysis was done on polygon areas for Flårjuven, Valterkulten, Slettfjell and Troll, and terrace area analysis was done for Flårjuven and Valterkulten. The results from these sites are presented in Table 7. The mean sampled polygon area for the varied from 20.93m² to 101.26m² over the four sites with the smallest polygon only 1.95m² in area and the largest reaching 276.53m². The mean terrace area was 183.28m² at Flårjuven and 63.68m² at Valterkulten with the smallest terrace

area at 22.95m² and the largest at 293.18m². Although the data show variable results it has shown that the aerial photograph modelling has given a new insight into landscape feature analysis and may be used for futures studies in this area.

The most comprehensive study on the polygon sizes was undertaken at Troll (pg. 95-96). No definite conclusions could be drawn up as the data showed variable results with regards to all samples taken and no link to the thermal data collected (Table 6, pg. 103-104). However, the samples have created a solid baseline dataset for future studies. Further investigation into ground properties is advised.

Table 7: Comparative table of polygon and terrace data.

Polygons		**Terraces**	
Flårjuven Polygon Area (m²) Statistics		**Flårjuven Terrace Area (m²) Statistics**	
Count:	31	**Count:**	7
Minimum:	12.29	**Minimum:**	90.92
Maximum:	109.26	**Maximum:**	293.18
Sum:	1385.23	**Sum:**	1282.98
Mean:	44.68	**Mean:**	183.28
Standard Deviation:	24.68	**Standard Deviation:**	66.23
Valterkulten Polygon Area (m²) Statistics		**Valterkulten Terrace Area (m²) Statistics**	
Count:	9	**Count:**	11
Minimum:	31.39	**Minimum:**	22.95
Maximum:	90.63	**Maximum:**	91.94
Sum:	581.63	**Sum:**	700.48
Mean:	64.63	**Mean:**	63.68
Standard Deviation:	23.19	**Standard Deviation:**	21.55
Slettfjell Polygon Area (m²) Statistics			
Count:	196		
Minimum:	1.95		
Maximum:	65.36		
Sum:	4103.09		
Mean:	20.93		
Standard Deviation:	14.77		
Troll Polygon Area (m²) Statistics			
Count:	44		
Minimum:	21.79		
Maximum:	276.53		
Sum:	4455.58		
Mean:	101.26		
Standard Deviation:	48.44		

5.4. Landscape features and variables

A comparative table of the sites and their features, maximum temperature, inland distance, height, maximum zero-degree isotherm depth and relative freeze/thaw cycle count is presented (Table 6, pg. 103-104). Comparing the collected data and results allows for a further consideration of what conditions are necessary for these landscapes to develop. Robertskollen, which has the minimum altitude site, had noticeably more biotic life but only sorted and non-sorted patterns were found. Furthermore, Vesleskarvet is the second lowest site and contains only sorted patterns. On the other hand, the other four sites which all have a height of over 1000m.a.s.l. displayed more predominant landscape features such as polygons, stripes and terraces. Feature formations can then be directly linked to height above sea level, the distance from the ice shelf (closer to the South Pole) and time period since deglaciation. The maximum recorded ground surface temperature varied and no conclusions can be drawn regarding the link to landscape features. The zero-degree isotherm depth has no link to landscape features found. Furthermore, no link between the freeze/thaw count and landscape features was found.

5.5. Slope movement

Site experiments were set up at three sites to investigate the movement of rock down slopes. The rocks were marked yellow and a point on each rock was marked with a permanent marker pen. The points were recorded with a DGPS in 2013. On return to the sites it was found that the paint and marker points had been dramatically weathered and it was not possible to take the new readings. It is recommended that coloured metal plates with a point indentation are glued to the rock surfaces in order to make this a long term experiment.

5.6. Recommendations for the future

The borehole thermal loggers have proven to be effective in assisting with understanding active layer dynamics. However, for warm sites like Robertskollen, it is recommended that 2m boreholes are set up in order to fully capture the depth of the zero-degree isotherm. Furthermore, for sites such as Slettfjell and Vesleskarvet where the zero-degree isotherm is relatively shallow, the shallow boreholes are sufficient. Due to the failure rate experienced over the years, it is also recommended that more loggers should be set up at each site but potentially at areas where topography, aspect and sediment types may vary. Furthermore, loggers should be set up at areas where snow cover is known to vary, in order to monitor these effects. A pyronometer should be set up at each site to measure the solar radiation. Working hand-in-hand with the thermal loggers it would help with the overall assessment of ground fluctuations.

The polygon study done at the Troll study area has set up, a good baseline data set of 30 in-depth samples. Future studies will be able to compare these data in a simple yet thorough manner.

The UAV, although a highly successful new technology for this study, has presented many recommendations for future work:

- The marker flags should be larger and of a brighter colour in order to stand out in the rocky areas.
- The number of marker flags should be increased to create georeferenced outputs for every flight and not only the final output mosaic of all the flights (four marker flags per flight).
- It is recommended that square solid marker flags pinned to the ground are used, rather than crosses or standing flags. Identifying crosses in the model proved complicated and could not be done in low quality model outputs.
- It would be a good idea to set up a 20m x 20m straight line square in the field in order to ensure the stitched image in post processing is in a true form.
- Lower height above ground surface flights should be used for areas where high quality output is needed. The nearer the photographs to the ground, the higher the object model output.
- Sensors such as LiDAR (Light Detection And Ranging) could be used in the UAV or MAV for specific projects. This equipment could be used in combination with the other data to give a more in-depth understanding of the topography.
- A base station could be setup in order to communicate with the UAV and fly accurate GPS navigated routes.
- An assessment of other modelling software could be done.

5.7 Concluding remarks

The six objectives of the project (Aims and Objectives, pg. 21-22) are summarised, as well as whether or not the objectives have been achieved. Furthermore, the role these findings may have in advancing our understanding of active layer dynamics and landscape features found in cold weather environments are addressed. Finally, the key results will be presented.

The first objective required determining air temperature, ground temperature and ground moisture variability and change at the six selected study sites. The data from these logger boreholes has given an insight into the exact processes which are occurring on the ground surface layer at the selected sites. Having both long-term monitoring and high-frequency monitoring sessions allowed for the detailing of the freeze/thaw cycle events. The data provided by the boreholes was used to create tables

and graphs which were comparable across sites. The areas where this data has been recorded for up to seven years has given an insight into short term variables. Furthermore, the different borehole depths have provided comparative data results and recommendations for future borehole depths. It is possible to get a rough estimation of the depth for future monitoring boreholes in WDML based on: attitude of the site, geology, age of sediments and distance from the ice shelf.

Accomplishment of the first objective fed into the second objective which was to determine the depth of the zero-degree isotherm and calculate the frequency of the freeze/thaw cycle events over the six study areas. The depth and freeze/thaw cycle events proved unrelated and varied significantly over the sites. It was concluded that altitude directly impacted the depth of the zero-degree isotherm and it was a combination of freeze/thaw events, geology and time period since deglaciation which determined the landforms found at the sites. The active layer depth is directly related to the thermal results. Shallow boreholes (more frequent sensor spacing) capture more cycle occurrences and are a more useful logger for most of the study areas. For extremely warm areas such as the Robertskollen site it is recommended that two metre borehole loggers are installed in order to capture a detailed understanding of the active layer.

The third objective delivered a portfolio of active layer and permafrost landforms. At all of the sites sorted and/or non-sorted ground was found. Vesleskarvet and Robertskollen were the only two sites at which only sorted and/or non-sorted ground was found. The other four sites had polygon formations and at Valterkulten and Flårjuven, terrace formations were also found. Finally, at the Slettfjell site striped formations were found; however, further investigation into these findings is advised as snow cover could have provided irregular results. Through fieldwork and post fieldwork studies, it was possible to document and map landforms in WDML.

The fourth objective aimed at developing and utilising new technologies to document these landforms. The UAV was built in order to fly over the areas of interest and take multiple aerial images for the creation of 3D models, ultra-high resolution mapping of landscape features and post fieldwork landscape feature analysis. The UAV proved to be an exceptional new tool for this project and has given insight into further studies in this field. Many different UAVs exist and with their increasing popularity the price is becoming highly competitive which makes it possible to buy these devices for even the smallest projects. Study areas which do not require a precise landing zone can be flown with fixed wing UAVs. Fixed wing UAVs have longer flight durations as they rely on only one motor and have a more efficient glide ratio. For large study areas a fixed wing should be used to reduce sample time but minimum flying speed is limited. In conclusion an UAV is an undisputed benefit to projects which require aerial photographs at low cost but, depending on the study area, the correct form of UAV should be used.

Objective five required landscape feature analysis baseline data to be collected and set up for the sites. Due to time constraints and weather conditions, it was not possible to collect certain data at some of the study sites. Landscape features (polygons, terraces, and stripes) were sampled and measured at selected sites and an inventory compiled. The weather only allowed for the UAV to be flown at selected sites and as a result, recommendations for future work are listed (pg. 108-109).

The final objective was to create DEMs of the areas of interest. After the trial and error UAV flights, it was possible to create high-quality mosaicked images which were imported into ArcMap and georeferenced. These images were then manipulated and adapted in order to achieve the final objective of creating DEMs, hillshading and topographic contour lines. It was not possible to produce these outcomes at Troll which was not setup and flown correctly. Flight planning is essential for aerial imagery modelling. The DEMs and hillshading gave insight into the topography of the study area which was not possible from field analysis. Future work in this field could be compared to this baseline data setup. If the same sites are modelled then the DEM outputs could be superimposed with this data and change can be monitored.

In contrast to the Arctic, the physical properties of Antarctic permafrost is less well known, especially with regards to the thermal regime, the active layer thickness and the presence of ground ice (Vieira *et al*., 2010). Borehole thermal logging is a key element in setting up baseline data for future studies and climate change modelling. Working hand-in-hand with aerial imagery modelling, it is possible to create a holistic understanding of cold weather environments. It is recommended that future studies in this field expand the study areas and compare findings to the baseline data created through this project.

Active layer processes and resultant landforms in Western Dronning Maud Land were investigated using multiple data sets obtained from thermal logger boreholes from 2007 to 2014 and aerial photography from 2013 to 2014. Key results from this study include: 1) The UAV has proved to be an indisputably effective tool with which to take aerial photographs for the creation of 3D models, ultra-high resolution mapping of landscape features and post fieldwork landscape feature analysis. 2) Permafrost is present at all the study areas in WDML. 3) The active layer thickness is directly linked to ground thermal properties but also to altitude. 4) The short term trends show a deepening in the depth of the zero-degree isotherm across all sites. 5) The short term trends show an increase in freeze/thaw cycles events across all the sites.

References

Adlam, L.S., Balks, M.R., Seybold, C.A. & Campbell, D.I. Temporal and spatial variation in active layer depth in the McMurdo Sound Region, Antarctica. *Antarctic Science*, 22(1):45-52.

Agisoft PhotoScan® User Manual: Professional Edition, Version 1.0.0. 2013. [Online]. Available: http://downloads.agisoft.ru/pdf/photoscan-pro_1_0_0_en.pdf [20/06/2014].

Alberts, F.G. (Ed.) 1995: *Geographic Names of the Antarctic*. National Science Foundation, Arlington. p. 834.

Anderson, D.G. & Bliss, L.C. 1998. Association of Plant Distribution Patterns and Microenvironments on Patterned Ground in a Polar Desert, Devon Island, N.W.T., Canada. *Arctic and Alpine Research*, 30(2):97-107.

André, M.F. 2003. Do periglacial landscapes evolve under periglacial conditions? Geomorphology, 52(1-2):149-164.

ATS. 1959. *The Antarctic Treaty*. Washington, D.C: Secretariat of the Antarctic Treaty.

Ballantyne, C. & Benn, D. 1994. Paraglacial Slope adjustment and resedimentation following recent glacier retreat, Fabergstolsdalen, Norway. *Arctic and Alpine Research*, 26:255-269.

Ballantyne, C. & Matthews, J. 1982. The development of sorted circles on recently deglaciated terrain, Jotunheimen, Norway. *Arctic and Alpine Research*, 14(4):341-354.

Ballantyne, C. & Matthews, J. 1983. Desiccation cracking and sorted polygonal development, Jotunheimen, Norway. *Arctic and Alpine Research*, 15(4):339-349.

Belcher, D., Veverka, J. & Sagan, C. 1971. Mariner Photography of Mars and Aerial Photography of Earth: Some Analogies. *Icarus*, 15:241-252.

Bendea, H., Chiabrandoa, F., Giulio Tonolob, F. & Marenchinoa, D. 2007. *Mapping of Archaeological Areas Using a Low-Cost UAV – The Augusta Bagiennorum Test Site*. XXI International CIPA Symposium, Athens, Greece.

Birkeland, P.W. 1984. *Soil and Geomorphology*. New York. Oxford University Press.

Black, R.F. 1976. Periglacial Feature Indicative of Permafrost: Ice and Soil Wedges. *Quaternary Research*, 6:3-26.

Blunier, T. & Brook, E.J. 2001. Timing of Millennial-Scale Climate Change in Antarctica and Greenland During the Last Glacial Period. *Science*, 291(5501):109-112.

Bockheim, J.G. 1995. Permafrost distribution in the southern circumpolar region and its relation to the environment: A review and recommendations for further research. *Permafrost and Periglacial Processes*, 6(1):27-45.

Bockheim, J.G. (Ed.) 2005. International Workshop on Antarctic Permafrost and Soils, Final Report. *National Science Foundation*, 84.

Bockheim, J.G., Campbell, I.B., Guglielmin, M. & López-Martínez, J. 2008. *Distribution of permafrost types and buried ice in ice free areas of Antarctica*. In 9th International Conference on Permafrost, Proceedings. University of Alaska Press, Fairbanks: 125–130.

Bockheim, J.G., Campbell, I.B. & McLeod, M. 2007. Permafrost Distribution and Active Layer Depths in the McMurdo Dry Valleys, Antarctica. *Permafrost and Periglacial Processes*, 18:217-227.

Bockheim, J.G. & Hall, K.J. 2002. Permafrost, active layer dynamics and Periglacial environments of continental Antarctica. Periglacial Research. *South African Journal of Science*, 98.

Bockheim, J.G., Vieira, G., Ramos, M., López-Martínez, J., Serrano, E., Guglielmin, M., Wilhelm, K. & Nieuwendam, A. 2013. Climate warming and permafrost dynamics in the Antarctic Peninsula region. *Global and Planetary Change*, 100: 215-223.

Boelhouwers, J., Holness, S. & Summer, P. 2003. The maritime Subantarctic: a distinct periglacial environment. *Geomorphology*, 52:39-55.

Bonan, G.B. 1989. A Computer Model of the Solar Radiation, Soil Moisture, and Soil Thermal Regimes in Boreal Forests. *Ecological Modelling*, 45:275-306.

Briggs, D. J. 1977a. *Sources and Methods in Geography – Soils*. London: Butterworths & Co. Ltd.

Briggs, D. J. 1977b. *Sources and Methods in Geography – Sediments*. London: Butterworths & Co. Ltd.

Brinkmann, M., Pearce, D.A., Convey, P. & Ott, S. 2007. The cyanobacterial community of polygon soils at an inland Antarctic nunatak. *Polar Biology*, 30:1505-1511.

Bristow, K.L. & Campbell, G.S. 1984. On the Relationship between Incoming Solar Radiation and Daily Maximum and Minimum Temperature. *Agricultural and Forest Meteorology*, 31:159-166.

Brown, J., Hinkel, K.M. & Nelson, F.E. 2000. The circumpolar active layer monitoring (calm) program: Research designs and initial results. *Polar Geography*, 24(3):166-258.

Brown, J., Hinkel, K. & Nelson, F.E. (comp.). 2003. Circumpolar Active Layer Monitoring (CALM) Program Network: Description and data. In Parsons, M. & Zhang, T. (Eds) *International Permafrost Association Standing Committee on Data Information and Communication (comp.).* Circumpolar Active Layer Permafrost System, Version 2.0. National Snow and Ice Data Center/World Data Center for Glaciology. Boulder. CD-ROM.

Cannone, N., Ellis Evans, J.C., Strachan, R. & Guglielmin, M. 2006. Interactions between climate, vegetation and active layer in maritime Antarctica. *Antarctic Science*, 18:323-333.

Cannone, N. & Guglielmin, M. 2010. Relationships between periglacial features and vegetation development in Victoria Land, continental Antarctica. *Antarctic Science*, 22:703-713.

Chao, H., Cao, Y. & Chen, Y. 2010. Autopilots for Small Unmanned Aerial Vehicles: A Survey. *International Journal of Control, Automation, and Systems*, 8(1):36-44.

Dragonfly Innovations Inc. 2014. *An Introduction to Unmanned Aerial Vehicles (UAVs)* [Online]. Available: http://www.draganfly.com/news/2008/08/24/introduction-to-unmanned-aerial-vehicles-uavs/. [20/05/2014].

Eisenbeiss, H. 2004. *A Mini Unmanned Aerial Vehicle (UAV): System Overview and Image Acquisition.* International Workshop on Processing and Visulaization Using High-resolution Imagery, Pitsanulok, Thailand.

French, H.M. & Guglielmin, M. 1999. Observations on the Ice-Marginal, Periglacial Geomorphology of Terra Nova Bay, Northern Victoria Land, Antarctica. *Permafrost and Periglacial Processes*, 10: 331-347.

French, H.M. 2006. *The Periglacial Environment*. Longman, London.

French, H.M. & Guglielmin, M. 2000a. Cryogenic Weathering of Granite, Northern Victoria Land, Antarctica. *Permafrost and Periglacial Processes*, 11:305-314.

French, H.M. & Guglielmin, M. 2000b. Frozen Ground Phenomena in the Vicinity of Terra Nova Bay, Northern Victoria Land, Antarctica: A Preliminary Report. *Physical Geography*, 82(4):513-526.

Gislason, S.R., Oelkers, E.H., Eiriksdottir, E.S., Kardjilov, M.I., Gisladottir, G., Sigfusson, B., Snorrason, A., Elefsen, S., Hardardottir, J., Torssander, P. & Oskarsson, N. 2009. Direct evidence of the feedback between climate and weathering. *Earth and Planetary Science Letters*, 277:213-222.

Goodfellow, B.W., Fredin, O., Derron, M.H. & Stroeven, A.P. 2009. Weathering processes and Quaternary origin of an alpine blockfield in Arctic Sweden. *Boreas*, 38:379-398.

Goryachkin, S.V., Karavaeva, N.A., Targulian, V.O. & Glazov, M.V. 1999. Arctic Soils: Spatial Distribution, Zonality and Transformation due to Global Change. P*ermafrost and Periglacial Processes*, 11:235-250.

Grosch, E.G., Bisnath, A., Frimmel, H.E. & Board, W.S. 2007. Geochemistry and tectonic setting of mafic rocks in Western Dronning Maud Land, East Antarctica: implications for the geodynamic evolution of the Proterozoic Maud Belt. *Journal of the Geological Society*, 164:465-475.

Gruber, S. 2012. Derivation and analysis of high-resolution estimate of global permafrost zonation. *The Cryosphere*, 6:221-223.

Guglielmin, M. 2006. Ground Surface Temperature (GST), Active Layer and Permafrost Monitoring in Continental Antarctica. *Permafrost and Periglacial Processes*, 17:133-143.

Guglielmin, M. 2012. Advances in permafrost and periglacial research in Antarctica: A review. *Geomorphology*, 155-156:1-6.

Guglielmin, M., Biasini, A. & Smiraglia, C. 2003. The Contribution of Geoelectrial Investigations in the Analysis of Periglacial and Glacial Landforms in Ice Free Areas of the Northern Foothills (Northern Victoria Land, Antarctica). *Geografiska Annaler*, 79A:1-2.

Guglielmin, M., Ellis Evans, J.C. & Cannone, N., 2008. Ground thermal regime under different vegetation conditions in permafrost areas and sensitivity to climate change: a case study at Signy Island (maritime Antarctica). *Geoderma*, 144:73-85.

Guglielmin, M., Fratte, M.D. & Cannone, N. 2014. Permafrost warming and vegetation changes in continental Antarctica. *Environmental Research Letters*, 9:14.

Guglielmin, M., Lewkowicz, A., French, H.M. & Strini, A. 2009. Lake-ice blisters, Terra Nova Bay area, Northern Victoria Land, Antarctica. *Geografiska Annaler*, 91A:99-111.

Hall, K.J. 2002. Review of Present and Quaternary periglacial processes and landforms of the maritime and sub-Antarctic region. Periglacial research. *South African Journal of Science*, 98.

Hall, K.J. & André, M.F. 2001. New insights into rock weathering from high-frequency rock temperature data: an Antarctic study of weathering by thermal stress. *Geomorphology*, 41:23-35.

Hall, K.J. & Walton, D.W.H. 1992. Rock weathering, soil development and colonization under a changing climate. Philosophical Transactions: *Biological Sciences*, 338(1285), Antarctica and Environmental Change. p. 269-277.

Hallet, B. 1990. Spatial self-organization in geomorphology: from periodic bedforms and patterned ground to scale-invariant topography. *Earth-Science Reviews*, 29:57-75.

Hallet, B., Sletten, R. & Whilden, K. 2011. Micro-relief development in polygonal patterned ground in the Dry Valleys of Antarctica. *Quaternary Research*, 75:347-355.

Hansen, C.D., Meiklejohn, K.I. & Nel, W. 2013. *The Characterisation of an Openwork Block Deposit, Northern Buttress, Vesleskarvet, Dronning Maud Land, Antarctica*. Grahamstown. Rhodes Univeristy

Harris, C. & Davies, M.C.R. 2000. Gelifluction: observations from large-scale laboratory studies. *Arctic, Antarctic, and Alpine Research*, 32:202-207.

Harris, C., Haeberli, W., Vonder Mu¨hll, D. & King, L. 2001. Permafrost monitoring in the high mountains of Europe: the PACE project in its global context. *Permafrost and Periglacial Processes*, 12:3-11.

Harris, C. & Matthews, J.A. 1984. Some observations on boulder cored frost boils. *Geographical Journal*, 150(1):63-73.

Harris, S.A. 1982. *Identification of permafrost zones using selected permafrost landforms*. Proc. 4th Canadian Permafrost Conf., Alberta. p. 49-58.

Hauck, G., Vieira, G., Gruber, S., Blanco, J. & Ramos, M. 2007. Geophysical identification of permafrost in Livingston Island, maritime Antarctica. *Journal of Geophysical Research*, 122, F02S19.

Haugland, J.E. 2004. Formation of patterned ground and fine-scale soil development within two late Holocene glacial chronosequences: Jotunheimen, Norway. *Geomorphology*, 61:287-301.

Haugland, J.E. 2006. Short-Term Periglacial Processes, Vegetation Succession, and Soil Development within Sorted Patterned Ground: Jotunheimen, Norway. *Arctic, Antarctic, and Alpine Research*, 38(1):82-89.

Idso, S.B., Aase, J.K. & Jackson, R.D. 1975. Net Radiation – Soil Heat Flux Relations as Influenced by Soil Water Content Variations. *Boundary-Layer Meteorology*, 9:113-122.

Intergovernmental Panel on Climate Change. 2014. *Climate Change 2013:* The Physical Science Basis. Working Group I Contribution to the Fifth Assessment Report of the Intergovernmental Panel on Climate, edited by Stocker, T.F *et al*., Cambridge Univ. Press, New York.

Julián, A. & Chueca, J. 2007. Permafrost Distribution from BTS Measurements (Sierra de Telera, Central Pyrenees, Spain): Assessing the Importance of Solar Radiation in a Mid-elevation Shaded Mountainous Area. *Permafrost and Periglacial Processes*, 18:137-149.

Kennicutt, M.C. & Chown, S.L. 2014. Six priorities for Antarctic science. *Nature*, 512:23-25.

Kennicutt, M.C., Chown, S.L., Cassano, J.J., Liggett, D., Peck, L.S., R. Massom, R., Rintoul, S.R., Storey, J., Vaughan, D.G., Wilson, T.J., Allison, I., Ayton, J., Badhe, R., Baeseman, J., Barrett, P.J., Bell, R.E., Bertler, N., Bo, S., Brandt, A., Bromwich, D., Cary, S.C., Clark, M.S., Convey, P., Costa, E.S., Cowan, D., Deconto, R., Dunbar, R., Elfring, C., Escutia, C., Francis, J., Fricker, H.A., Fukuchi, M., Gilbert, N., Gutt, J., Havermans, C., Hik, D., Hosie, G., Jones, C., Kim, Y.D.., Le Maho, Y.., Lee, S.H., Leppe, M., Leitchenkov, G., Li, X., Lipenkov, V., Lochte, K., López-Martínez, J., Lüdecke, C., Lyons, W., Marenssi, S., Miller, H., Morozova, P., Naish, T., Nayak, S., Ravindra, R., Retamales, J., Ricci, C.A., Rogan-Finnemore, M., Ropert-Coudert, Y., Samah, A.A., Sanson, L., Scambos, T., Schloss, I.R., Shiraishi, K., Siegert, M.J., Simões, J.C., Storey, B., Sparrow, M.D., Wall, D.H., Walsh, J.C., Wilson, G., Winther, J.G., Xavier, J.C., Yang, H. & Sutherland, W.J. 2014. A roadmap for Antarctic and Southern Ocean science for the next two decades and beyond. *Antarctic Science*, 1-16.

Kerfoot, D.E. 1972. Thermal Contraction Cracks in an Arctic Tundra Environment. *Arctic*, 25(2).

Kessler, M.A. & Werner, B.T. 2003. Self-Organization of Sorted Patterned Ground. *Science*, Vol. 299: 380-383.

Krantz, W.B. 1990. Self-organization manifest as patterned ground in recurrently frozen soils. *Earth-Science Reviews*, 29:117-130.

Lavelle, M. 2012. *Good Gas, Bad Gas. National Geographic*. [Online]. Available: http://ngm.nationalgeographic.com/2012/12/methane/lavelle-text. [18/08/2014].

Lee, J.E., le Roux, P.C., Meiklejohn, K.I. & Chown, S.L. 2012. 2013. Species distribution modelling in low-interaction environments: Insights from terrestrial Antarctic system. *Austral Ecology*, 38: 279-288.

Levy, J.S., Head, J.W. & Marchant, D.R. 2008a. The role of thermal contraction crack polygons in cold-desert fluvial systems. *Antarctic Science*, 20:565-579.

Levy, J.S., Head, J.W. & Marchant, D.R. 2009a. Cold and dry processes in the Martian Arctic: geomorphic observations at the Phoenix landing site and comparisons with terrestrial cold desert landforms. *Geophysical Research Letters*, 36, L21203.

Levy, J.S., Head, J.W. & Marchant, D.R. 2009b. Thermal contraction crack polygons on Mars: Classification, distribution, and climate implications from HiRISE observations. *Journal of Geophysical Research*, 114, E01007.

Levy, J.S., Head, W.J., Marchant, D.R. & Kowalewski, D.E. 2008b. Identification of sublimation-type thermal contraction crack polygons at the proposed NASA Phoenix landing site: Implications for substrate properties and climate-driven morphological evolution. *Geophysical Research Letters*, Vol. 35, L04202.

Levy, J.S., Marchant, D.R. & Head, J.W. 2010. Thermal contraction crack polygons on Mars: A synthesis from HiRISE, Phoenix, and terrestrial analog studies. *Icarus*, 206:229-252.

Lewkowicz, A.G. & Harris, C. 2005. Frequency and magnitude of active-layer detachment failures in discontinuous and continuous permafrost, northern Canada. *Permafrost and Periglacial Processes*, 16:115-130.

Lucchitta, B.K. 1981. Mars and Earth: Comparison of Cold-Climate Features. *Icarus*, 45:264-303.

Lucieer, A., Robinson, S. & Turner, D. 2010. *Using an unmanned aerial vehicle (UAV) for ultra-high resolution mapping of Antarctic moss beds*. 15th Australasian Remote Sensing & Photogrammetry Conference. Alice Springs.

Lucieer, A., Robinson, S., Turner, D., Harwin, S. & Kelcey, J. 2012. *Using a micro-UAV for ultra-high resolution multisensory observations of Antarctic moss beds.* International Archives of the Photogrammetry, Remote Sensing and Spatial Information Sciences, XXXIX-B1:429-433.

Lundqvist, J., Lilliesköld, M. & Ostmark, K. 1995. Glacial and periglacial deposits of the Tumbledown Cliffs area, James Ross Island, West Antarctica. *Geomorphology*, 11:205-214.

Marchant, D.R. & Head, J.W. 2007. Antarctic dry valleys: Microclimate zonation, variable geomorphic processes, and implications for assessing climate change on Mars. *Icarus*, 192:187-222.

Marshall, D.J., Crafford, J.E., Krynauw, J.R., Drummond, A.E. & Newton, I.P. 1995. The biology, physic-chemistry and geology of a nunatak pond at Valterkulten, Western Dronning Maud Land, Antarctica. *South African Journal of Antarctic Research*, 25(1 & 2).

Matsuoka, N., Abe, M. & Ijiri, M. 2003. Differential frost heave and sorted patterned ground: field measurements and a laboratory experiment. *Geomorphology*, 52:73-85.

Matthews, J.A., Shakesby, R., Berrisford, M. & McEwen, L. 1998. Periglacial patterned ground on the Styggedalsbreen glacier foreland, Jotunheimen, southern Norway: micro-topographic, paraglacial and geoecological controls. *Permafrost and Periglacial Processes*, 9:147-166.

Mellon, M.T., Malin, M.C., Arvidson, R.E., Searls, M.L., Sizemore, H.G., Heet, T.L., Lemmon, M.T., Keller, H.U. & Marshall, J. 2009. The periglacial landscape at the Phoenix landing site, *Journal of Geophysical Research*, 114.

Minsley, B.J., Abraham, J.D., Smith, B.D., Cannia, J.C., Voss, C.I., Jorgenson, M.T., Walvoord, M.A., Wylie, B.K., Anderson, L., Ball, L.B., Deszcz-Pan, M., Wellman, T.P. & Ager, T.A. 2012. Airborne electromagnetic imaging of discontinuous permafrost. *Geophysical Research Letters*, 39, L02503.

National Snow and Ice Data Center. 2005. *Frozen Ground Data Center*. CIRES and the University of Colorado Boulder. [Online]. Available: http://nsidc.org/fgdc/glossary/definitions.pdf [22/03/2013].

Obleitner, R. 1994. Climatological features of glacier and valley winds at the Hintereisferner (Ötztal Alps Austria). *Theoretical and Applied Climatology*, 49:225–239.

Pewe, T.L. 1959. Sand wedge polygons (Tesselations) in the McMurdo Sound Region, Antarctica. *American Journal of Science*, 257:545-552.

Ray, R.J. & Krantz, W.B. 1983. A model for sorted and patterned-ground regularity. *Journal of Glaciology*, 29(102).

Reijmer, C. H. and van den Broeke, M. R. 2001. Moisture source of precipitation in Western Dronning Maud Land, Antarctica. *Antarctic Science*, 13:210-20.

Remondino, F., Barazzetti, L., Nex, F., Scaioni, M. & Sarazzi, D. 2011. UAV Photogrammetry for Mapping and 3D Modeling – Current Status and Future perspectives. *International Archives of the Photogrammetry, Remote Sensing and Spatial Information Sciences*, XXXVIII-1, C22.

Rossbacher, L.A. & Judson, S. 1981. Ground Ice on Mars: Inventory, Distribution, and Resulting Landforms. *Icarus*, 45:39-59.

Sack, D. & Orme, A.R. 2013. Introduction to the foundations of geomorphology. In: Shroder, J. (Editor in Chief), Orme, A.R., Sack, D. (Eds.), *Treatise on Geomorphology*. Academic Press, San Diego, CA, vol. 1, The Foundations of Geomorphology. p. 1-10.

SANAP. 1992. *South African National Antarctic Program (SANAP) Antarctic Field Manual*. Pretoria: Department of Environmental Affairs.

SANAP. 2012. *Sanap – Research*. [Online]. Available http://www.sanap.ac.za/sanap_research/sanap_research.html. [13/10/2014].

SASCAR. 1984. *South African Antarctic Earth Science Research Programme*. South African National Scientific Programmes Report, 81. Pretoria.

SCAR. 2010. *Scientific Committee on Antarctic Research*. [Online]. Available: http://www.scar.org/about/ [22/05/2013].

SCAR. 2014. *Report of the SCAR Delegation to CEP XVII and XXXVII ATCM in Brasilia, Brasil, 28 April – 7 May 2014*. XXXIII SCAR Delegates Meeting. Auckland, New Zealand.

Schenk, T. 1997. Towards automatic aerial triangulation. *Journal of Photogrammetry & Remote Sensing*, 52:110-121.

Schenk, T. 2004. From point-based to feature-based aerial triangulation. *Journal of Photogrammetry & Remote Sensing*, 58:315-329.

Schuur, E.A.G., Bockheim, J., Canadell, J.G., Euskirchen, E., Field, C.B., Goryachkin, S.V., Hagemann, S., Kuhry, P., Lafleur, P.M., Lee, H., Mazhitova, G., Nelson, F.E., Rinke, A., Romanovsky, V.E., Shiklomanov, N., Tarnocai, C., Venevsky, S., Vogel, J.G. & Zimov, S.A. 2008. Vulnerability of Permafrost Carbon to Climate Change: Implications for the Global Carbon Cycle. *BioScience*, 58(8):701-714.

Serrano, E., López-Martínez, J., Cuchi, J.A., Durán, Mink, S. & Navas, A. 2008. *Permafrost in the South Shetland Islands (maritime Antarctica): spatial distribution pattern*. In: Kane, D., Hinkel, K. (Eds.), Proc. Ninth Internat. Permafrost Conf., 29 June–3 July 2008, Fairbanks, Alaska, Extended Abstracts, 1. p. 1621-1625.

Seybold, C.A., Balks, M.R. & Harms, D.S. 2010. Characterization of active layer water contents in the McMurdo Sound region, Antarctica. *Antarctic Science*, 22(6):633-645.

Shaw, J.D., Terauds, A., Riddle, M.J., Possingham, H.P. & Chown, S.L. 2014. Antarctica's Protected Areas Are Inadequate, Unrepresentative, and at Risk. *PLOS Biology*, 12(6).

Skuce, A. 2012. *Subcap Methane Feedbacks, Part 1: Fossil methane seepage in Alaska*. [Online]. Available: http://www.skepticalscience.com/crycapone.html [18/08/2014].

Terauds, A., Steven, L., Chown, S.L., Morgan, F., Peat, H.J., Watts, D.J., Keys, H., Convey, P. & Bergstrom, D.M. 2012. Conservation biogeography of the Antarctic. *Diversity and Distributions, (Diversity Distributions)*, 18:726-741.

Trenberth, K.E., Fasullo, J.T. & Kiehl, J. 2009. *Earth's Global Energy Budget*. American Meterological Society.

Turner, D., Lucieer, A. & Watson, C. 2012. An Automated Technique for Generating Georectified Mosaics from Ultra-High Resolution Unmanned Aerial Vehicle (UAV) Imagery, Based on Structure from Motion (SfM) Point Clouds. *Remote Sensing*, 4:1392-1410.

Turner, J., Bindschadler, R.A., Convey, P., di Princo, G., Fahrbach, E., Gutt, J., Hodgson, D.A., Mayewski, P.A. & Summerhayes, C.P. 2009. *Antarctic Climate Change and the Environment*. Scientific Commitee on Antartic Research.

van Den Broeke, M.R. 1997. Structure and diurnal variation of the atmospheric boundary layer over a mid-latitude glacier in summer. *Boundary-Layer Meteorology*, 83:183-205.

van Everdingen, R.O. 2005. *Multi-Language Glossary of Permafrost and Related Ground-Ice Terms*. International Permafrost Association. Canada.

van Gasselt, S., Reiss, D., Thorpe, A.K. & Neukum, G. 2005. Seasonal variations of polygonal thermal contraction crack patterns in a south polar trough, Mars. *Journal of Geophysical Research*, 110.

Vieira, G. 2014. *High resolution mapping of ice-free environments: examples from the West Antarctic Peninsula region*. SCAR Open Science Conference and COMNAP Symposium Success through International Cooperation, 26.

Vieira, G., Bockheim, J., Guglielmin, M., Balks, M., Abramov, A.A., Boelhouwers, J., Cannone, N., Ganzert, L., Gilichinsky, D.A., Goryachkin, S., López-Martínez, J., Meiklejohn, I., Raffi, R., Ramos, M., Schaefer, C., Serrano, E., Simas, F., Sletten, R. & Wagner, D. 2010. Thermal State of Permafrost and Active Layer Monitoring in the Antarctic: Advances During the International Polar Year 2007–2009. *Permafrost and Periglacial Processes*, 21:182-197.

Vieira, G., Lopez-Martinez, J., Serrano, E., Ramos, M., Gruber, S., Hauck, C. & Blanco, J.J. 2008. *Geomorphological observations of permafrost and ground-ice degradation on Deception and Livingston Islands, Maritime Antarctica*. In Proceedings of the 9th International Conference on Permafrost, 29 June–3 July 2008, Fairbanks, Alaska, Extended Abstracts, Vol. 1, Kane D, Hinkel K (eds). University of Alaska Press: Fairbanks. p. 1839-1844.

Washburn, A.L. 1979. Geocryology: *A Survey of Periglacial Processes and Environments*. Wiley, New York. p. 406.

Zhang, T., Osterkamp, T.E. & Stamnes, K. 1997. Effects of Climate on the Active Layer and Permafrost on the North Slope of Alaska, U.S.A. *Permafrost and Periglacial Processes*, 8:45-67.

Zongjian, L. 2008. UAV for Mapping - Low Altitude Photogrammetric Survey. The International Archives of the Photogrammetry, *Remote Sensing and Spatial Information Sciences*. XXXVII, B1.

Appendix A: Borehole logger issues and solutions

Site	Logger	Data Download	Issue	Solution	Comment
Flårjuven	XR5 New	10-01-2014	Radiation shield base ripped, replaced with new base	New base to radiation shield installed	n/a
Flårjuven	XR5 Old	10-01-2014	Logger faulty and not reading temperature correctly	New logger installed - temperature reading correctly	Discard ambient temperature data
Flårjuven	ACR	10-01-2014	n/a	n/a	n/a
Flårjuven	Decagon 5	10-01-2014	Battery @ 12%	n/a	n/a
Robertskollen	XR5	12-01-2014; 23-01-2014	New mounting base installed, batteries at 7.20V	New base to radiation shield installed	n/a
Robertskollen	Decagon 5	12-01-2014; 23-01-2014	Battery @ 5%	n/a	n/a
Robertskollen	ACR	12-01-2014; 23-01-2014	bu	n/a	n/a
Slettfjell	ACR	11-01-2014	n/a	n/a	n/a
Slettfjell	XR5	11-01-2014	New mounting base installed, batteries at 7.01V	Old loggers used with replacement batteries	n/a
Slettfjell	Decagon 5	11-01-2014	Battery @ 29%	n/a	n/a
Troll	XR5 New	29-12-2013	Radiation shield @ 47cm above the ground; Decagon 5 exposed	Sensor re-buried	Discard Decagon 5 moisture data
Troll	XR5 Old	29-12-2013	Batteries flat @ around August 2013; CH1 broken off	Batteries changed; CH1 re-attached	2014/15 Take Over: Discard CH data
Troll	ACR Center	29-12-2013; 31-12-2013; 02-01-2014; 04-01-2014; 06-01-2014; 08-01-2014	Near surface sensor exposed	Sensor re-buried	Discard near surface sensor data
Troll	ACR Crack	29-12-2013; 31-12-2013; 02-01-2014; 04-01-2014; 06-01-2014; 08-01-2014	Near surface sensor exposed;	Sensor re-buried	Discard near surface sensor data
Troll	Decagon 5 Center	29-12-2013	Battery @ 8%; Sensor exposed; Battery @ 4% on 08/01/14	Sensor re-buried	Discard Decagon 5 moisture data
Troll	Decagon 5	29-12-2013	Battery @ 35%; Battery @ 33% on	n/a	n/a

	Crack		08/01/14		
Valterkulten	Decagon 5	09-01-2014	Battery @ 45%	n/a	n/a
Valterkulten	XR5	09-01-2014	Radiation shield broken off, replaced with a new off, 2.5cm and 5cm are connected in reverse.	New radiation shield attached	Discard ambient temperature data
Valterkulten	ACR	09-01-2014	n/a	n/a	n/a
Vesleskarvet	XR5	27-12-2013	CH1 & 2 broken off; channels repaired 08/01/14	Ch1 & 2 re-attached	n/a
Vesleskarvet	ACR	27-12-2013; 08-01-2014; 10-01-2014; 12-01-2014; 14-01-2014; 16-01-2014; 18-01-2014; 20-01-2014	n/a	n/a	n/a

Appendix B: Study area soil samples coordinates and altitude

Site	Type	Location	Description	Latitude	Longitude	m.a.s.l.
Flårjuven	Soil	Old Logger	Flarjuven Old Logger	S72° 01' 26.4"	W003° 22' 47.6"	1278
Flårjuven	Soil	Polygons	Poly 1 Centre Flarjuven	S 72° 00' 42.9"	W 003° 23' 04.4"	1247
Flårjuven	Soil	Polygons	Poly 1 Crack Flarjuven	S 72° 00' 42.9"	W 003° 23' 04.4"	1247
Flårjuven	Soil	Polygons	Poly 2 Centre Flarjuven	S 72° 00' 42.4"	W 003° 23' 03.8"	1242
Flårjuven	Soil	Polygons	Poly 2 Crack Flarjuven	S 72° 00' 42.4"	W 003° 23' 03.8"	1242
Flårjuven	Soil	Polygons	Poly 3 Centre Flarjuven	S 72° 00' 42.2"	W 003° 23' 01.9"	1242
Flårjuven	Soil	Polygons	Poly 3 Crack Flarjuven	S 72° 00' 42.2"	W 003° 23' 01.9"	1242
Flårjuven	Soil	Polygons	Poly 4 Centre Flarjuven	S 72° 00' 41.7"	W 003° 23' 02.8"	1242
Flårjuven	Soil	Polygons	Poly 4 Crack Flarjuven	S 72° 00' 41.7"	W 003° 23' 02.8"	1242
Flårjuven	Soil	Polygons	Poly 5 Centre Flarjuven	S 72° 00' 41.6"	W 003° 23' 03.9"	1242
Flårjuven	Soil	Polygons	Poly 5 Crack Flarjuven	S 72° 00' 41.6"	W 003° 23' 03.9"	1242
Flårjuven	Soil	Sope Transect	Flar Ter M1	S 72° 00' 43.9"	W 003° 22' 53.3"	1262
Flårjuven	Soil	Sope Transect	Flar Ter B1	S 72° 00' 43.9"	W 003° 22' 53.0"	1260
Flårjuven	Soil	Sope Transect	Flar Ter M2	S 72° 00' 44.0"	W 003° 22' 52.9"	1261
Flårjuven	Soil	Sope Transect	Flar Ter B2	S 72° 00' 44.2"	W 003° 22' 52.5"	1265
Flårjuven	Soil	Sope Transect	Flar Ter M3	S 72° 00' 44.2"	W 003° 22' 52.4"	1265
Flårjuven	Soil	Sope Transect	Flar Ter B3	S 72° 00' 44.3"	W 003° 22' 52.0"	1265
Flårjuven	Soil	Sope Transect	Flar Ter M4	S 72° 00' 44.5"	W 003° 22' 51.4"	1268
Flårjuven	Soil	Sope Transect	Flar Ter B4	S 72° 00' 44.7"	W 003° 22' 51.4"	1270
Flårjuven	Soil	Sope Transect	Flar Ter M5	S 72° 00' 44.7"	W 003° 22' 51.0"	1270
Flårjuven	Soil	Sope Transect	Flar Ter B5	S 72° 00' 44.9"	W 003° 22' 50.5"	1271
Flårjuven	Soil	Sope Transect	Flar Ter M6	S 72° 00' 45.2"	W 003° 22' 50.5"	1274
Flårjuven	Soil	Sope Transect	Flar Ter B6	S 72° 00' 45.3"	W 003° 22' 49.8"	1277
Flårjuven	Soil	Sope Transect	Flar Ter M7	S 72° 00' 45.4"	W 003° 22' 49.5"	1278
Flårjuven	Soil	Sope Transect	Flar Ter B7	S 72° 00' 45.6"	W 003° 22' 49.0"	1280

Flårjuven	Soil	Polygons	Soil from inside contraction crack	n/a	n/a	n/a
Flårjuven	Soil	Polygons	Rock with precipitate from inside polygon	n/a	n/a	n/a
Flårjuven	Soil	Polygons	Inside polygon	n/a	n/a	n/a
Flårjuven	Soil	Polygons	Soil from XR5 logger site	n/a	n/a	n/a
Slettfjell	Soil	Logger	Slettfjell Logger 1	S72° 08' 14.2"	W003° 17' 02.8"	1472
Slettfjell	Soil	South of Logger	Slettfjell Logger South	S72° 08' 14.4"	W003° 17' 03.3"	1543
Slettfjell	Soil	Polygons	Slettfjell Gypsum	n/a	n/a	n/a
Troll	Soil	Polygons	00 Center	S72° 00' 08.3"	E002° 34' 18.5"	1175
Troll	Soil	Polygons	00 Crack	S72° 00' 08.3"	E002° 34' 18.5"	1175
Troll	Soil	Polygons	01 Centre	S72° 00' 41.7"	E002° 33' 07.2"	1500
Troll	Soil	Polygons	01 Crack	S72° 00' 41.7"	E002° 33' 07.2"	1500
Troll	Soil	Polygons	3 Center	S72° 00' 19.4"	E002° 34' 14.2"	1256
Troll	Soil	Polygons	3 Crack	S72° 00' 19.4"	E002° 34' 14.2"	1256
Troll	Soil	Polygons	4 Center	S72° 00' 38.5"	E002° 33' 22.0"	1482
Troll	Soil	Polygons	4 Crack	S72° 00' 38.5"	E002° 33' 22.0"	1482
Troll	Soil	Polygons	5 Center	S72° 00' 09.4"	E002° 32' 37.7"	2060
Troll	Soil	Polygons	5 Crack	S72° 00' 09.4"	E002° 32' 37.7"	2060
Troll	Soil	Polygons	6 Center	S72° 00' 07.2"	E002° 34' 27.5"	2020
Troll	Soil	Polygons	6 Crack	S72° 00' 07.2"	E002° 34' 27.5"	2020
Troll	Soil	Polygons	7 Center	S72° 00' 24.5"	E002° 33' 23.4"	1353
Troll	Soil	Polygons	7 Crack	S72° 00' 24.5"	E002° 33' 23.4"	1353
Troll	Soil	Polygons	8 Center	S72° 00' 11.5"	E002° 33' 11.5"	2040
Troll	Soil	Polygons	8 Crack	S72° 00' 11.5"	E002° 33' 11.5"	2040
Troll	Soil	Polygons	9 Center	S72° 00' 41.7"	E002° 33' 04.7"	1504
Troll	Soil	Polygons	9 Crack	S72° 00' 41.7"	E002° 33' 04.7"	2504
Troll	Soil	Polygons	10 Center	S72° 00' 39.2"	E002° 32' 55.3"	1329
Troll	Soil	Polygons	10 Crack	S72° 00' 39.2"	E002° 32' 55.3"	1329

Troll	Soil	Polygons	11 Center	S72° 00' 11.2"	E002° 34' 55.9"	2030
Troll	Soil	Polygons	11 Crack	S72° 00' 11.2"	E002° 34' 55.9"	2030
Troll	Soil	Polygons	12 Center	S72° 00' 09.7"	E002° 33' 06.5"	2050
Troll	Soil	Polygons	12 Crack	S72° 00' 09.7"	E002° 33' 06.5"	2050
Troll	Soil	Polygons	13 Center	S72° 00' 08.7"	E002° 34' 22.1"	2030
Troll	Soil	Polygons	13 Crack	S72° 00' 08.7"	E002° 34' 22.1"	2030
Troll	Soil	Polygons	14 Center	S72° 00' 27.0"	E002° 32' 40.6"	1318
Troll	Soil	Polygons	14 Crack	S72° 00' 27.0"	E002° 32' 40.6"	1318
Troll	Soil	Polygons	15 Center	S71° 59' 53.9"	E002° 34' 50.9"	2030
Troll	Soil	Polygons	15 Crack	S71° 59' 53.9"	E002° 34' 50.9"	2030
Troll	Soil	Polygons	16 Center	S72° 00' 22.3"	E002° 32' 47.4"	1303
Troll	Soil	Polygons	16 Crack	S72° 00' 22.3"	E002° 32' 47.4"	1303
Troll	Soil	Polygons	17 Center	S72° 00' 01.8"	E002° 34' 15.6"	2100
Troll	Soil	Polygons	17 Crack	S72° 00' 01.8"	E002° 34' 15.6"	2100
Troll	Soil	Polygons	18 Center	S72° 00' 40.0"	E002° 33' 09.4"	1495
Troll	Soil	Polygons	18 Crack	S72° 00' 40.0"	E002° 33' 09.4"	1495
Troll	Soil	Polygons	19 Center	S72° 00' 34.2"	E002° 33' 37.4"	1457
Troll	Soil	Polygons	19 Crack	S72° 00' 34.2"	E002° 33' 37.4"	1457
Troll	Soil	Polygons	20 Center	S72° 00' 27.4"	E002° 32' 37.7"	1322
Troll	Soil	Polygons	20 Crack	S72° 00' 27.4"	E002° 32' 37.7"	1322
Troll	Soil	Polygons	21 Center	S72° 00' 30.6"	E002° 33' 45.0"	1430
Troll	Soil	Polygons	21 Crack	S72° 00' 30.6"	E002° 33' 45.0"	1430
Troll	Soil	Polygons	22 Center	S72° 00' 06.6"	E002° 33' 30.2"	2100
Troll	Soil	Polygons	22 Crack	S72° 00' 06.6"	E002° 33' 30.2"	2100
Troll	Soil	Polygons	23 Center	S72° 00' 04.0"	E002° 32' 24.0"	2030
Troll	Soil	Polygons	23 Crack	S72° 00' 04.0"	E002° 32' 24.0"	2030
Troll	Soil	Polygons	24 Center	S72° 00' 45.7"	E002° 32' 48.1"	
Troll	Soil	Polygons	24 Crack	S72° 00' 45.7"	E002° 32' 48.1"	

Troll	Soil	Polygons	25 Center	S72° 00' 08.3"	E002° 33' 24.1"	2100
Troll	Soil	Polygons	25 Crack	S72° 00' 08.3"	E002° 33' 24.1"	2100
Troll	Soil	Polygons	26 Center	S72° 00' 43.9"	E002° 32' 06.4"	2020
Troll	Soil	Polygons	26 Crack	S72° 00' 43.9"	E002° 32' 06.4"	2020
Troll	Soil	Polygons	27 Center	S72° 00' 10.8"	E002° 34' 45.8"	2040
Troll	Soil	Polygons	27 Crack	S72° 00' 10.8"	E002° 34' 45.8"	2040
Troll	Soil	Polygons	28 Center	S72° 00' 38.5"	E002° 33' 07.9"	1477
Troll	Soil	Polygons	28 Crack	S72° 00' 38.5"	E002° 33' 07.9"	1477
Troll	Soil	Polygons	29 Center	S72° 00' 30.6"	E002° 34' 11.6"	1356
Troll	Soil	Polygons	29 Crack	S72° 00' 30.6"	E002° 34' 11.6"	1356
Troll	Soil	Polygons	30 Center	S72° 00' 13.0"	E002° 33' 09.0"	2020
Troll	Soil	Polygons	30 Crack	S72° 00' 13.0"	E002° 33' 09.0"	2020
Valterkulten	Soil	Slope Transect	Valt Terr Midd1	S71° 53' 48.6"	W003° 13' 36.4"	1005
Valterkulten	Soil	Slope Transect	Valt Terr B1	S71° 53' 48.6"	W003° 13' 36.2"	1002
Valterkulten	Soil	Slope Transect	Valt Terr Midd2	S71° 53' 48.4"	W003° 13' 36.1"	1007
Valterkulten	Soil	Slope Transect	Valt Terr B2	S71° 53' 48.5"	W003° 13' 36.2"	1006
Valterkulten	Soil	Slope Transect	Valt Terr Midd3	S71° 53' 48.2"	W003° 13' 36.1"	1008
Valterkulten	Soil	Slope Transect	Valt Terr B3	S71° 53' 48.4"	W003° 13' 36.3"	1006
Valterkulten	Soil	Slope Transect	Valt Terr Mid4	S71° 53' 48.2"	W003° 13' 35.6"	1009
Valterkulten	Soil	Slope Transect	Valt Terr B4	S71° 53' 48.2"	W003° 13' 35.9"	1009
Valterkulten	Soil	Slope Transect	Valt Terr Mid5	S71° 53' 48.0"	W003° 13' 35.7"	1011
Valterkulten	Soil	Slope Transect	Valt Terr Bot5	S71° 53' 48.2"	W003° 13' 35.6"	1009
Valterkulten	Soil	Slope Transect	Valt Terr Mid6	S71° 53' 47.8"	W003° 13' 35.3"	1013
Valterkulten	Soil	Slope Transect	Valt Terr Bot6	S71° 53' 47.9"	W003° 13' 35.4"	1012
Valterkulten	Soil	Slope Transect	Valt Terr Mid7	S71° 53' 47.6"	W003° 13' 34.8"	1017
Valterkulten	Soil	Slope Transect	Valt Terr Bot7	S71° 53' 47.7"	W003° 13' 35.1"	1015
Valterkulten	Soil	Slope Transect	Valt Terr Mid8	S71° 53' 47.4"	W003° 13' 34.6"	1019
Valterkulten	Soil	Slope Transect	Valt Terr Bot8	S71° 53' 47.5"	W003° 13' 34.7"	1017

Valterkulten	Soil	Slope Transect	Valt Terr Mid9	S71° 53' 47.3"	W003° 13' 34.1"	1021
Valterkulten	Soil	Slope Transect	Valt Terr Bot9	S71° 53' 47.4	W003° 13' 34.6"	1019

Appendix C: Flårjuven polygons data samples

A Axis			B Axis	Slope						Soil Moisture					
Length (m)	Orientation (magnetic, degrees)	TRUE	Length (m)	Orientation (magnetic, degrees)	TRUE	Gradient (degrees	Slope=a axis	Perimeter	Height	Centre	Crack	Comment	Snow-Crack	Lat	Long
12.1	134	112.18	7.1	134	112.18	12.1	TRUE	32.55	1247			In crack, slight increase in slope to the	Y	-72.01191667	-3.384555556
8.2	80	58.18	4.3	80	58.18	8.2	TRUE	20.2	1242			In crack	Y	-72.01177778	-3.384388889
8.8	103	81.18	7.3	103	81.18	8.8	TRUE	25.4	1242			In crack	Y	-72.01172222	-3.383861111
13.1	85	63.18	9.4	85	63.18	13.1	TRUE	34.4	1242			In crack	Y	-72.01158333	-3.384111111
8.7	72	50.18	6.6	72	50.18	8.7	TRUE	29.65	1242			In crack	Y	-72.01155556	-3.384416667
10.2	94.8	73.0	6.9	94.8	73.0	10.2	5	28.4	1243.0				0		
13.1	134.0	112.2	9.4	134.0	112.2	13.1	0	34.4	1247.0				5		
8.2	72.0	50.2	4.3	72.0	50.2	8.2		20.2	1242.0						
2.2	24.7	24.7	1.8	24.7	24.7	2.2		5.7	2.2						

Appendix D: Troll polygons data samples

			A Axis			B Axis	Slope						Soil Moisture					
Number	Date	Site	Length (m)	Orientation (magnetic, degrees)	TRUE	Length (m)	Orientation (magnetic, degrees)	TRUE	Gradient (degrees)	Slope=a axis	Perimeter	Height	Centre	Crack	Comment	Snow-Crack	Lat	Long
TR800	2013/12/30	Mimelia	11.8	31.1	9.28	6	344	322.18	17	FALSE	31.1	1175	2050	2030	No snow	N	-72.002300000000	2.571810000000
TR801	2013/12/29	Mimelia	17.2	45	23.18	12.1	345	323.18	12	FALSE	44.7	1500	2070	2030	No snow	N	-72.011600000000	2.552040000000
TR802	2013/12/30	Mimelia	18.8	345	323.18	15	345	323.18	16	TRUE	56	1256	2060	2030	Snow in crack, no large boulders	Y	-72.005400000000	2.570580000000
TR803	2013/12/29	Mimelia	14.2	350	328.18	13.6	350	328.18	11.5	TRUE	39.8	1482	2030	2030	Snow in crack	Y	-72.010700000000	2.556090000000
TR804	2013/12/30	Mimelia	10	21	359.18	5	57	35.18	8	FALSE	23.9	2060	2050	1131	Snow in crack	Y	-72.002600000000	2.543840000000
TR805	2013/12/30	Mimelia	19.2	4	342.18	15	344	322.18	18	FALSE	53	2020	2040	1185	Snow in crack, large boulders	Y	-72.002000000000	2.574270000000
TR806	2013/12/29	Mimelia	22.9	15	353.18	20	15	353.18	14.5	TRUE	66.2	1353	2020	2020	Snow in crack	Y	-72.006800000000	2.556490000000
TR807	2013/12/30	Mimelia	30	290	268.18	9.3	9	347.18	23	FALSE	38	2040	2070	1144	Snow in crack, very elevated centre,	Y	-72.003200000000	2.553210000000
TR808	2013/12/29	Mimelia	21.1	346	324.18	15.6	346	324.18	10	TRUE	59.3	1504	2010	2020	No snow	N	-72.011600000000	2.551340000000
TR809	2013/12/30	Mimelia	15.9	348	326.18	11.3	348.00	326.18	12	TRUE	44.1	1329	2030	2040	Snow in crack	Y	-72.010900000000	2.548700000000
TR810	2013/12/30	Mimelia	9	325	303.18	8.4	325	303.18	21	TRUE	25.2	2030	2050	1291	Snow in crack	Y	-72.003100000000	2.582180000000
TR811	2013/12/30	Mimelia	8.2	82	60.18	8.5	8	-13.82	12	FALSE	24	2050	2040	1146	No snow, no large boulders	N	-72.003444444444	2.547222222222
TR812	2013/12/30	Mimelia	7.2	348	326.18	6	348	326.18	13	TRUE	22	2030	2030	1183	Snow in crack	Y	-72.002400000000	2.572830000000
TR813	2013/12/29	Mimelia	14	8	-13.82	9.6	8	-13.82	8	TRUE	41.5	1318	2020	2030	Snow in crack, no large boulders, lots	Y	-72.007500000000	2.544620000000
TR814	2013/12/30	Mimelia	8	34	12.18	6.1	311	289.18	18	FALSE	18.3	2030	2040	1177	Snow in crack	Y	-71.998750000000	2.579694444444
TR815	2013/12/29	Mimelia	14	12.5	-9.32	10.3	12.5	-9.32	10	TRUE	37.6	1303	2050	2110	Snow in crack, no large boulders, lots	Y	-72.006200000000	2.546530000000
TR816	2013/12/30	Mimelia	10.8	75	53.18	6.4	355	333.18	11	FALSE	29.8	2100	2040	1125	Snow in crack	Y	-72.000722222222	2.571000000000
TR817	2013/12/29	Mimelia	17.1	5	-16.82	17	5	-16.82	9	TRUE	51	1495	2020	2020	No snow	N	-72.011100000000	2.552550000000
TR818	2013/12/29	Mimelia	14.5	345	323.18	12	345	323.18	14	TRUE	42.6	1457	2040	2050	Snow in crack, large boulders	Y	-72.009500000000	2.560360000000
TR819	2013/12/29	Mimelia	19.5	20	-1.82	16.6	20	358.18	8.5	TRUE	55	1322	2010	2140	Snow in crack	Y	-70.007805555556	2.543694444444
TR820	2013/12/29	Mimelia	14.8	50	28.18	14.4	5	343.18	16	FALSE	43	1430	2060	2050	Snow in crack, large boulders	Y	-72.008500000000	2.562470000000
TR821	2013/12/30	Mimelia	21.3	59	37.18	9.5	59	37.18	8	TRUE	37.6	2100	2210	1123	Snow in cracks, no boulders, centre r	Y	-72.002100000000	2.558430000000
TR822	2013/12/30	Mimelia	10.7	116	94.18	9.9	56	34.18	14	FALSE	33.2	2030	2030	1180	Snow in crack	Y	-72.003666666667	2.538888888889
TR823	2013/12/29	Mimelia	12.3	335	313.18	11.9	335	313.18	9.5	TRUE	37.2		2020	2030	Snow in crack	Y	-72.012700000000	2.546670000000
TR824	2013/12/30	Mimelia	11.3	303	281.18	8.2	348	326.18	10	FALSE	30.7	2100	2050	1125	Snow in crack, no large boulders, cen	Y	-72.002300000000	2.556680000000
TR825	2013/12/30	Mimelia	12.3	72	50.18	7.3	37	15.18	13	FALSE	33	2020	2030	1231	Snow in crack	Y	-72.006000000000	2.540944444444
TR826	2013/12/30	Mimelia	16.8	326	304.18	11.4	335	313.18	19	FALSE	47.5	2040	2070	1257	Snow in crack	Y	-72.003000000000	2.579400000000
TR827	2013/12/29	Mimelia	18.2	57	35.18	17.7	350	328.18	12	FALSE	51	1477	2030	2020	Snow in crack	Y	-72.010700000000	2.552230000000
TR828	2013/12/30	Mimelia	17.6	0	-21.82	14.1	0	338.18	16.5	TRUE	52	1356	2050	2040	Snow in crack, large boulders	Y	-72.008500000000	2.569850000000
TR829	2013/12/30	Mimelia	12.1	61	39.18	11	7	345.18	27	FALSE	38	2020	2100	1157	Snow in cracks	Y	-72.003600000000	2.552530000000
Mean			15.0	147.6	161.8	11.3	192.4	242.6	13.7	15	40.2	1704.4	2047.3	1638.2		5		
Max			30.0	350.0	359.2	20.0	355.0	358.2	27.0	15	66.2	2100.0	2210.0	2140.0		25		
Min			7.2	0.0	-21.8	5.0	0.0	-16.8	8.0		18.3	1175.0	2010.0	1123.0				
StDev			5.1	146.0	152.9	3.9	163.6	144.7	4.7		11.9	345.9	36.7	442.4				
Mode			14.0	345.0	323.2		345.0	323.2	12.0		38.0		2050.0	2030.0				
										50						83.3333333		

Appendix E: Troll polygon sample sieved weights

Sample	Frozen (with plastic)	Plastic	Tin	Melted (with tin)	Dried (with tin)	8000	4000	2000	1000	500	250	125	63	<63
00CE	658.7	19.04	10.52	650.37	650.00	524.07	505.72	484.88	586.49	573.03	438.15	281.22	444.25	244.15
00CR	807.8	17.67	10.65	800.83	799.87	642.91	504.77	510.22	517.10	474.23	394.29	298.11	446.02	421.52
01CE	473.6	18.17	11.72	466.94	464.53	530.90	505.62	440.99	480.00	484.86	452.82	310.52	446.09	243.77
01CR	772.5	21.9	10.4	907.46	907.19	656.09	714.84	589.83	547.13	481.35	397.10	271.19	438.47	243.25
02CE	762.7	17.49	12.31	757.18	756.14	563.46	519.58	510.32	491.50	489.81	411.01	304.64	451.30	421.99
02CR	883.2	17.64	11.67	877.45	876.73	649.44	607.19	546.29	571.48	542.56	429.06	278.10	439.84	243.48
03CE	586.2	18.19	12.04	579.89	57.26	556.35	458.46	440.12	436.07	444.20	411.04	343.28	466.18	427.64
03CR	838.1	17.52	10.52	831.12	830.68	672.63	715.67	545.67	511.38	468.71	395.91	270.47	438.26	243.36
04CE	672.1	25.22	10.58	657.6	657.15	559.57	526.36	505.75	474.73	438.04	384.91	306.65	448.29	422.07
04CR	579.7	25.64	10.52	564.55	563.36	556.77	459.59	439.51	443.68	471.85	417.76	307.53	453.00	423.04
05CE	797.6	17.79	11.76	791.62	790.79	717.22	542.68	501.24	549.85	526.35	423.70	276.81	440.26	244.08
05CR	623.8	19.4	11.74	616.06	609.35	638.56	552.88	490.36	508.17	483.08	406.39	275.87	438.98	243.42
06CE	726.8	19.6	10.1	717.34	716.49	502.54	481.93	426.56	480.02	635.27	609.10	325.19	444.27	243.90
06CR	608.2	18.25	11.87	601.97	601.44	573.64	544.44	497.64	538.91	521.52	407.83	268.15	437.39	243.18
07CE	531.6	23.65	11.96	519.01	519.48	656.28	552.66	458.13	475.84	457.85	394.32	271.53	439.89	243.55
07CR	801.3	31.77	10.65	779.81	749.83	586.04	520.22	473.00	544.44	595.15	481.15	293.90	444.37	243.42
08CE	719.8	18.48	11.8	712.98	697.61	602.11	481.68	470.20	455.10	442.39	423.97	351.54	456.81	422.66
08CR	703.5	18.94	10.55	695.39	695.15	529.03	620.04	556.42	567.58	511.18	394.53	267.24	438.10	243.33
09CE	812.05	17.65	11.69	806.96	805.22	585.36	510.09	514.17	495.67	509.35	415.95	307.35	453.30	422.50
09CR	621.8	17.27	12.26	616.88	616.32	596.96	522.69	495.29	469.97	424.19	359.66	289.84	444.82	420.95
10CE	814.2	25.31	11.76	800.89	798.78	628.32	495.50	452.30	533.20	616.70	515.40	303.91	441.38	243.26
10CR	516.28	23.69	12.23	504.57	503.13	580.72	504.93	471.98	438.20	401.46	352.14	291.90	447.62	421.47
11CE	514.7	24.2	11.76	502.32	500.81	534.42	491.74	440.54	497.66	523.54	456.44	298.06	446.80	243.62

11CR	622.3	23.58	11.85	610.41	603.44	611.22	459.61	445.97	451.42	454.44	401.71	615.91	449.81	421.79
12CE	602.5	17.52	11.69	596.71	594.98	544.97	461.56	444.03	464.84	484.70	413.24	318.26	450.19	421.65
12CR	672.2	18.59	12.08	478.27	477.77	591.39	503.96	447.70	488.57	482.87	421.53	285.71	442.86	243.74
13CE	852.8	17.92	11.8	846.81	845.22	553.47	482.54	499.73	504.50	527.44	460.43	327.42	463.48	433.88
13CR	714.6	17.55	11.87	709.12	708.78	575.08	601.65	530.32	547.10	520.55	410.81	271.80	438.48	243.35
14CE	681.93	25.23	11.83	668.28	667.23	516.41	528.31	476.68	554.50	575.63	460.06	300.24	443.66	243.58
14CR	675.3	30.2	12.12	656.08	639.58	520.84	509.54	467.71	569.88	610.63	438.40	271.98	438.29	243.36
15CE	654.5	17.37	11.88	640.06	638.94	511.70	498.62	460.00	516.23	561.29	518.51	317.78	442.85	243.24
15CR	704.3	20.23	11.73	693.93	682.04	695.98	521.53	478.45	447.98	415.99	367.06	296.87	446.08	421.37
16CE	617.2	25.99	11.7	603.39	589.10	647.37	459.81	436.48	438.45	440.54	395.21	305.16	452.38	422.41
16CR	603.3	25.43	11.69	588.44	586.92	652.69	475.25	446.51	446.00	441.07	373.63	292.39	445.70	421.78
17CE	783	18.66	11.9	774.81	77305.00	534.67	497.24	448.17	550.21	672.63	509.42	298.47	443.79	243.85
17CR	818.8	17.8	12.25	812.37	811.68	619.38	637.92	556.56	551.92	506.66	413.05	274.30	438.80	243.49
18CE	668.1	18.77	12.07	661.15	659.35	569.35	531.89	481.76	519.72	534.06	465.77	300.37	443.73	243.79
18CR	724.5	17.95	11.62	718.26	717.77	727.24	613.25	500.94	509.26	470.87	383.77	263.09	436.89	243.12
19CE	658.3	18.24	8.98	649.33	648.62	593.50	494.88	450.54	531.84	569.76	447.09	295.76	450.94	244.09
19CR	596.1	18.34	11.81	588.27	574.22	605.00	478.65	451.66	434.75	437.40	392.80	304.50	452.50	425.22
20CE	592.8	18.55	11.72	584.47	575.19	502.95	501.72	458.23	520.62	555.55	472.03	306.32	446.23	243.45
20CR	855.9	19.22	11.73	848.1	845.11	660.77	544.92	520.33	487.80	470.13	398.62	299.99	448.23	422.83
21CE	602.5	27.4	11.71	492.31	491.75	522.68	459.46	448.61	457.93	437.06	389.41	309.04	452.13	423.41
21CR	650.5	30.75	11.76	631.08	612.98	569.17	596.00	478.79	507.25	509.86	417.27	279.14	441.04	243.50
22CE	617.8	25.95	11.86	603.15	602.46	647.13	474.26	453.72	438.24	439.84	387.70	299.50	449.03	421.56
22CR	830.6	24.93	11.85	817.86	816.66	626.76	500.44	486.81	471.57	493.73	449.87	318.97	453.33	422.73
23CE	680.6	17.67	10.4	673.39	673.01	514.66	486.12	499.83	489.12	481.69	418.81	315.27	454.39	422.81
23CR	731.3	20.03	8.9	719.57	716.80	606.48	673.70	581.43	523.07	441.62	376.50	266.05	437.71	243.18
24CE	717.7	25.82	11.7	703.18	679.87	543.40	487.07	472.47	466.41	474.26	431.79	325.15	463.15	424.96
24CR	534.2	25.73	11.74	520.22	518.81	630.11	503.86	451.72	427.58	404.77	353.20	289.06	445.24	421.56
25CE	668.9	26.88	11.73	652.36	651.44	504.55	497.01	551.28	528.87	460.72	357.41	290.13	448.15	421.54

25CR	727.4	24.3	11.8	715.26	714.54	567.50	520.74	439.65	518.55	609.53	504.30	298.80	442.18	243.61
26CE	421	18.11	10.5	413.55	413.27	517.54	452.58	456.15	548.11	409.84	362.31	294.09	448.95	423.43
26CR	701.9	17.66	10.52	694.96	694.56	679.76	586.28	508.55	527.26	482.11	393.11	268.50	438.11	243.42
27CE	724	19.69	10.67	715.02	714.55	544.47	471.79	449.68	458.95	527.33	465.15	320.52	457.58	427.95
27CR	773.4	18.44	10.64	765.65	765.19	593.51	496.81	507.83	493.47	442.90	412.54	318.83	457.15	424.38
28CE	866.4	18.09	10.52	859.04	858.33	576.12	534.00	482.70	489.40	546.31	443.75	312.50	458.26	424.44
28CR	735.4	19.7	10.52	726.15		633.26	604.31	528.93	528.72	488.11	407.29	278.28	440.37	243.58
29CE	720.8	23.7	10.57	707.77	707.54	647.03	521.72	503.00	496.23	442.37	352.63	287.33	445.22	421.30
29CR	823.8	25.29	10.49	809.23	806.36	601.50	487.20	471.72	475.35	517.71	461.13	322.66	455.51	422.64

Appendix F: Troll fines analysis results

Record Number	Sample Name	Dx (10)	Dx (50)	Dx (90)	Residual	Weighted Residual
0	Centre	12.4	41.2	82.1	0.88	0.94
0	Crack	17.6	51.3	99	1.31	1.34
2	Centre	7.34	37.7	76.8	0.93	1
2	Crack	32.1	59.6	101	1.23	1.11
4	Centre	13.3	43	84.7	0.32	0.33
4	Crack	6.03	32.4	71.2	0.41	0.46
6	Centre	15.1	49.2	88.3	0.38	0.39
8	Centre	4.89	31.2	71	0.69	0.78
10	Crack	9.29	42.7	76.7	0.41	0.43
12	Centre	5.55	39.5	79	0.42	0.44
12	Crack	28.8	55.4	92.9	0.53	0.43
14	Centre	19.9	51.4	90.4	0.44	0.42
16	Centre	7.65	34	75	0.38	0.34
16	Crack	9.7	40.4	85.5	0.38	0.4
18	Centre	12.3	45.5	83.3	0.39	0.38
20	Crack	12.1	40.5	82.2	0.3	0.35
22	Centre	9.88	43.3	84.5	0.72	0.79
22	Crack	6.88	37.3	72.6	1.08	1.17
24	Centre	9.03	40	78	0.73	0.79
24	Crack	10.5	42.8	86.5	0.86	0.93
26	Centre	11.5	37.7	75.4	0.33	0.35
26	Crack	16.6	51.3	102	0.33	0.31
28	Centre	8.91	37.1	74.8	0.52	0.53
28	Crack	59.2	117	198	0.47	0.47

Appendix G: Structure from Motion results on a single object